Petrogenesis of High Heat Producing Granite: Implication for Mt Painter Province, South Australia

Kamonporn Kromkhun, (M.Sc)

Geology and Geophysics
School of Earth & Environmental Science
University of Adelaide

Thesis submitted for the degree of Doctor of Philosophy
in the Faculty of Science, University of Adelaide

January 2010

Chapter 4 Geochronology

The chemical and physical properties of zircon and its average closure temperature for the U-Th-Pb decay system make it a very useful mineral to date the original crystallization of magmatic rocks (Košler and Sylvester, 2003). The chemical and physical stability of zircons also allow them to be preserved as xenocrysts in magmatic rocks. Cathodoluminescence (CL) and back-scattered electron (BSE) images of zircons reveal their morphology and can help distinguish complex zircon growth histories (Corfu et al., 2003).

This study uses the LA-ICPMS technique to analyse the U, Th and Pb content from 30-50 μm laser ablation spots in single zircon crystals to examine the age relationships between the igneous rocks of the Mt Painter Inlier. Samples covering felsic and mafic igneous suites were selected for the geochronological study (Figure 4.1). Zircon crystals were separated from their host and studied for their morphology and internal structure using the CL image. The detailed methodology is presented in Appendix 1.

4.1 Result

4.1.1 Pepegoona Volcanics

Sample MN003 from the Pepegoona Volcanics was collected from the east of study area. Zircons from MN003 range from 50 to 250 μm in size and the length-to-width ratio of zircon range from 2:1 up to 4:1 (Figure 4.2a). Zircons are commonly euhedral and some show well-formed pyramidal terminations. In transmitted light, the zircons are generally pale yellow to colourless and show growth zoning. Most zircons exhibit secondary minerals on their surfaces resulting from metamorphism and/or hydrothermal alteration. A few zircons contain xenocrystic cores. Zircons from the Pepegoona volcanic have U concentration in range between 542 and 4756 ppm and Th concentration range between 318 and 2745 ppm. The Th/U ranges from 0.53 to 0.63.

The results of single zircon U-Pb analyses from the Pepegoona Volcanics are shown in Figures 4.2b and 4.2c. The shaded frequency bars and solid lines represent those analyses that are less than 10% discordant. They

yield $^{207}Pb/^{206}Pb$ ages ranging from 1585 to 1622 Ma. The dashed histogram line displays all age data. The calculated concordia age of the Pepegoona Volcanics zircons (n=15, exclude discordant zircons) yield an age of 1603±19 Ma (MSWD = 2.4; Figure 4.2d) that is interpreted to be the volcanic extrusive age.

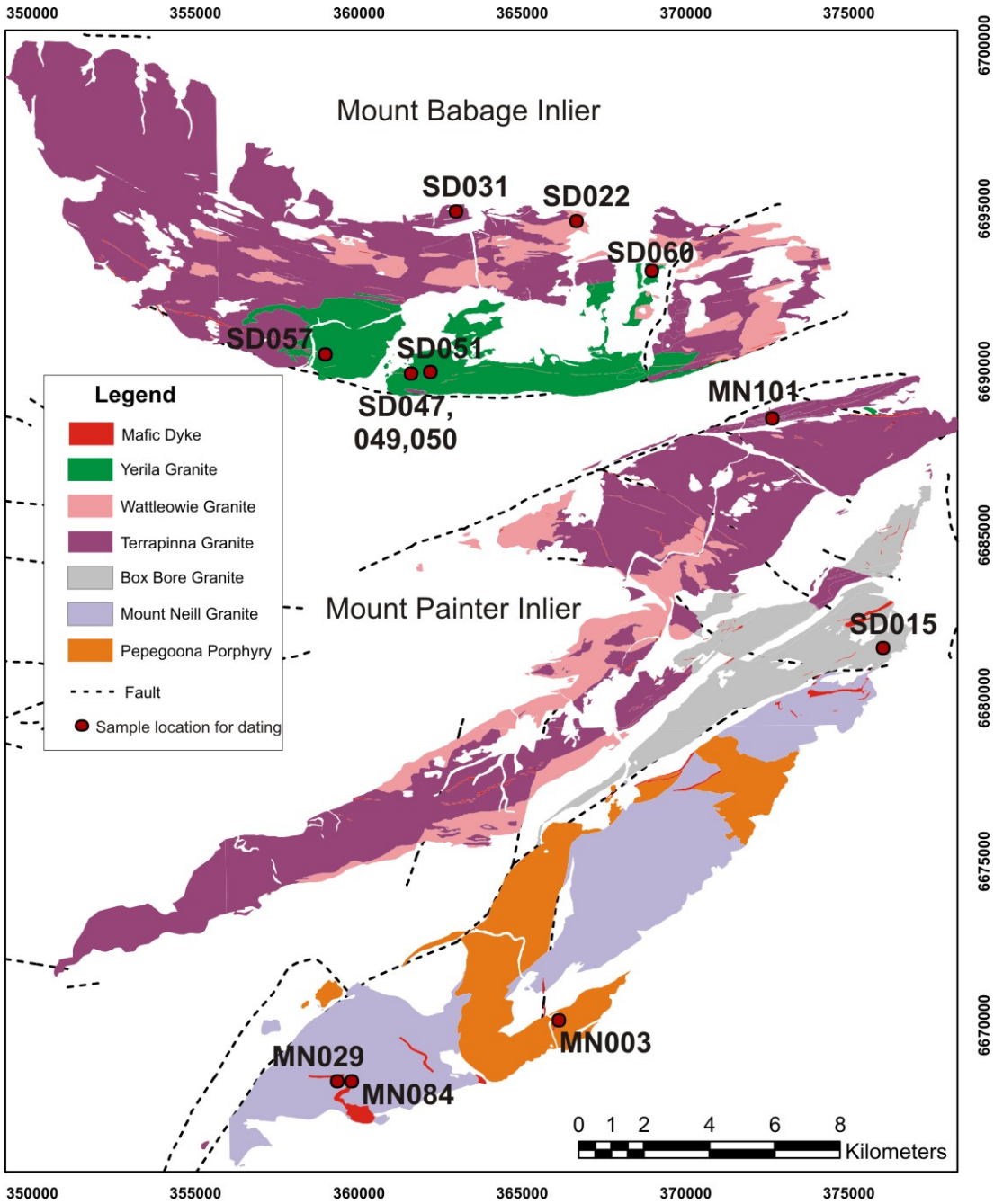

Figure 4.1 Location of mafic and felsic samples selected for U-Pb zircon dating.

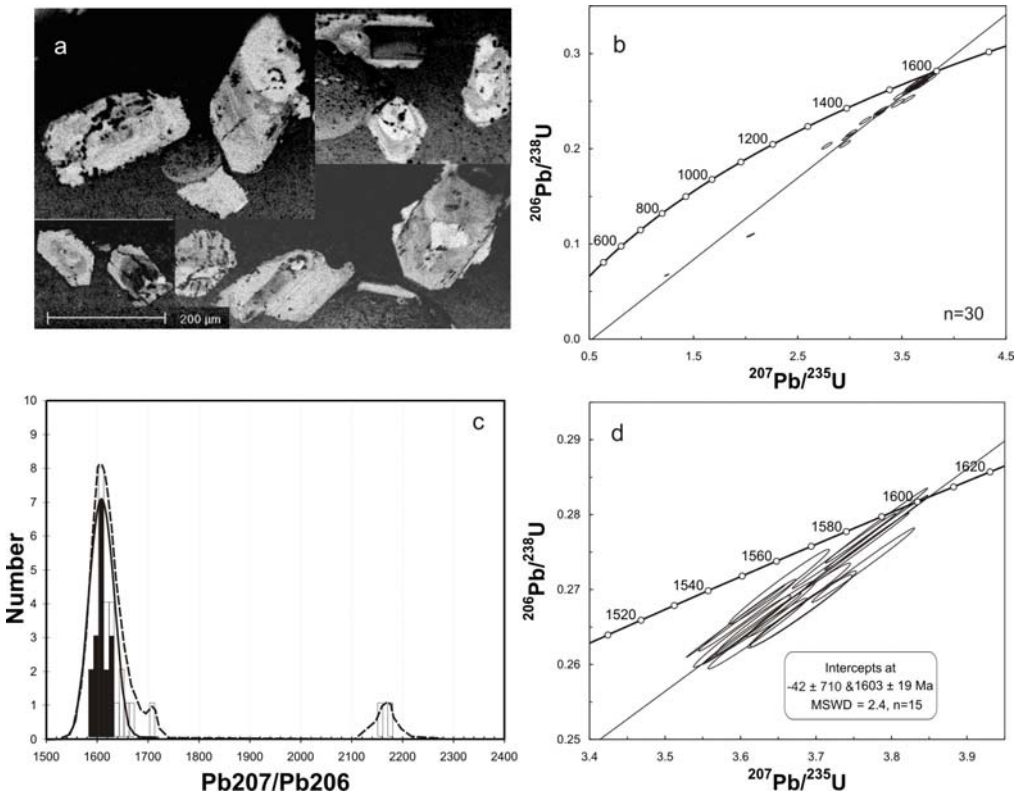

Figure 4.2 The U-Pb zircon age results for the Pepegoona Volcanics. a) CL image of Pepegoona zircons showing euhedral and overgrowth zoning. b) Concordia diagram for all zircon analyses, c) Probability plot of 207Pb/206Pb age; solid histogram for concordant zircon and no fill histogram for all analyses (n=30), d) U-Pb concordia plot of zircons from MN003 showing an intercept age for magma crystallization age of 1603 ±19 Ma

4.1.2 Mt Neill Granite

Sample MN029 from the Mt Neill granite was selected for U-Pb zircon dating. The zircons range in size from 100 to 300 μm and have length-to-width ratios of 2:1 to 4:1. The crystals are commonly euhedral and often show broken grains with dark patches resulted from post-metamorphism and post-alteration (1575-15600 Ma; Srewart and Foden, 2001). They are pale yellow to colourless and contain very rare xenocryst cores. The CL image clearly shows oscillatory growth zoning typical of magmatic zircons (Figure 4.3a). Mt Neill granite zircons contain U concentration between 178 and 3175 ppm and Th concentration between 69 and 1210 ppm and have Th//U ratios from 0.3 to 0.5.

All thirty-nine zircon U-Pb age analysis from Mt Neill granites have less than 10% discordance and have $^{207}Pb/^{206}Pb$ ages ranging from 1549.7 to 1718.6 Ma (Figure 4.3b). Figure 4.3c presents a frequency histogram of the age distribution for Mt Neill Granite zircons. The calculated concordia age of Mt Neill granite zircons (n=20: exclude discordant zircons) is 1590±5 Ma (MSWD = 1.6; Figure 4.3d), which excludes discondant zircons.

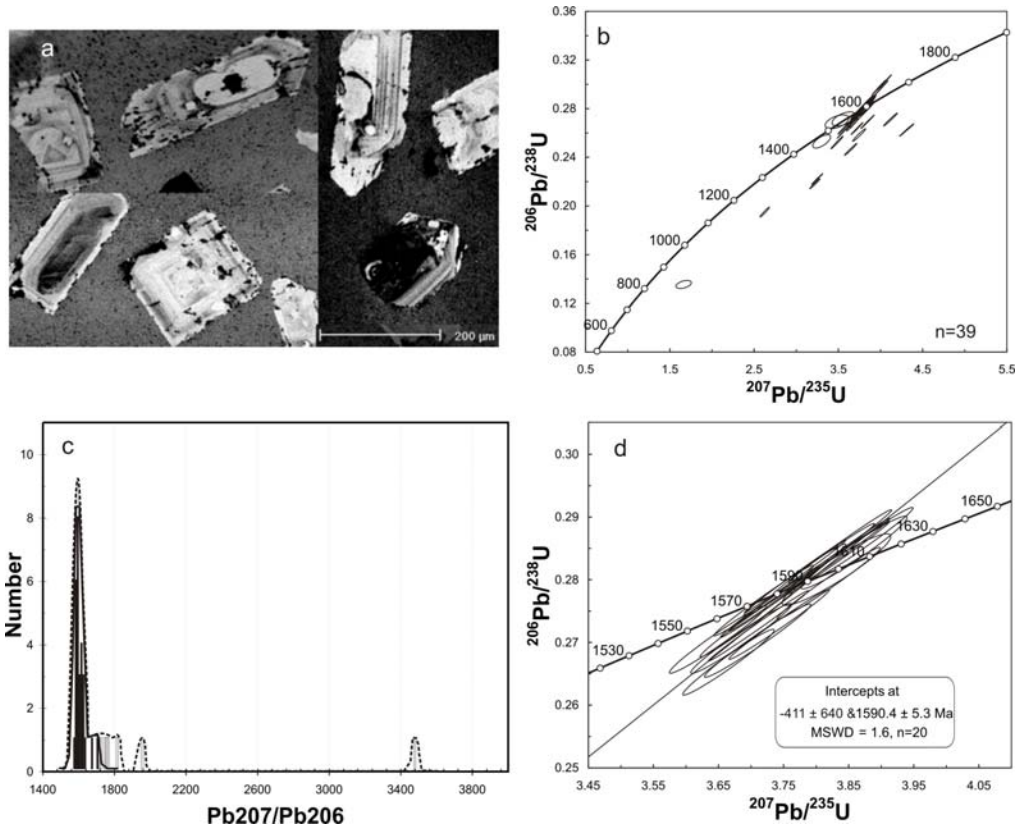

Figure 4.3 Result of U-Pb zircon age from MN029 (Mt Neill granite); a) CL image of Mt Neill granitic zircons showing euhedral and overgrowth zoning, b) Concordia diagram for all zircon analyses, c) Probability plot of $^{207}Pb/^{206}Pb$ age; solid histogram for concordant zircon and no fill histogram for all analyses (n=39), d) U-Pb concordia plot of zircons from MN003 showing an intercept age for magma crystallization age of 1590 ±5.3 Ma.

4.1.3 Box Bore Granite

Zircons from the strongly deformed Box Bore granite were separated from sample SD015. The zircons are between 150 to 500 µm in size with length-to-width ratios of 2:1 to 3:1 (Figure 4.4a). Most zircons are pale yellow, pale brown to colourless and euhedral to subhedral. They contain rare xenocrystic cores. CL images display low luminescence and oscillatory

zoning patterns. The zircons often show the effects of metamorphism and alteration. They contain very high U and Th contents with the U concentration between 1283 to 4193 ppm and Th concentration between 502 and 1972 ppm (Th/U ratio range between 0.4 and 1.8).

Thirty zircons were analysed to calculate the U-Pb age. Only twelve zircons are less than 10% discordant and their $^{207}Pb/^{206}Pb$ ages range from 1538 to 1608 Ma. Zircons that are more than 10% discordant yield ages scattered between 1389.3 and 2373.6 Ma (Figure 4.4b). The shaded bar and solid line in Figure 4.4c represent U-Pb ages of Box Bore granite zircons with less than 10% discordance and the dashed histogram line displays all analysed data. The calculated concordia age of sixteen zircons excluding discordant zircons from Box Bore granite yield an age of 1586 ±45Ma (MSWD=16; Figure 4.4d).

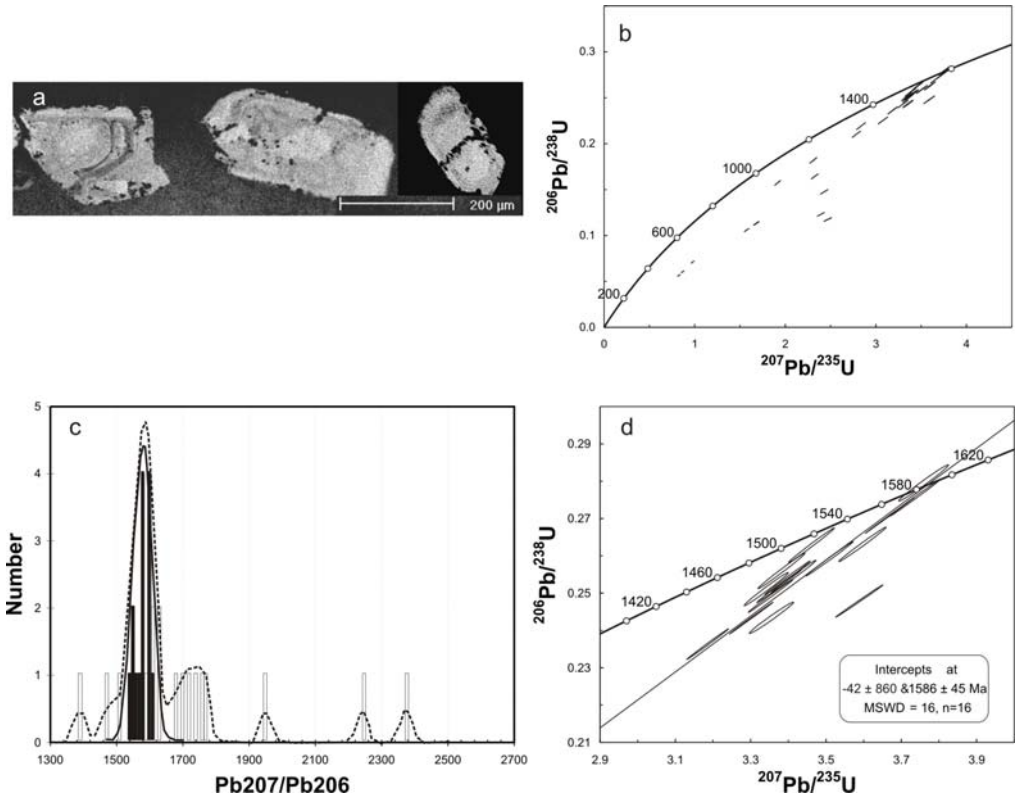

Figure 4.4 U-Pb zircon age of Box Bore granite from SD015. a) CL image of zircons from Box Bore granite, b) Concordia diagram for all zircon analyses (n=30), c) Probability plot of $^{207}Pb/^{206}Pb$ age; solid histogram for concordant zircon and no fill histogram for all analyses (n=30), d) U-Pb concordia plot of zircons from MN003 showing an intercept age for magma crystallization age of 1586±45 Ma.

4.1.4 Terapinna Granite

Sample MN101 from the Terrapinna granite was selected for U-Pb zircon dating. The length of zircons typically ranges from 100 to 200 μm and their length-to-width ratios from 1:1 up to 3:1 (Figure 4.5a). They are anhedral to euhedral and some show well-formed pyramidal terminations. Anhedral zircons commonly contain xenocrystic cores suggesting mixing of older with younger zircons. The CL images display oscillatory zoning patterns within euhedral zircons and overgrowth rims on anhedral zircons. In transmitted light, the zircons are typically colourless. Most zircons exhibit secondary minerals on their surface resulting from metamorphism and/or hydrothermal alteration. Terrapinna Granite zircons have Th contents ranging between 187 and 1696 ppm and U content ranging between 1014 and 6508 ppm with Th/U ranging between 0.2 and 0.7.

Analyses of fifty-one single zircons from Terrapinna granite show most zircons are discordant giving a wide $^{207}Pb/^{206}Pb$ age ranges from 1513 to 4212 Ma (Figure 4.5b). Only nineteen spots are less than 10% discordant and most zircons yield $^{207}Pb/^{206}Pb$ ages within the Mesoproterozoic period. However, three concordant zircons (exclude discordant zircons) give significantly older ages of 1893, 2319 and 2702 Ma. Sixteen concordant zircons give a weighted average age of 1569±20 Ma (Figure 4.5c). These sixteen analyses were used to calculate a concordia age of the Terrapinna Granite of 1569±22 Ma (MSWD=4; Figure 4.5d).

4.1.5 Wattleowie Granite

Sample SD022 from the Wattleowie Granite was selected for zircon age dating. These zircons are commonly between 100 and 500 μm in size (average size of 200 μm) with the length-to-width ratios are between 1:1 and 4:1. They are pale yellow to colourless and euherdral to subhedral with poor-developed prismatic crystals. Most zircons display oscillatory growth zoning and some clearly show xenocrystic cores mantled by younger zircon (Figure 4.6a).

Forty analyses of Wattleowie granite zircons were conducted and plotted in Isoplot (Figure 4.6b) with only fifteen spots being less than 10% discordant. The shaded bar and solid line in Figure 4.6c represent U-Pb ages of Wattleowie Granite zircons with less than 10% discordance and the dashed histogram line displays all analysed data. Most crystals give concordia ages (exclude discordant zircons) in range 1503 to 1590 Ma but three concordant analyses from inherited cores give significantly older $^{206}Pb/^{207}Pb$ ages of 2411, 1720 and 1649 Ma (Figure 4.6c). The calculated concordia age of none-xenocrystic zircons from the Wattleowie Granite is 1562±7 Ma (MSWD=20; Figure 4.6d).

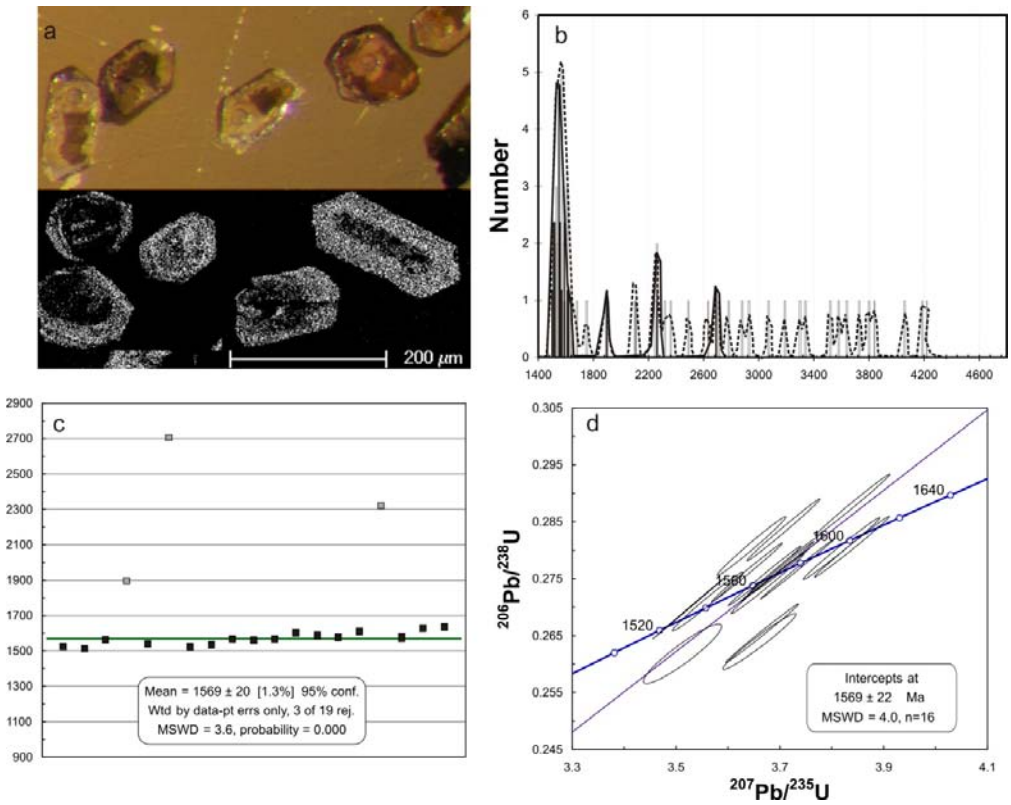

Figure 4.5 U-Pb zircon age of Terrapinna granite (MN101). a) Photograph and CL image of zircons from Terrapinna granite, b) Probability plot of $^{207}Pb/^{206}Pb$ age; solid histogram for concordant zircon and no fill histogram for all analyses (n=51), c) Weight average of $^{207}Pb/^{206}Pb$ age at 1569±20 Ma, d) U-Pb concordia diagram of MN101 zircons showing an intercept age for magma crystallization age of 1569±22 Ma.

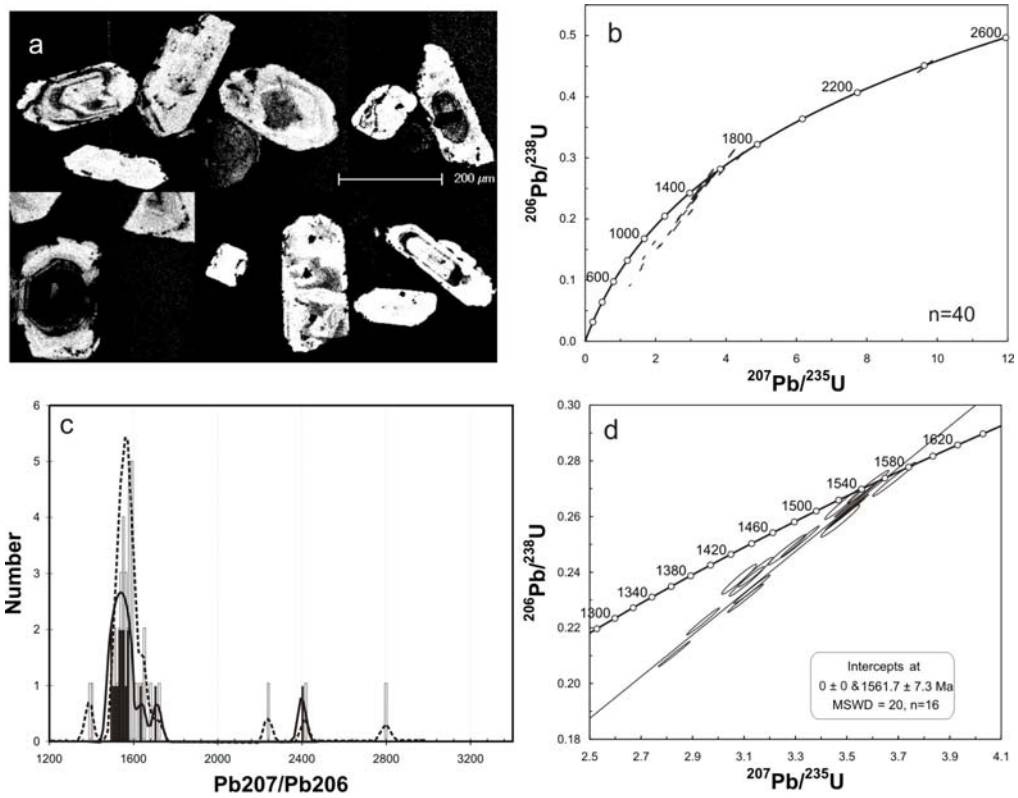

Figure 4.6 The U-Pb zircon dating of Wattleowie granite (SD022). a) Cl image of zircons from sample SD022, b) Concordia diagram for all zircon analyses (n=40), c) Probability plot of $^{207}Pb/^{206}Pb$ age; solid histogram for concordant zircon and no fill histogram for all analyses (n=40), d) U-Pb concordia plot of zircons from Wattleowie granite showing an intercept age for magma crystallization age of 1562±7 Ma.

4.1.6 Yerila Granite

Zircons for the Yerila Granite were separated from Sample SD060. The zircons range in length from 50 to 250 μm with length-to-width ratios of 1:1 to 4:1 (Figure 4.7a). They are typically pale brown to colourless and subhedral to euhedral. The subhedral zircons often contain xenocrystic cores. Euhedral zircons display oscillatory growth zoning. Most zircons contain Th-U enriched minerals (detail in Chapter 5) and/or recrystallised texture. Zircons are highly enriched in U and Th. They have U concentrations ranging from 1503 to 23289 ppm and Th ranging from 4012 to 12581 ppm with Th/U ratios ranging from 0.3 to 6.1.

Twenty nine zircons were analysed and yielded $^{206}Pb/^{207}Pb$ ages between 1503 and 1729 Ma (Figure 4.7b). However, only seventeen zircons are less than 10% discordant. The shaded bar and solid line in Figure 20c represent U-Pb ages of Yerila zircons with less than 10% discordance and the

dashed histogram line displays all analysed data. The calculated concordia age of ten zircons (exclude discordant zircons) from Yerila granite shows the upper intercept age of 1556 ± 20 Ma (MSWD=1.2; Figure 4.7d). The lower interception age at 990±200 Ma might reflect the time of metamorphism.

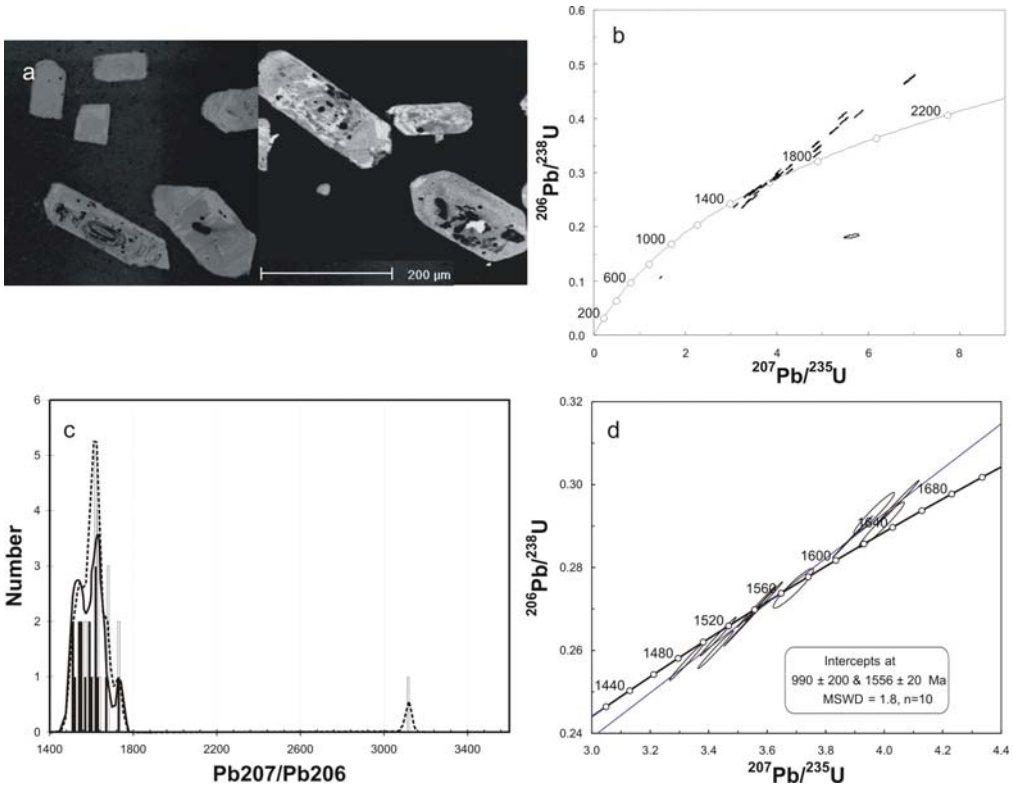

Figure 4.7 U-Pb zircon dating of Yerila granite (SD060). a) CL image of zircons from sample SD060, b) Concordia diagram for all zircon analyses (n=29), c) Probability plot of $^{207}Pb/^{206}Pb$ age; solid histogram for concordant zircon and no fill histogram for all analyses (n=29), d) U-Pb concordia plot of zircons from Yerila granite showing an intercept age for magma crystallization age of 1556±20 Ma and lower interception for Pb loss at 990±220 Ma.

4.1.7 Microgranular enclaves of Yerila Granita

Samples SD047, SD049, SD050 and SD065 are from microgranular enclaves within the Yerila Granite.

a) Mafic microgranular enclave

Zircons from mafic microgranular enclaves (Sample SD047 and SD050) are commonly 100 to 350 µm in size with an average of 200 µm. They are generally euhedral with length and width ratios of 2:1 to 5:1, are brown to pale yellow in colour and show oscillatory growth zoning. The zircons normally contain inclusions of U-Th minerals (Figure 4.8a) and recrystallization textures. They contain very high U and Th contents with U

content between 25269 and 36961 ppm and Th content between 5793 and 40738 ppm and the Th/U ratio average of 0.48.

Thirty-four spots on zircons from sample SD047 were analysed for U-Pb and most crystals give concordant ages except six spots showing greater than 10% discordance. Only one spot has an older age suggesting an inherited component. Figure 4.8b shows U-Pb concordia plot for all analyses. The shaded bar and solid line in Figure 4.8c represent U-Pb ages of zircons from mafic enclaves with less than 10% discordance and the dashed histogram line displays all analysed data. Concordant zircons from the mafic enclave give $^{206}Pb/^{207}Pb$ ages ranging between 1348 and 1549 Ma. The calculated concordia from sixteen spots (exclude discordant zircons) has an upper intercept age of 1529 ± 9 Ma (MSWD=1.9; Figure 3.8d) with a lower intercept age of 578±120 Ma suggesting Pb loss during the Delamerian Orogen.

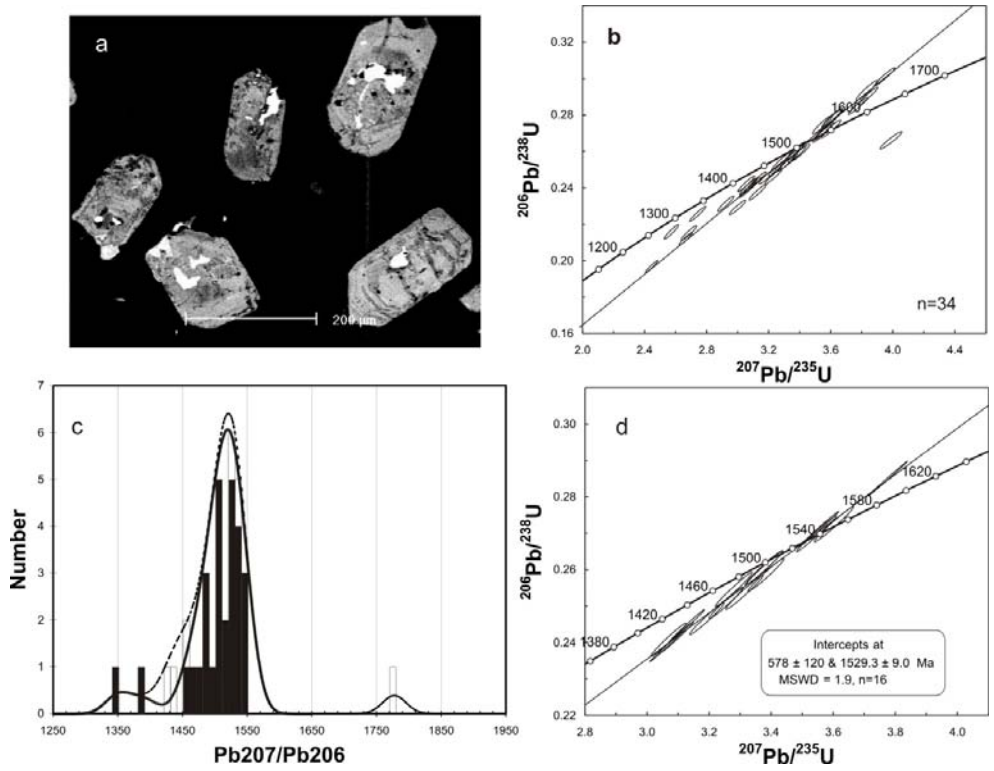

Figure 22 U-Pb zircon dating of mafic enclave (SD047). a) CL image of zircons from sample SD047 showing U-enriched mineral inclusion, b) Concordia diagram for all zircon analyses (n=34), c) Probability plot of $^{207}Pb/^{206}Pb$ age; solid histogram for concordant zircon and no fill histogram for all analyses (n=34), d) U-Pb concordia plot of zircons from the mafic enclave showing an intercept age for magma crystallization age of 1529±9 Ma.

Mafic enclave zircons from sample SD050 were analysed with 21 of 38 analysed spots being less than 10% discordant. Concordant zircon crystals (Figure 4.9a) yield $^{206}Pb/^{207}Pb$ ages ranging between 1406 and 1542 Ma (Figure 4.9b). The shaded bar and solid line in Figure 4.9c represent U-Pb ages with less than 10% discordance and the dashed histogram line displays all analysed data. The calculated concordia age from twenty-six spots (exclude discordant zircons) exhibits the upper intercept age of 1509 ± 17 Ma (MSWD=19; Figure 4.9d) with lower interception age of 439±99 Ma suggesting Pb loss during the Delamerian Orogen.

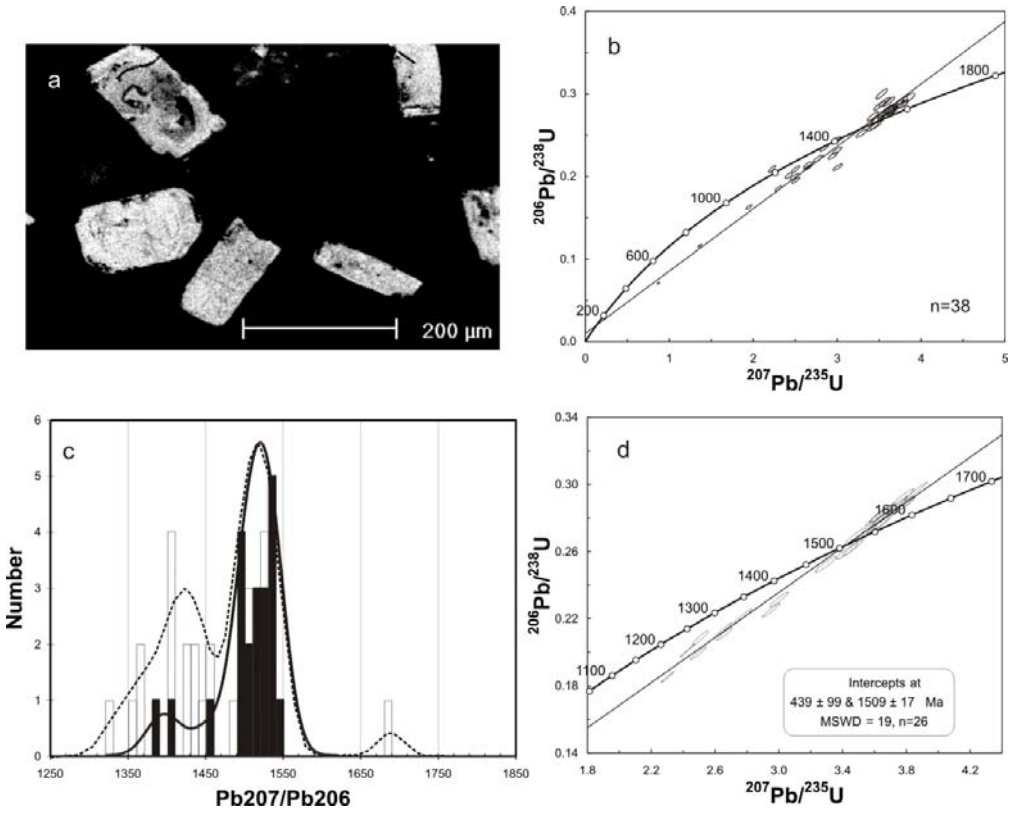

Figure 4.9 U-Pb zircon dating of mafic enclave (SD050). a) CL image of zircons from sample SD050, b) Concordia diagram for all zircon analyses, c) Probability plot of $^{207}Pb/^{206}Pb$ age; solid histogram for concordant zircon and no fill histogram for all analyses (n=38), d) U-Pb concordia plot of zircons from the mafic enclave showing an intercept age for magma crystallization age of 1509±17 Ma with lower interception age of 439±99 Ma.

Sample SD065 is from a mafic enclave within the Yerila granite and was collected from the northern Mt Babbage Inlier. The zircons are 50 to 100 μm in size. They are normally subhedral to euhrdral (Figure 4.10) with some showing xenocrystic cores and U-Th mineral inclusion. Most zircons from SD065 are discordant. Only three zircon grains are less than 10% discordance yielding $^{206}Pb/^{207}Pb$ age of 1557 to 1648 Ma. The shaded bar and solid line in Figure 4.11a represent U-Pb ages with less than 10% discordance and the dashed histogram line displays all analysed data. The calculated concordia age from eighteen spots (exclude discordant zircons) exhibits the upper intercept age of 1572 ± 27 Ma (MSWD=37; Figure 4.11b) with lower interception age of 0 Ma. All analyses plot away from concordia curve indicating Pb loss. Ages of SD065 mafic enclave zircons are significantly older than previous mafic enclave zircons (sample SD047 and SD050) but their ages overlap with the Yerila Granite.

Xenotime is found as overgrowth around zircons from this sample (Fig 4.12a) and yields and age around 1085 Ma (Figure 4.12b). This age could be related to the Paralana Granodiorite or a Musgravian magmatic event, which the Musgravian magmatic event ages ranging between 1086 and 1051 Ma suggested by Newmann (1996) and Paul (1998).

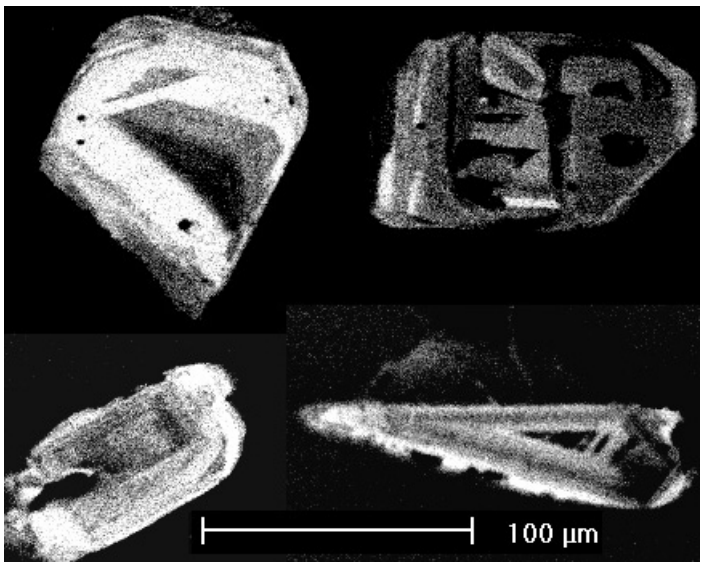

Figure 4.10 CL image of zircons from sample SD065 showing growth zoning.

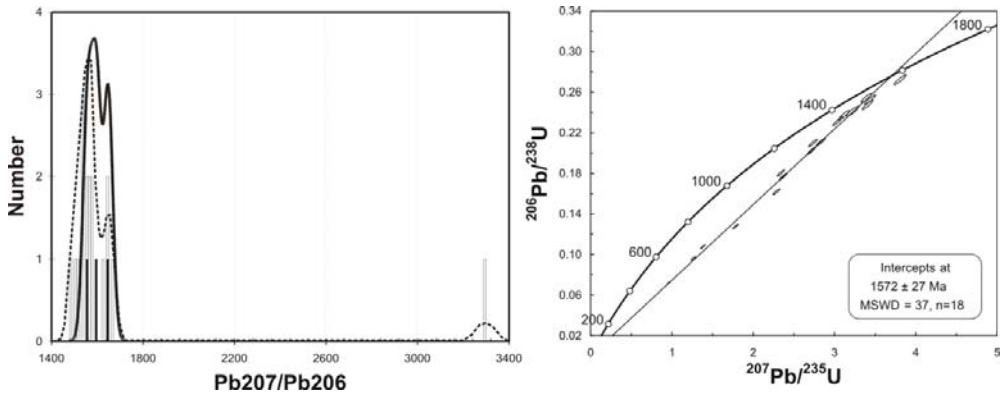

Figure 4.11 U-Pb zircon dating of mafic enclave (SD065). a) Probability plot of $^{207}Pb/^{206}Pb$ age; solid histogram for concordant zircon and no fill histogram for all analyses, b) U-Pb concordia plot of zircons from the mafic enclave showing an intercept age for magma crystallization age of 1572±27 Ma.

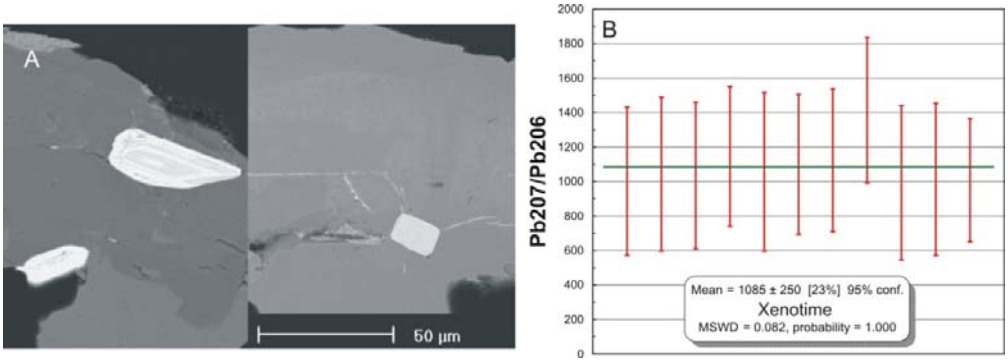

Figure 4.12 Xenotime from Sample SD065; a) BSE image of zircons within xenotime grains from sample SD065, b) Weight average of $^{206}Pb/^{207}Pb$ age of xenotime.

b) Felsic microgranular enclave

Zircons from the felsic microgranular enclave (SD049) are rare and smaller in size than zircons from the mafic enclaves. The size of felsic enclave zircons ranges between 50 and 250 µm with length and width ratios of 1:1 to 3:1. They are pale brown to colourless and euhedral to subhedral, often showing broken grains with U-Th mineral replacement (Figure 4.13a). These zircons contain high U and Th concentrations (U content between 8427 and 442942 ppm and Th content between 7113 and 225845 ppm).

Twenty-eight spots on felsic enclave zircons were analysed, however, only eight analyses are concordant (less than 10% discordant). Most zircons are affected by Pb loss and give $^{206}Pb/^{207}Pb$ age between 1775 to 1343 Ma (Figure 4.13b). The shaded bar and solid line in Figure 4.13c represent U-Pb ages with less than 10% discordance and the dashed histogram line displays

all analysed data. The calculated concordia age from sixteen spots (exclude discordant zircons) exhibits the upper intercept age of 1504 ±29Ma (Figure 4.13d).

The zircon morphology and U-Pb ages of the felsic and mafic enclaves are different. Felsic enclave zircons give significantly older ages that probably result from contamination by older zircons. In contrast, mafic enclave zircons have more magmatic zircon characteristics.

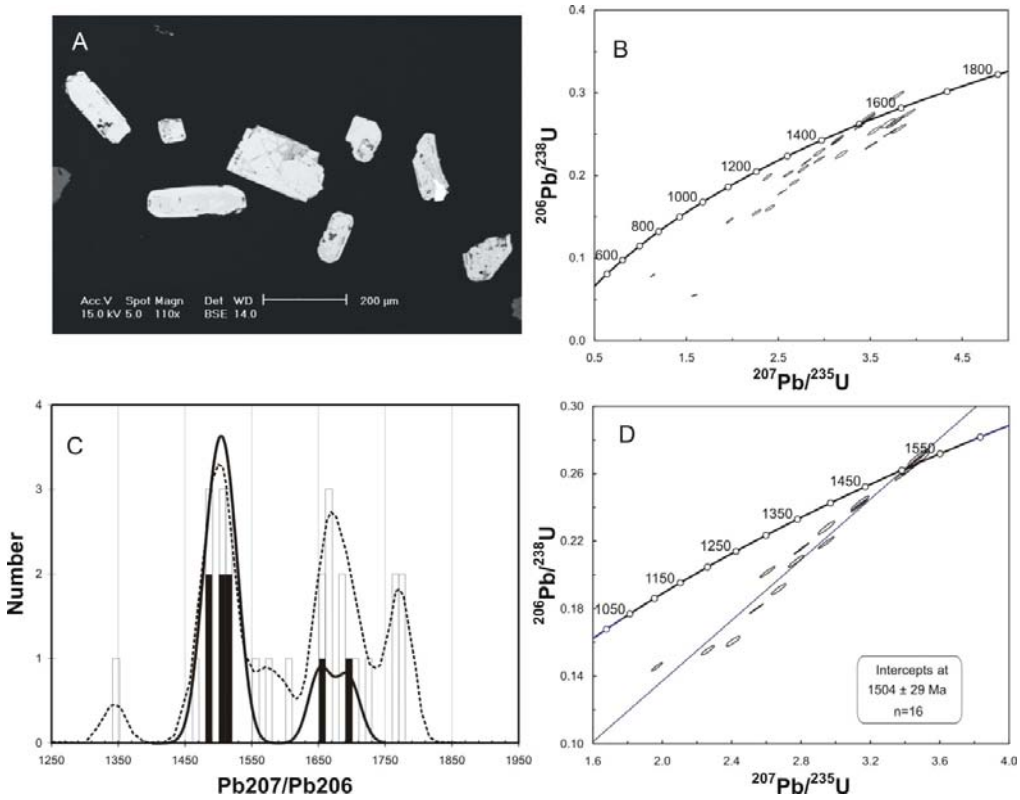

Figure 4.13 U-Pb zircon dating of felsic enclave (SD49). a) BSE image of zircons from sample SD049, b) Concordia diagram for all zircon analyses, c) Probability plot of $^{207}Pb/^{206}Pb$ age; solid histogram for concordant zircon and no fill histogram for all analyses, d) U-Pb concordia plot of zircons from the felsic enclave showing intercept age for magma crystallization age of 1504±29 Ma.

4.1.8 Mafic Dyke

Four samples from mafic dykes were selected for zircon dating; MN084, SD031, SD051 and SD057. Sample locations are shown in Figure 4.1.

a) MN084

A sample of mafic dyke (MN084) was collected from outcrop crosscutting the Mt Neill Granite and Pepegoona Volcanics. Zircons from this sample are pale purple and euhrdral to subhedral. Zircon grains range in size from 50 to 200 μm (Figure 4.14a). The large zircons are typically broken. Most zircons show oscillatory growth zoning with some subhedral zircons contain xenocrystic cores. The zircons have U contents between 488 and 674 ppm and Th contents between 125 and 210 ppm.

Twenty analyses on zircon crystals from sample MN084 were conducted and give $^{206}Pb/^{207}Pb$ ages between 1564 and 1696 Ma (Figure 4.14b). Four of the twenty analyses are inherited zircons (showing more than 10% discordance). Most concordant crystals give $^{206}Pb/^{207}Pb$ age ranging from 1558 to 1588 Ma but two analyses show older ages of 1615 and 1658 Ma that are interpreted to be inherited. The shaded bar and solid line in Figure 4.14c represent U-Pb ages with less than 10% discordance and the dashed histogram line displays all analysed data. The calculated concordia age from fifteen analyses (exclude discordant zircons) shows the upper intercept age of 1572±4 Ma (MSWD=22; Figure 4.14d).

b) SD031

Sample SD031, was collected from a mafic dyke cross-cutting the Terrapinna and Wattleowie granites in the northern Mt Babbage Inlier. The zircons from this sample are pale brown to colourless and 100 to 300 μm in size with length and width ratios of 1:1 to 3:1 (Figure 4.15a). They are mainly euhedral with minor subhedral zircons containing xenocrystic cores and clearly present oscillatory growth zone. Cracks and healed cracks from metamorphism and alteration are common. U-Th minerals are also found as inclusion. U and Th contents are very high with U concentrations ranging from 30367 to 97359 ppm and Th concentrations ranging from 7047 and 2944 ppm. The Th/U ratio of the zircon is ~0.2 to 0.3.

Forty-three analyses on zircon crystals from sample SD031 were conducted and provided $^{206}Pb/^{207}Pb$ ages ranging between 1523 and 1848 Ma (Figure 4.15b). Thirty analysed spots are less than 10% discordant and have $^{206}Pb/^{207}Pb$ ages in the range 1523 to 1638 Ma. The shaded bar and solid line in Figure 4.15c represent U-Pb ages with less than 10% discordance and the

dashed histogram line displays all analysed data. The concordia age from twenty four analysed spots (exclude discordant zircons) shows the upper intercept age of 1557±4 Ma (MSWD=1.01; Figure 4.15d). Some zircons crystals that contain xenocrystic cores give older $^{206}Pb/^{207}Pb$ ages than those with oscillatory growth zoning and no inherited zircon cores (Figure 4.16).

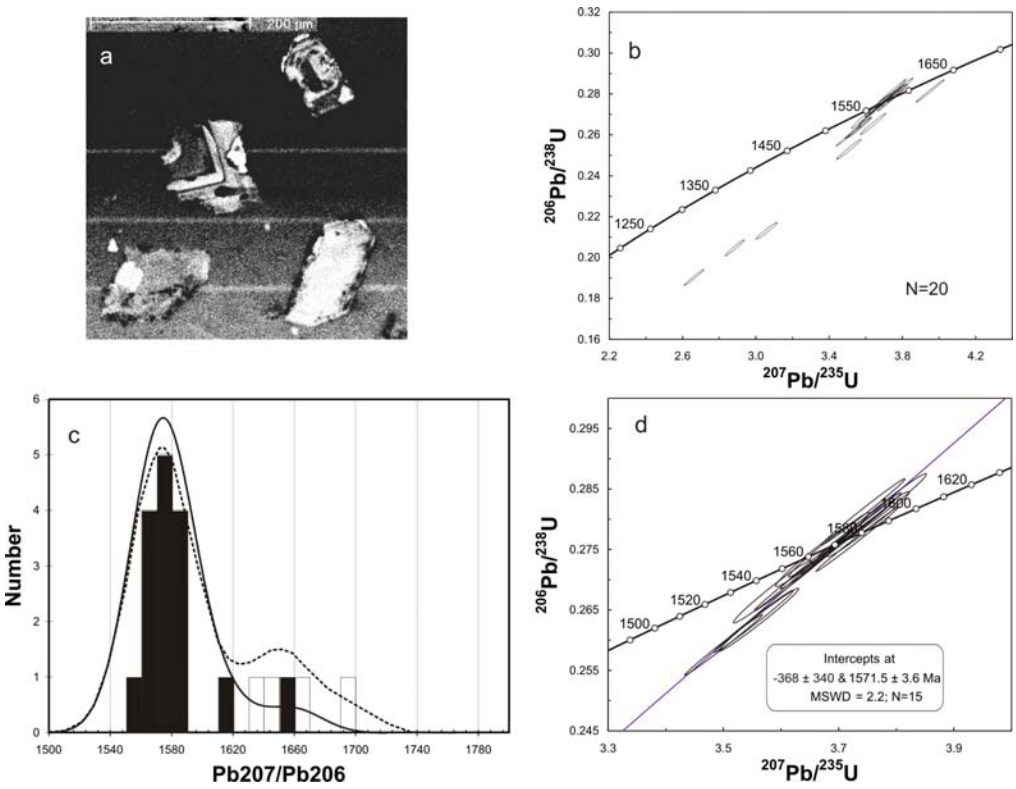

Figure 4.14 U-Pb zircon dating of mafic dyke (MN084) intruding Mt Neill granite; a) CL image of zircons from sample MN084, b) Concordia diagram for all zircon analyses, c) Probability plot of $^{207}Pb/^{206}Pb$ age; solid histogram for concordant zircon and no fill histogram for all analyses (n=20), d) U-Pb concordia plot of zircons from the mafic dyke showing an intercept age for magma crystallization age of 1572±4 Ma.

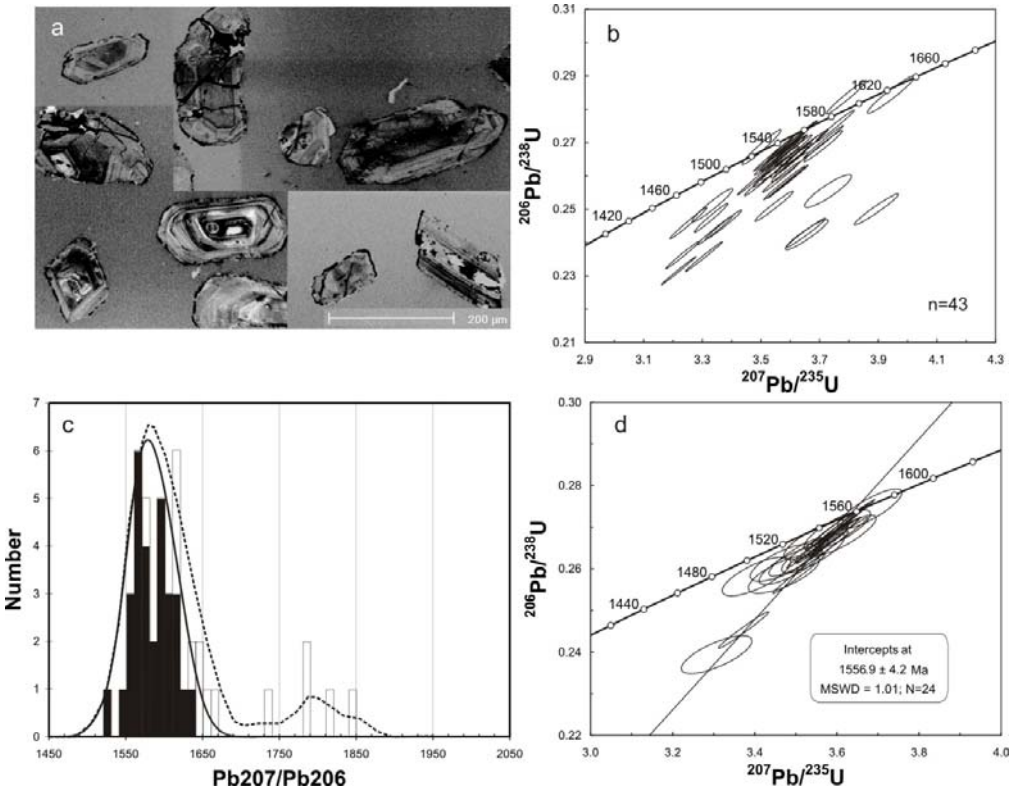

Figure 4.15 U-Pb zircon dating of mafic dyke (SD031) intruding Terrapinna and Wattleowie granites; a) CL image of zircons from sample SD031, b) Concordia diagram for all zircon analyses, c) Probability plot of $^{207}Pb/^{206}Pb$ age; solid histogram for concordant zircon and no fill histogram for all analyses (n=43), d) U-Pb concordia plot of zircons from the mafic dyke showing an intercept age for magma crystallization age of 1557±4 Ma.

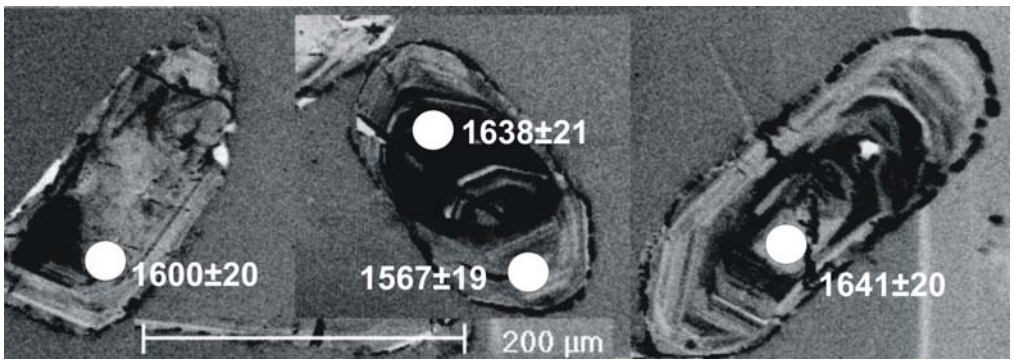

Figure 4.16 CL image of inherited zircons and the $^{207}Pb/^{206}Pb$ age on the zircon xenocrystic core and rim.

c) SD051

Zircons from Sample SD051 were collected from a mafic dyke crosscutting the gneissic Terrapinna Granite. They are pale brown to colourless and subhedral, ranging in size from100 to 500 µm in size and showing broken grains (Figure 4.17). Growth zoning is rarely preserved. They have high concentration of U and Th with U between 6107 and 175512 ppm

and Th content between 5897 and 189525 ppm and the Th/U ration ranges from 0.6 to 2.2.

The zircon ages for this sample are widely spread. Most analyses indicate strongly discordant zircons; however, five of forty zircon U-Pb age analyses have less than 10% discordance. Those zircon crystals yield $^{206}Pb/^{207}Pb$ age from 795 to 854 Ma. The shaded bar and solid line in Figure 4.18a represent U-Pb ages with less than 10% discordance and the dashed histogram line displays all analysed data. The concordia age from twenty four analysed spots (exclude discordant zircons) shows the upper intercept age of 800±29Ma (Figure 4.18b).

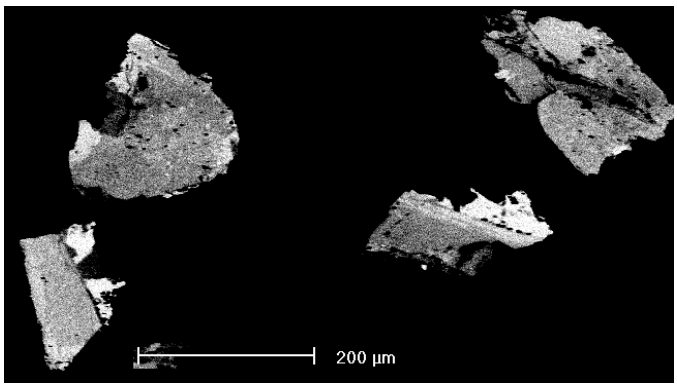

Figure 4.17 CL image of mafic dyke zircons from sample SD051

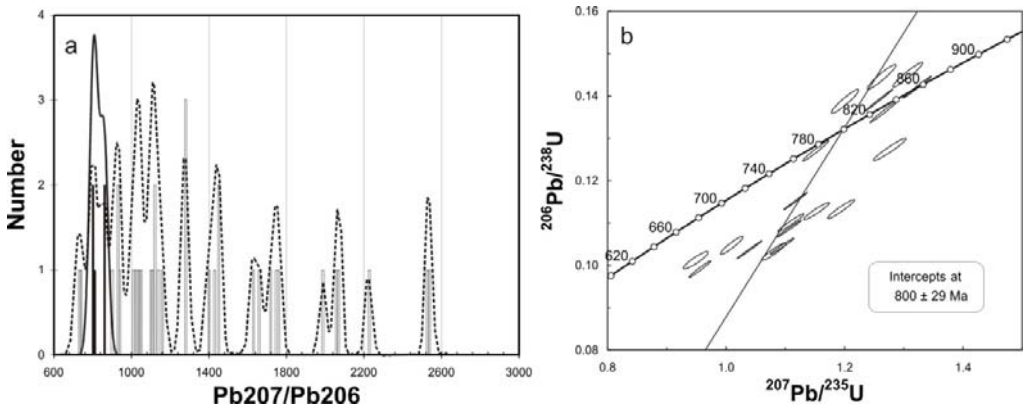

Figure 4.18 U-Pb zircon dating of mafic dyke (SD051) crosscutting Terrapinna granite; a) Probability plot of $^{207}Pb/^{206}Pb$ age; solid histogram for concordant zircon and no fill histogram for all analyses (n=40), b) U-Pb concordia plot of zircons (n=20) from the mafic dyke showing an intercept age for magma crystallization age of 800±29 Ma.

d) SD057

Sample SD057 is from a mafic dyke crosscutting the Yerila Granite at Birthday Well (Figure 4.1). Zircons from SD057 are pale brown and euhedral. They are 100 to 150 µm in size with length and width ratios of 2:1 to 3:1 and

are typically free of xenocrystic cores. U-Th mineral inclusions and dark patches resulted from metamorphism and alteration are common. U and Th concentrations of these zircons range from 2098 to 14858 ppm for U and 418 to 1804 ppm. The Th/U ratio is 0.1 to 2.2 with average of 0.9.

Twenty-eight zircon crystals from sample SD057 were analysed, giving $^{206}Pb/^{207}Pb$ ages between 1425 and 1526 Ma (Figure 4.19a). The shaded bar and solid line in Figure 4.19b represent U-Pb ages with less than 10% discordance and the dashed histogram line displays all analysed data. Twenty-three analyses are concordant (less than 10% discordant) and mostly yield $^{206}Pb/^{207}Pb$ age average weight of 1511±17 (Figure 4.19c). The concordia age from sixteen analysed spots (exclude discordant zircons) shows the upper intercept age of 1515±7 Ma (MSWD=1.7; Figure 4.19d) with lower interception of 337±96 Ma.

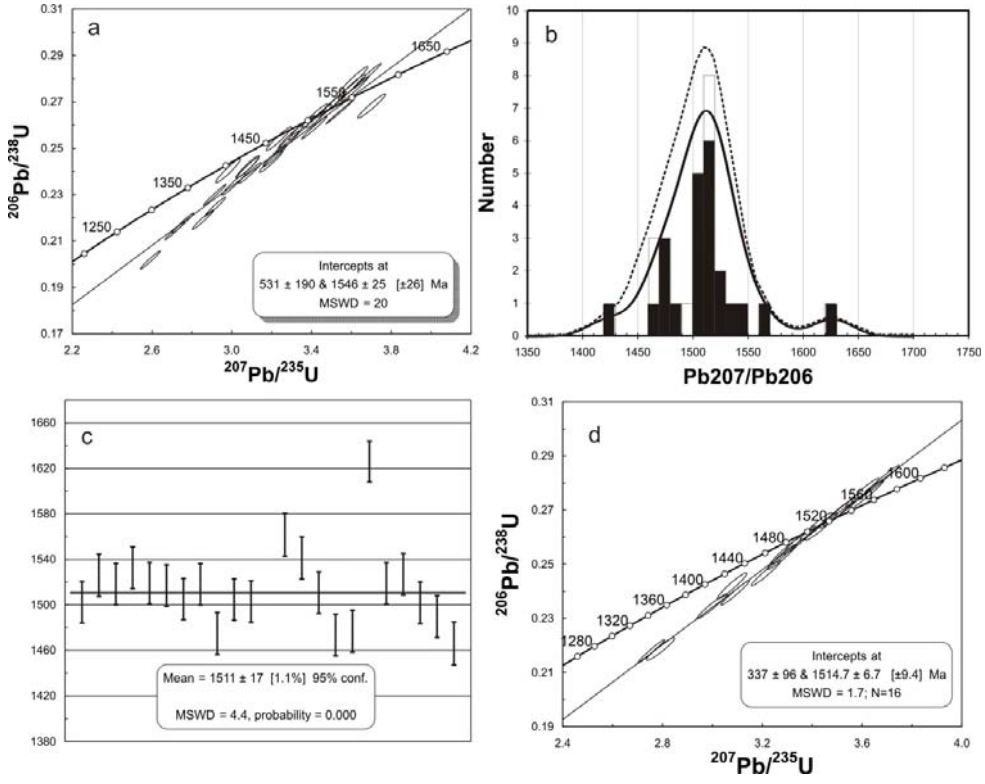

Figure 4.19 U-Pb zircon dating of mafic dyke (SD057) intruding Yerila granite; a) Concordia diagram for all zircon analyses, b) Probability plot of $^{207}Pb/^{206}Pb$ age; solid histogram for concordant zircon and no fill histogram for all analyses, c) Weighted average of $^{207}Pb/^{206}Pb$ age of SD057 zircons, d) U-Pb concordia plot of zircons from the mafic dyke showing intercept age for magma crystallization age of 1514±7 Ma and the lower interception age of 337±96 Ma.

4.2 Discussion

4.2.1 Crystallization age of the Mt Painter Province felsic and mafic igneous rocks

The U-Pb age of magmatic zircons provide important data to unravel the magmatic crystallization history of the Mt Painter Province magmatic rocks. The results of this study together with previous studies (Table 4.1) confirm that the volcanic and granitic rocks (including Pepegoona Volcanic, Mt Neill, Box Bore, Terpainna, Wattleowie and Yerila Granites) in the Mt Painter Inlier were emplaced during the Mesoproterozoic. However, the results indicate that the Mt Painter Province magmatic emplacement sequence took place over a period of approximately 100 Myr from 1603 to 1504 Ma. This time period of magmatic activity is more extensive than previous reports. Moreover, microgranular enclaves and mafic dykes were also emplaced during the Mt Painter Province felsic igneous activity.

The oldest Mesoproterozic igneous rocks of the Mt Painter Province are the Pepegoona Volcanics which yield a crystallization age of 1604±19 Ma. These volcanics normally occur together associated with the Mt Neill Granite which has a slightly younger crystallization age of 1590±5 Ma. The age of the Mt Neill Granite from this study suggests that the granite was emplaced earlier than previous study reported (Table 4.1). The overlap of ages between the Pepegoona Volcanics and the Mt Neill Granite together with field evidence (detail in Chapter 2) are interpreted to indicate that they formed during the same magmatic event, the first in the area.

Previously, the Box Bore Granite had a reported crystallization age of 1555±15 Ma (Teale, 1995). In this study, the U-Pb zircon age of the Box Bore Granite yielded an age of 1586±45 Ma which is within error of the age of Teale (1995). However, some analyses suggest that the Box Bore granite contains inherited zircons. These may have been inherited from the Pepegoona Volcanics and the Mt Neill Granite. Zircon U-Pb dating of the Terrapinna Granite yields an age of 1569±22 Ma which is slightly older than previously reported (1557±6 Ma; Sheard et al, 1992; Teale, 1995), although within error. Concordant zircons from the co-magmatic Wattleowie Granite have a magmatic crystallization age of 1562±7 Ma, which overlaps the age of

1557±6 Ma reported by Sheard et al. (1992). The crystallization age of the Yerila Granite from this study is 1556±20 Ma which is the same as the age of 1556±6 Ma reported by Johnson (1980). The Box Bore, Terrapinna, Wattleowie and Yerila Granites are interpreted to have formed from the second magmatic event, shortly after the Pepegoona Volcanics and Mt Neill Granite magmatic event.

U-Pb ages from zircons from the microgranular enclaves within the Yerila Granite yield magma crystallization ages of 1529±9 Ma (mafic enclave-SD047), 1509±17 Ma (mafic enclave-SD050), 1572±27 Ma (mafic enclave-SD065) and 1504±29 Ma (felsic enclave-SD049). Some analyses of enclave zircons are within error of Yerila zircons. This may be evidence for magma mingling between a felsic magma and more mafic magma. However, some microgranular enclves have significantly younger crystallization ages than the Yerila Granite; these enclaves could be later intrusions (e.g. lamprophyre dyke).

Some mafic dykes crosscutting Mesopreoterozic felsic igneous rocks in the Mt Painter Province contain zircons which are appropriate for U-Pb age analyses. Sample MN084, an andesite dyke crosscutting the Mt Neill Granite, contains magmatic zircons that yield a magma crystallization age of 1571±4 Ma. The mafic dyke from which sample SD031 crosscuts the co-magmatic Terapinna and Wattleowie granites contains abundant zircons that yield a crystallization age of 1557±4 Ma. Sample SD057, andesitic basalt, collected from a mafic dyke that crosscuts the Yerila granite. Zircons for this sample yield an age of 1515±7 Ma which is similar to a microgranular enclave age. Sample SD051 from a mafic dyke crosscutting the Terrapinna Granite yields a U-Pb zircon age of 800±29 Ma. The Neoproterozoic volcanic age of sample SD051 could be related to the Wooltana volcanic event or the Gairdner Dyke Swarm which occurs at 827±6 Ma (Wingate et al., 1998). Most mafic dykes age from this study indicate overlapping ages or slightly younger ages comparing to felsic igneous rocks.

4.2.2 Difficulty of the Mt Painter Province zircon dating

The U-Pb zircon age analyses in this study are comparable to previous work geochronological studies of the Mt Painter Province which used

SHRIMP and LA-ICPMS. However there are some difficulties in interpreting the geochronological data resulting from a number of processes including; igneous and metamorphic overgrowths, inheritance, annealing after radioactive damage, hydrothermal precipitation and dissolution (Bomparola et al., 2006). Moreover, LA-ICPMS analyses for U-Pb zircon age calculations may not be sufficiently precise to differentiate short time intervals within individual magmatic intrusions (Kosler and Sylvester, 2003).

Many zircons of the Mt Painter Province igneous rocks in this study clearly contain inherited zircons and juvenile-magmatic zircons. Most igneous zircons typically display subhedral to euhedral crystals, oscillatory zoning, Ce and Eu anomalies in the REE patterns, and Th/U ratios >0.3. Detailed analyses of zircon compositions are given in Chapter 3. Metamorphic zircons are typically anhedral, show as low-luminescence with xenocrystic cores and have low Th/U ratios, and could be differentiated from igneous zircons by using CL and BSE imaging. However, the small size of zircons together with the size of the laser spot and depth of analysis (analysis pit size of about 35 and 60 μm; width and depth, respectively) could cause laser ablating into different growth zones. Inherited zircons with high percentage of discordance are common in this study and could lead to the misinterpretation of magma crystallization ages. The inherited zircons and contamination by older zircons indicate that the Mt Painter Province magmas contained older age zircons. Some older zircons have been reset and overgrown during the Mesoproterozoic magmatic event. The Terrapinna and Wattleowie granites contain xenocrystic older zircons yielding U-Pb ages of 1.7, 1.9, 2.4 and 2.7 Ga, strongly suggesting that basement of the the Mt Painter Province consists of older, possibly Archaean basement. Although, there is only pre-Neoproterozoic evolution reported in the the Mt Painter Province area, the age ranges of the older zircons from this study work could indicate that these zircons may have formed in the Sleafordian Orogeny (2450 Ma; Fraser et al., 2010), the Kimban Orogeny (1740-1690 Ma; Hand et al., 2007) and rift related magmatism of the Willyama supergroup (1700-1720 Ma; Paul, 1998).

There are explanations for the discordance seen in many of the zircons analysed in this study; Pb loss by diffusion has disturbed the U-Pb systematic of zircons; mixing of zircon population more than one age; and single zircon

experience overgrowth zoning many times (Hanchar and Miller, 1993 and references therein; Lee et al., 1997). In addition, a few zircons from this study could reflect anatexis, during which zircons usually grow in a dissolution precipitation-recrystallization process presenting wider and sparser oscillatory zoning (Wang et al, 2006). The lower intercept from the concordia age calculation could suggest ages of thermal metamorphism. The zircons generally have high U and Th concentrations that could cause annealing due to the alpha decay particle of U and Th (metamict) which decreasing with age. Furthermore, radiation damage could open fractures causing Pb gain.

Previous studies have shown that the Mt Painter Province area experienced at least one Neoproterozoic thermal event and two Palaeozoic thermal events; the intrusion of the Gairdner Dyke Swarm on the Stuart Shelf at 827±6 Ma (Wingate et al., 1998) and extrusion of the Wooltana Volcanics at ~820 Ma (Crawford and Hilyard, 1990) , the Delamerian Orogeny (520-490 Ma; Foden et al., 1999) and a thermal event marked by the intrusion of the British Empire Granite in the Ordovician, which has been linked to the Alice Springs Orogeny (Elburg et al., 2003). Neoproterozoic magmatic activity (~800 Ma) may have been related to a mantle plume with the high temperatures involved in such an event possibly disturbing the U-Pb systematic of some zircons.

In this study, the lower interception ages are around the ages of the Wooltana and Gairdner volcanic activity and the Delamarian Orogeny and British Empire Granite. All of these events may have caused U remobilisation resetting the U-Pb system in monazite and Pb loss (Elburg et al, 2003).

4.3 Summary

Based on the U-Pb zircon ages presented in this study, the mafic and felsic magma evolution of the Mt Painter Province occurred during the Mesoproterozoic era between ~1603 and ~1504 Ma. Table 4.1 summarises ages of different magmatic suites and Figure 5.20 shows the Mesoproterozic magmatic evolution form data of this study.

Table 4.1 Crystallization ages of mafic and felsic igneous rocks at Mt Painter Province

Suites	This Study		Previous Study	
	Sample	U-Pb age (Ma)	Age	Source
Pepegoona Volcanic	MN003	1603±19	1645 (Rb-Sr)	Compston et al. (1966)
Mt Neill Granite	MN029	1590±5	1569±14 (U-Pb)	Fanning et al. (1995)
Box Bore Granite	SD015	1586±45	1555±15 (U-Pb)	Teale et al. (1995)
Terrapinna Granite	MN101	1569±22	1556±4 (U-Pb)	Thornton (1980)
Watlleowie Granite	SD022	1562±7	1557±6 (U-Pb)	Sheard et al. (1992)
Yerila Granite	SD060	1556±20	1556±6 (U-Pb)	Johnson (1980)
Enclave	SD047	1529±9		
Enclave	SD049	1504±29		
Enclave	SD050	1509±17		
Enclave	SD065	1572±27		
Mafic Dyke	MN084	1571±4		
Mafic Dyke	SD031	1557±4		
Mafic Dyke	SD051	800±29		
Mafic Dyke	SD057	1515±7		

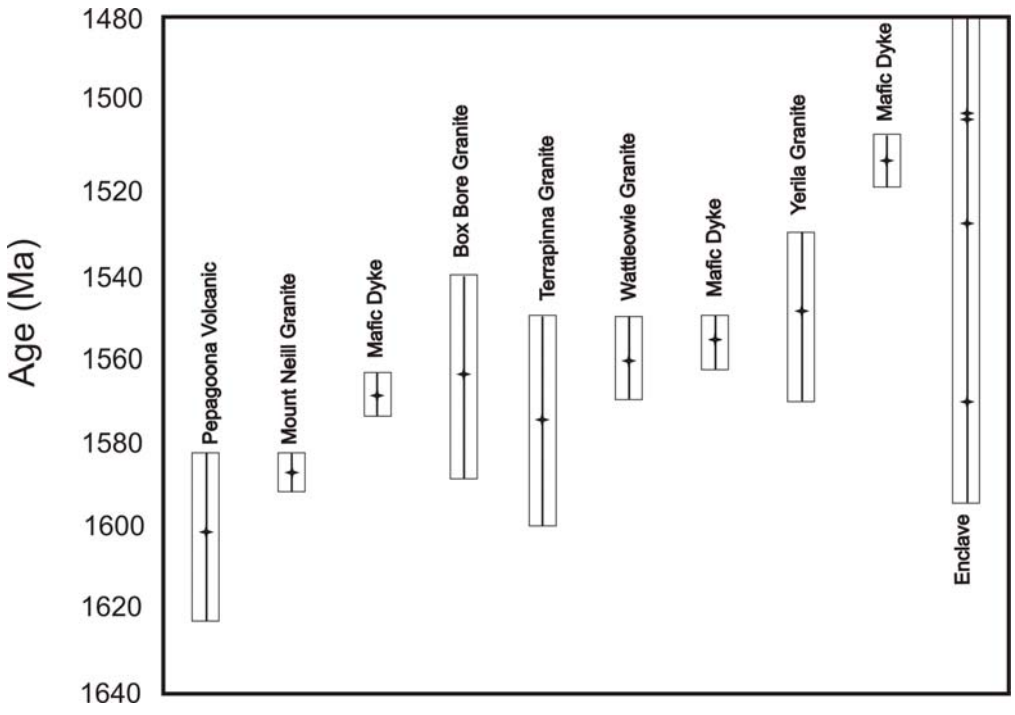

Figure 5.20 Magmatic evolutions of Mesoproterozoic mafic-felsic igneous rocks from Mt Painter Province.

Chapter 5 Geochemistry

Major and trace element geochemistry of felsic and mafic igneous rocks within the Mt Painter Province were analysed in this study. Interpretation and discussion of the geochemical characteristics of the Mt Painter mafic and felsic rock samples are supplemented with geochemical data from previous studies (Johnson, 1980; Neumann, 2001; Stewart and Foden, 2001). Detailed methodologies for the sample preparation and analyses are reported in Appendix 1.

The geochemical study aims to address the following issues:

a. Classification of the sampled rocks based on geochemical characteristics;
b. Differentiation between the different mafic and felsic units based on their geochemical characteristics and;
c. Development of petrogenetic models and interpretation of geological setting.

The classification and geochemical interpretation will be presented in two main groups according to the lithology and petrography presented in Chapter 2; that is felsic igneous rocks and mafic igneous rocks. Each group will be studied using major and trace element characteristics and demonstrated through several different diagrams which are used to interpret typology, source of magma and related processes of the felsic and mafic igneous rocks.

5.1 Result

5.1.1 Major elements

a) Felsic igneous rocks

Felsic igneous rocks include the Pepegoona Volcanics, Mt Neill, Box Bore, Terrapinna, Watlleowie and Yerila Granites, and microgranular enclaves of the Yerila Granite. SiO_2 of these felsic rocks varies widely between 67 and 80 wt% (Appendix 5). The Box Bore and Wattleowie

Granites are the most felsic among those suites. The Yerila Granite has the lowest average percentage of SiO_2 (average of 69 wt%).

The TAS (Total-alkali-silica) diagrams after Cox et al. (1989) are used for classifying granitic and volcanic samples. Granitic samples from this study mainly plot within the granite field in this TAS classification (Figure 5.1). The microgranular enclaves from the Yerila Granite plot within the granodiorite and diorite fields. The Pepegoona Volcanics are classified as rhyolite with four samples being dacite and trachydacite (Figure 5.2). Most samples of the Mt Painter Province are potassic in composition however a few samples from the Mt Neill and Yerila Granites show a sodic nature (Figure 5.3), which is as a result of Na-K metasomatic alteration between 1575-1560 Ma (Elburg et al., 2002). Some samples that have been affected by metamorphism and metasomatism are enriched in K_2O. These felsic igneous rocks have an Alumina Saturation Index (ASI) of between 1.07 and 1.38. The binary plot after Maniar and Picolli (1989) shows that the Mt Neill, Wattleowie and Terrapinna Granites and the Pepegoona Volcanics are peralumious, however, the Yerila and Box Bore Granites and the microgranular enclaves plot on the metaluminous and peraluminous boundary (Figure 5.4).

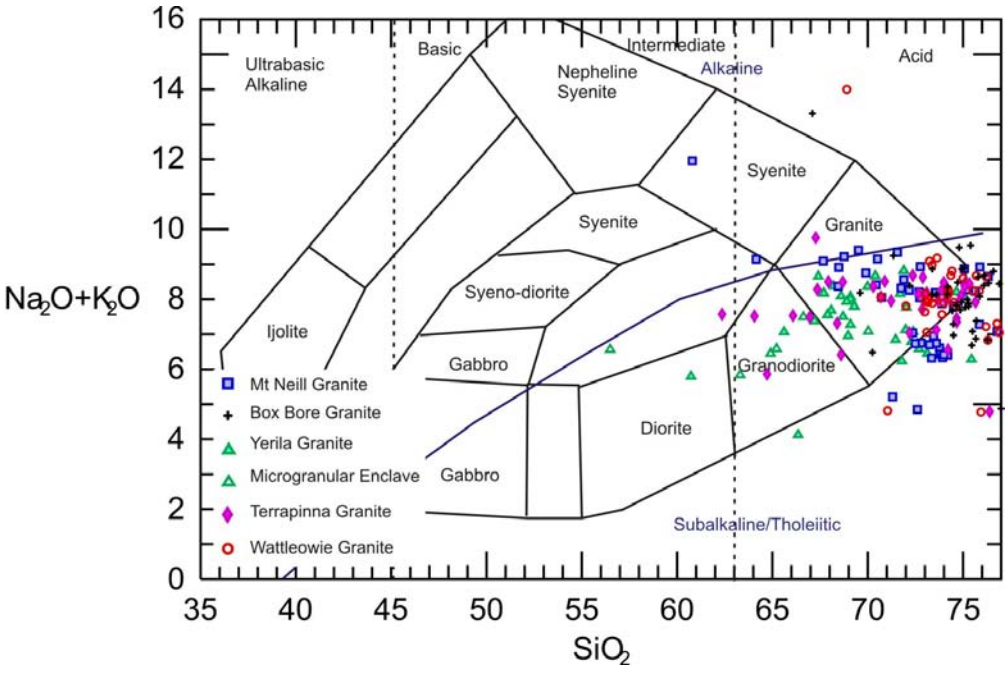

Figure 5.1 Classification of plutonic igneous rocks after Cox et al. (1989) using SiO_2 versus Na_2O+K_2O for granitic rocks of Mount Painter Province.

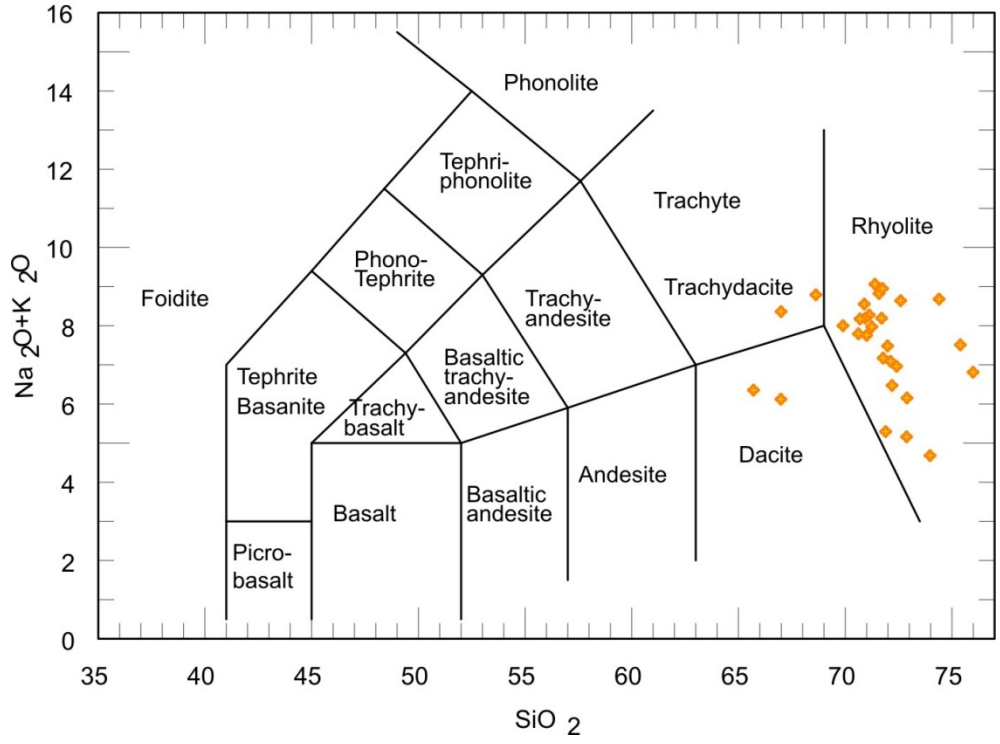

Figure 5.2 The total alkali versus silica (TAS) diagram of the Pepegoona Volcanics.

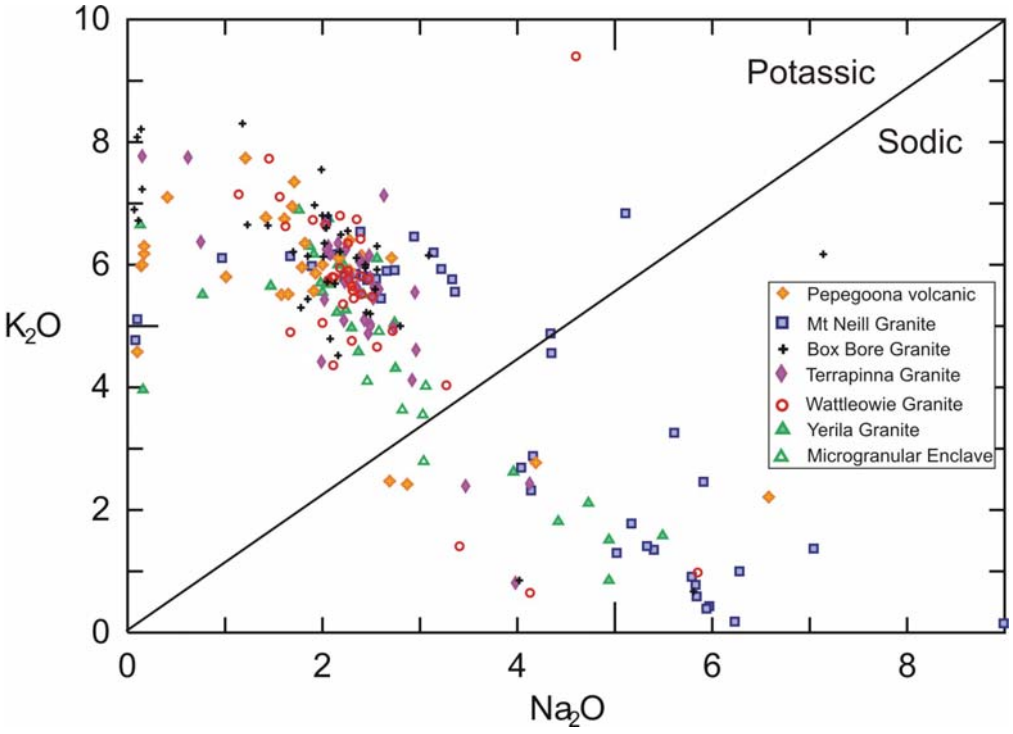

Figure 5.3 Diagram of Na_2O versus K_2O for the Mt Painter felsic igneous rocks. Most samples are potassic series with minor of sodic series.

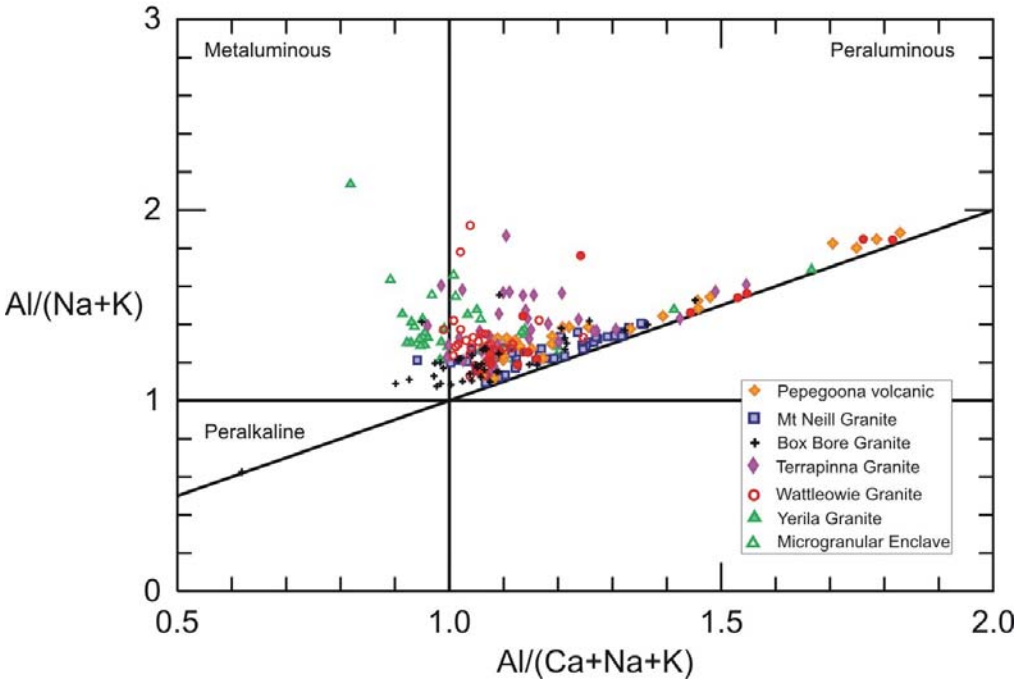

Figure 5.4 Alumina index from binary plot (after Manaiar and Picolli, 1989) of Mt Painter felsic igneous rocks.

Harker diagrams (SiO_2 versus major elements) of the felsic units are shown in Figure 5.5a to 5.5h. Relationships of SiO_2 and other major elements are mostly linear arrays showing negative trends (decrease of e.g. Al_2O_3, Fe_2O_3, CaO and TiO_2 while increase of SiO_2). Only SiO_2 versus Na_2O and K_2O (Figure 5.5f and 5.6g) show less defined trends that due to alteration. The Harker diagrams highlight different general geochemical variation trends. Most granitic suites including Mt Neill, Terrapinna, Wattleowie and Box Bore Granites generally show similar trends in all major elements. The Pepegoona Volcanics exhibit different linear arrays in MnO, K_2O and P_2O diagrams and sometimes differ in ratios. Harker trends of the Yerila granite and associated microgranular enclaves can differ significantly from other felsic rocks (e.g Figure 5.5a and 5.5f).

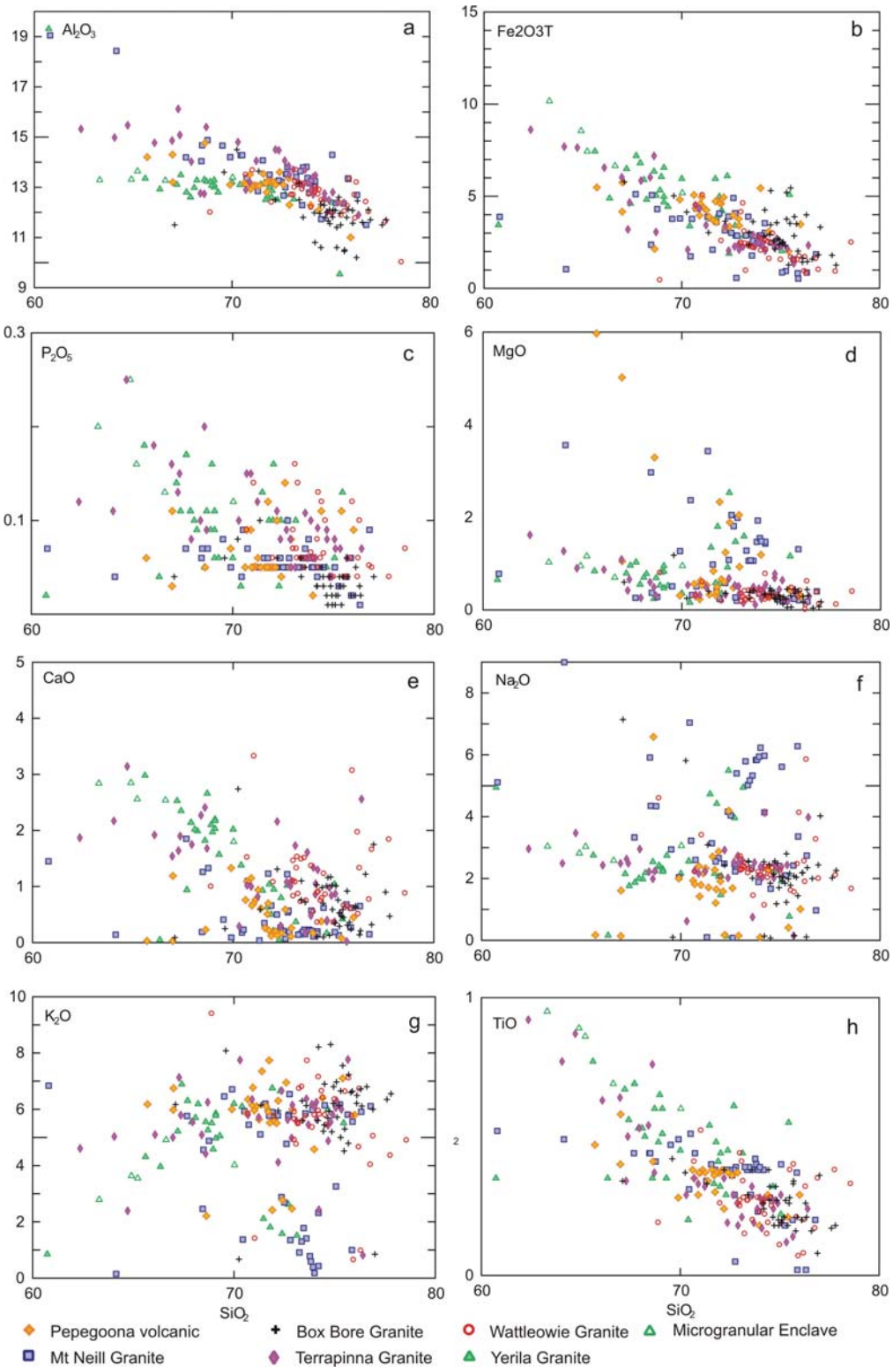

Figure 5.5 a to h Harker variation diagrams (SiO_2 versus other major elements) for felsic igneous rocks of Mt Painter Province.

The mesonormative calculation for the felsic rocks in this study is based on the accepted CIPW calculations of Johannsen (1931) using an Excel spread sheet developed by Kurt Hollocher, Geology Department, Union College, NY. The felsic volcanic and granitic rocks contain variable normative quartz concentrations ranging from 28.78 to 35.35 (Table 5.1). Representing corundum in the norm suggests that they mostly are peraluminous with normative corundum in range 3.25 to 0.31. The QAP (Quartz-Alkali-feldspr-Palgioclase) diagram after Le Maître (1989) for the felsic rocks suggests that they mostly are monzogranite and syenogranite (Figure 5.6). Some samples from the Mt Neill and Yerila Granites and Pepegoona Volcanic plot in granodiorite and tonalite due to alteration.

Table 5.1 Normative minerals of the granitic and volcanic igneous rocks calculated from average values of major element concentrations.

	PV	MN	BB	TP	WG	YG
Quartz	33.58	29.73	35.91	27.31	34.18	29.03
Plagioclase	21.51	41.32	21.91	26.49	24.96	26.6
Orthoclase	29.85	16.36	35.07	32.22	33.94	31.21
Corundum	3.25	2.57	0.83	2.09	0.96	0.31
Hypersthene	8.73	7.09	4.27	8.73	4.39	9.31
Ilmenite	0.7	0.78	0.46	0.93	0.46	1.08
Magnetite	0.32	0.23	0.19	0.35	0.17	0.36
Apatite	0.12	0.14	0.07	0.25	0.14	0.25
Zircon	0.09	0.09	0.04	0.07	0.03	0.13
Na2SO4	0.02	0.02	0.02	0.02	0.02	0.04

PV – Pepegoona Volcanics, MN – Mt Neill Granite, TP – Terrapinna Granite, BB – Box Bore Granite, WT – Wattleowie Granite, YG – Yerila Granite.

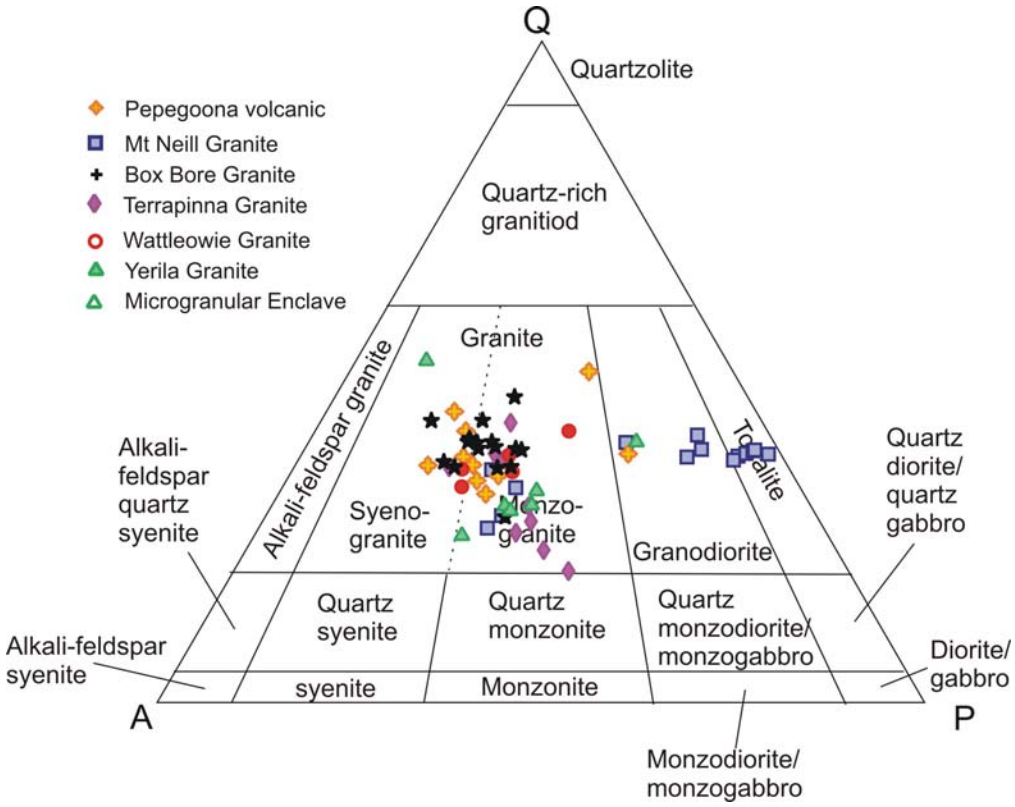

Figure 5.6 QAP diagram of felsic igneous rocks from Mount Painter.

b) Mafic igneous rock

Mafic igneous rocks in the Mt Painter Province have a crosscutting relationship with felsic igneous rocks and metasedimentary basements. Based on petrography, lithology (see Chapter 2) and geochronology (see Chapter 4), the mafic dykes are be divided into three groups including Group I - Paleozoic mafic dyke (PMF; n=8), Group II- Neoproterozoic mafic dyke (NMF; n=1) and Group III- Mesoproterozoic mafic dykes (MMF; n=14).

Mafic dykes for Mt Painter have a range of SiO_2 of 34-58 wt% with a majority between 49 to 58 wt% (Figure 5.7). Three samples, which have SiO_2 content below 40 wt% suggesting accumulation from fractional crystallisation, will not be considered in this chapter. The MgO content is variable (2.7-13.4 wt%) with Group I showing highest MgO concentration. Sample SD057 of Group III has very high MgO compared to other samples, which may be due to accumulation. The Mg# (Magnesium number) of the mafic dykes varies from 26.4 to 84.5. Group I mafic dykes contain the highest Mg# (average of 55), which may indicate their composition is closest to the parent magma. Group II has the lowest Mg# (32) and Group III has Mg#

average of 43. Binary plots of Mg# with major elements are used to assess possible magmatic fractionation trends (Figure 5.7). Binary diagrams of Mg# versus Al_2O_3 and CaO exhibit positive trends while TiO_2, P_2O_5 and FeO show negative trends in all groups. Binary plots of SiO_2 and Na_2O vs Mg# show unclear relationships.

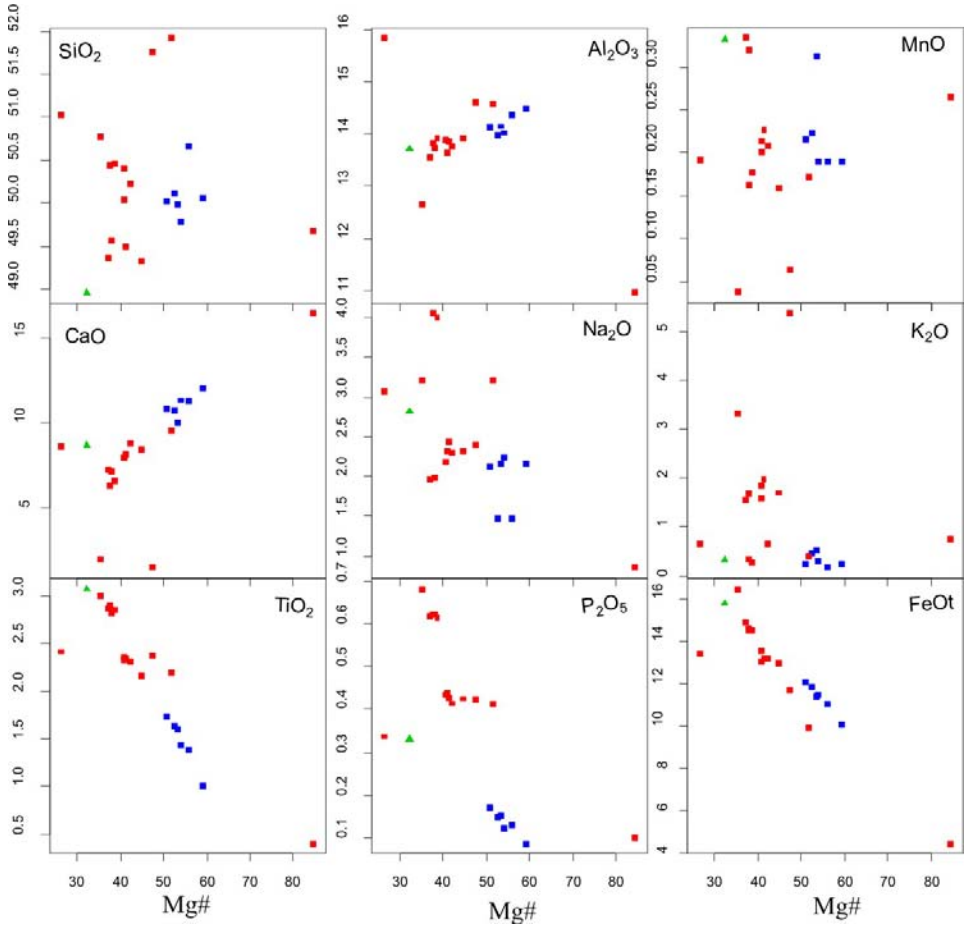

Figure 5.7 Binary plots of Mg number versus major elements for mafic igneous rock from Mount Painter Province (symbols blue-Group I; green- Group II; red -Group III).

Mafic dykes mainly plot into a basalt field with two samples as basaltic trachy-andesite of the TAS diagram (Figure 5.8). A ternary diagram of Al_2O_3-FeO_{tot}+TiO_2-MgO after Jensen (1976; Figure 5.9) for mafic dyke samples shows that Group I mainly plots within high Mg-tholeiitic basalt and Group II and III plot within high Fe-tholeiitic basalt. However, SD057 from Group III is in Komatiitic field due to its high MgO content. A wide variety of $Al2O_3/FeO_{tot}$ ratios may indicate differing degrees of alteration within suites. The AFM (Alkalis-FeO*-MgO) diagram clearly shows that most mafic dykes are tholeiitic (Figure 5.10; after Irvine and Baragar, 1971). However, two

samples from Group II mafic dyke plot within the calc-alkaline field, which may be due to alteration.

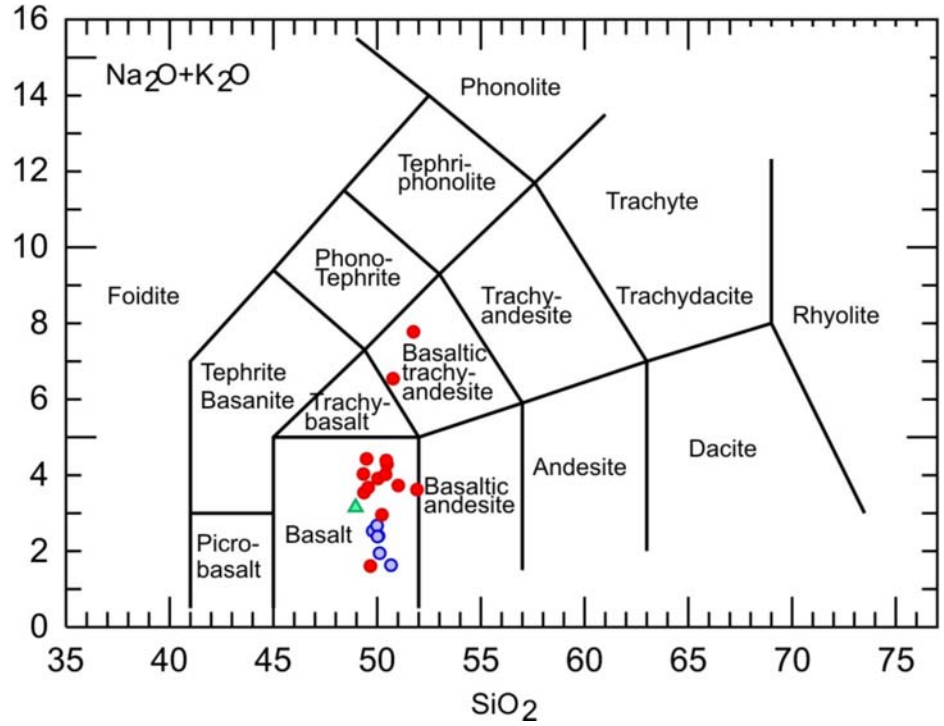

Figure 5.8 TAS diagram of mafic dykes classified as large majority of basalt and minor basaltic trachy-andesite (symbols blue-Group I; green-Group II; red -Group III).

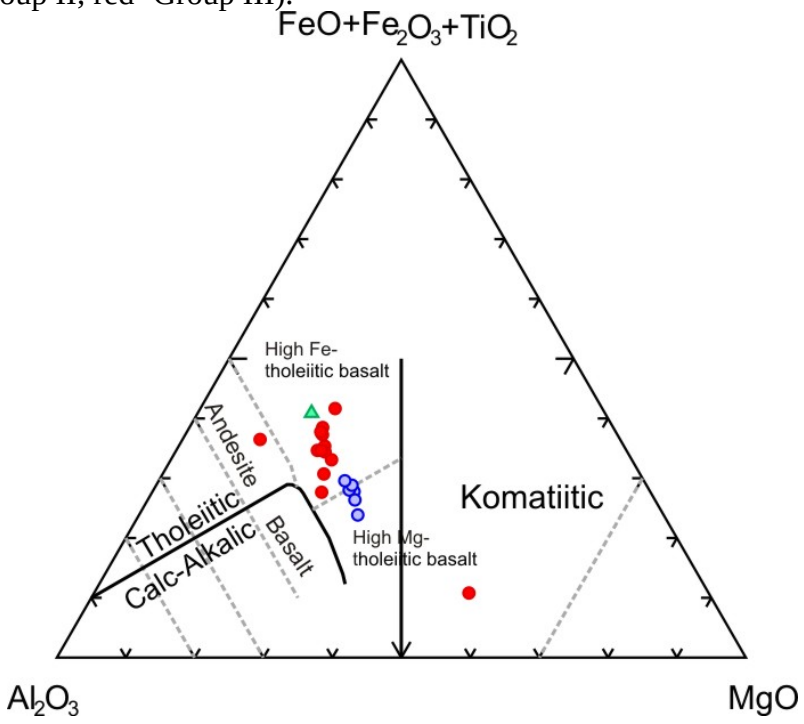

Figure 5.9 Ternary diagram of Al_2O_3-FeO_{tot}+TiO_2-MgO after Jensen (1976) for mafic dyke samples showing tholeiitic basaltic compositions (symbols blue-Group I; green- Group II; red -Group III).

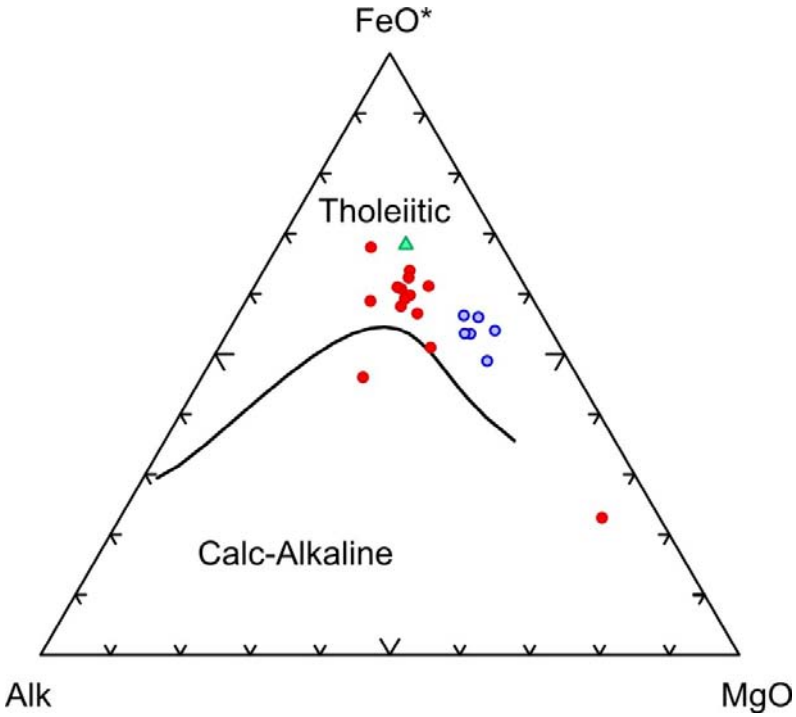

Figure 5.10 AFM diagram after Irvine and Baragar (1971) of mafic dykes showing most mafic dykes are tholeiitic (symbols blue-Group I; green- Group II; red -Group III).

Normative calculation for mafic dykes generally shows small amounts of normative quartz (Table 5.2). The silica-understaurated samples commonly contain normative hypersthene classifying as hypersthene basalt.

Table 5.2 Normative minerals of the mafic dykes calculated from major element geochemistry.

Group I	**SD041**	**MN099**	**SD029**	**SD063**	**774-146**	**SD023**	**SD020**	**774-169**
Quartz			0.26	3.39		3.97	0.79	1.51
Plagioclase	54.06	53.23	52.56	48.91	52.59	50.66	53.24	53.41
Orthoclase	1.75	2.13	4.06	3.53	1.48	1.35	1.91	1.37
Diopside	22.55	21.42	16.45	17.20	21.85	17.47	18.56	17.80
Hypersthene	15.40	17.24	23.69	23.92	21.61	23.90	22.27	22.88
Olivine	4.20	3.28			0.28			
Ilmenite	1.25	1.78	2.00	2.04	1.32	1.73	2.17	2.00
Magnetite	0.48	0.55	0.55	0.58	0.49	0.53	0.58	0.57
Apatite	0.20	0.27	0.34	0.34	0.23	0.29	0.38	0.34
Zircon	0.01	0.01	0.01	0.01	0.01	0.01	0.01	0.01
Chromite	0.04	0.04	0.04	0.04	0.13	0.04	0.04	0.12
Na_2SO_4	0.04	0.04	0.04	0.04		0.04	0.04	
Total	99.98	99.99	100.00	100.00	99.99	99.99	99.99	100.01

Table 5.2 (continued) Normative minerals of the mafic dykes calculated from major element concentrations.

Group II	**SD051**		**SD051**
Quartz	0.77	Magnetite	0.77
Plagioclase	55.73	Apatite	0.75
Orthoclase	2.65	Zircon	0.20
Diopside	13.27	Chromite	
Hypersthene	21.93	Na_2SO_4	0.04
Ilmenite	3.87	Total	99.98

Group III	**SD044**	**SD005**	**HPG14**	**MN090**	**SD007**	**MN077**	**SD022**	**SD039**	**MN084**
Quartz	3.67	1.03	2.09	1.93	4.16				3.34
Plagioclase	60.70	48.27	47.36	58.09	51.72	38.42	48.67	47.85	46.62
Orthoclase	4.75	11.78	13.45	3.19	4.94	24.35	12.58	14.60	11.86
Diopside	9.91	11.41	10.70	15.35	12.06	0.00	12.78	12.97	6.48
Hypersthene	16.55	22.83	21.81	17.33	22.49	27.19	18.29	16.62	25.86
Olivine						2.43	3.30	3.33	
Ilmenite	2.96	2.95	2.90	2.67	2.89	3.77	2.71	2.91	3.60
Magnetite	0.64	0.65	0.62	0.47	0.64	0.80	0.63	0.63	0.73
Apatite	0.75	1.00	0.97	0.91	0.93	1.55	0.97	0.97	1.41
Zircon	0.03	0.04	0.04	0.04	0.04	0.05	0.03	0.03	0.05
Chromite		0.01	0.01	0.01	0.01		0.01	0.01	0.01
Na_2SO_4	0.04	0.04	0.04	0.02	0.12	0.02	0.04	0.08	0.04
Total	100.00	100.01	99.99	100.01	100.00	100.01	100.01	100.00	100.00

	MN087	**SD004**	**MN055**	**MN086**	**773-41**	**37012**	**774-39**	**SD057**
Quartz	3.26				8.66	11.35	23.78	
Plagioclase	46.65	29.03	61.35	61.26	52.95	48.31	52.43	35.62
Orthoclase	12.71	38.48	2.08	2.52	20.36	19.40	3.82	5.55
Diopside	6.06		7.30	6.76			12.49	43.35
Hypersthene	25.59	23.27	20.90	21.29	14.49	17.27	4.79	4.52
Olivine		2.30	2.69	2.40				9.87
Ilmenite	3.54	2.93	3.53	3.59	1.86	1.67	1.44	0.50
Magnetite	0.70	0.56	0.70	0.70	0.45	0.54	0.33	0.22
Apatite	1.41	0.94	1.36	1.39	0.32	0.60	0.72	0.23
Zircon	0.05	0.04	0.04	0.04	0.12	0.11	0.12	0.07
Chromite	0.01	0.01	0.01	0.01			0.08	
Na_2SO_4	0.02	0.04	0.04	0.04				0.06
Total	100.00	100.00	100.00	100.00	100.01	100.00	100.00	99.99

5.1.2 Trace elements

a) Felsic igneous rocks

Granitic and felsic volcanic rocks are typically enriched in trace elements, particularly U, Th, Rb, Zr, Nb, Y, Ce and REEs and depleted in Sr and Eu (Figure 5.11). The Yerila Granite and its enclaves have extremely high trace element concentrations such as U (average of 114 and 192 ppm; for the

Yerila granite and its enclaves, respectively), Th (average of 380 and 662 ppm), Ce (average of 757 and 1084 ppm), Y (average of 201 and 344 ppm), La (average of 492 and 618 ppm) and Nd (average of 117 and 420 ppm). The Box Bore Granite contains lower concentrations of trace elements than the Yerila Granite but is still more enriched in these elements than other granitic and volcanic units. The Mt Neill Granite and Pepegoona Volcanic contain same amount of trace elements that are relatively less than the Yerila and Box Bore granites but more than the Terrapinna and Wattleowie granites. Trace element concentrations of the Wattleowie granite are lower than in the other groups.

b) Mafic dykes

Each three groups of mafic dykes contain different concentrations of trace elements. Group I has low trace element concentrations, whereas Group II and III are enriched in trace elements (Figure 5.12). Group I mafic dyke displays enrichment of Mg#, Cr and Ni that may suggest a primitive magma. In contrast, lower Mg#, Cr and Ni in Group II and III could suggest that they involve high differentiated magmas. Binary diagrams of Zr versus trace elements for Group I and Group III (except SD057 which contains high Mg#) mafic dykes display in Figure 5.12. They clearly show two separate fractionation trends (ratios and/or relationship). Group II is not included in Figure 5.12 due to its extremely high Zr contents which may be due to zircon accumulations.

The Th/U ratios of granitic, felsic volcanic, microgranular enclave and mafic dykes range between 0.3 to 16.5 with the majority between 2 to 6 (Appendix 5), suggesting that U and Th is mainly controlled by magmatic effects with minor hydrothermal U mobilisation.

The incompatible element diagrams or spider diagrams of the Mt Painter igneous rocks that normalise to primordial mantle value of Wood et al. (1979) are shown in Figure 5.13. Relative to primitive mantle, Rb, Th, U, La, Pb, Nd, Sm and Y concentrations are generally high whereas Ba, Nb, Ce, P, Sr, Zr and Ti are low. These characteristics are found in most Mt Painter igneous units except the Wattleowie Granite, which display slightly different

trends with no positive Th and U anomalies and low trace element concentration. The Yerila Granite and its enclaves exhibit very high trace elements concentrations in the spider diagrams.

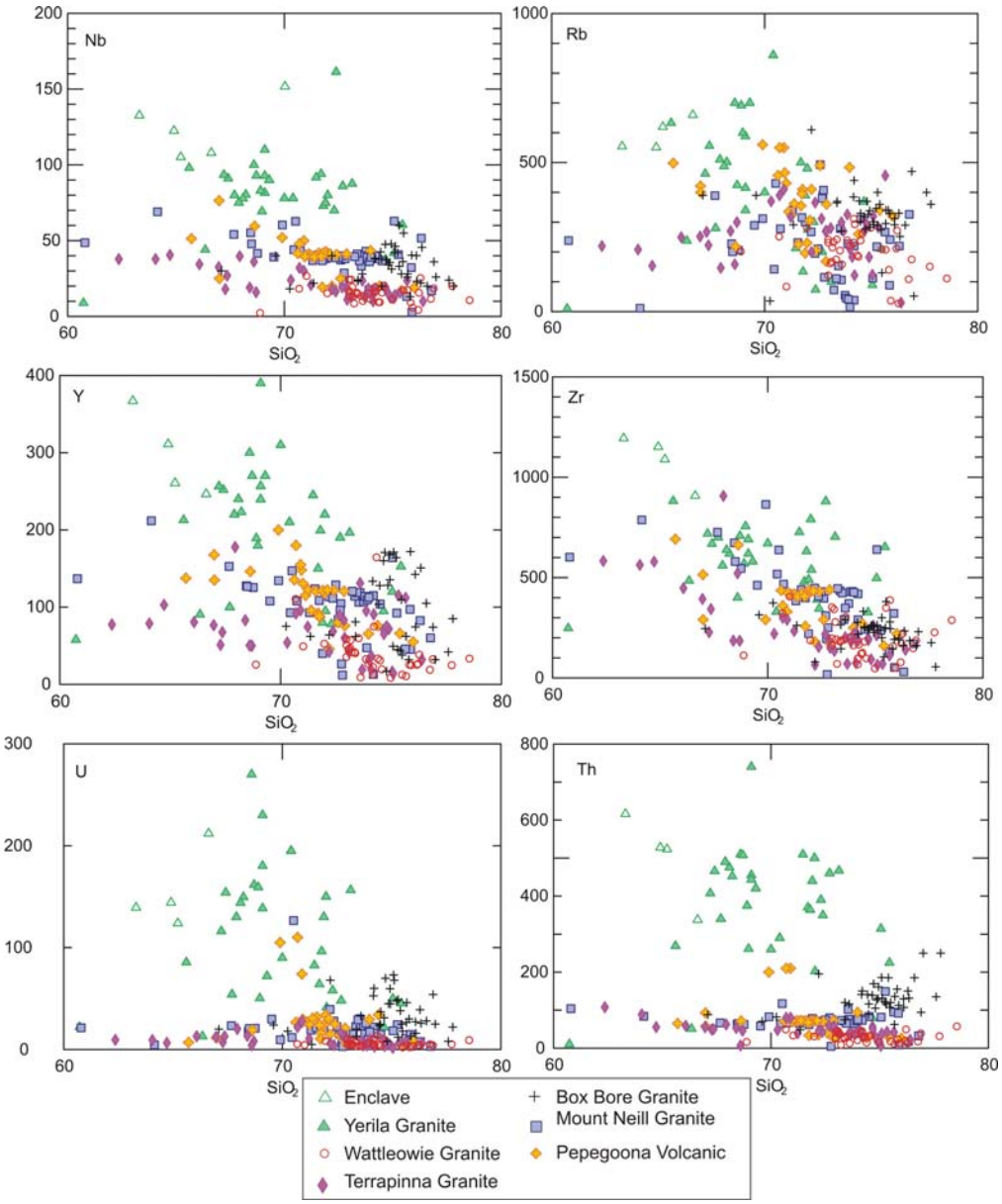

Figure 5.11 Harker variation diagrams (SiO_2 versus selected trace elements) for felsic igneous rocks of Mount Painter Province.

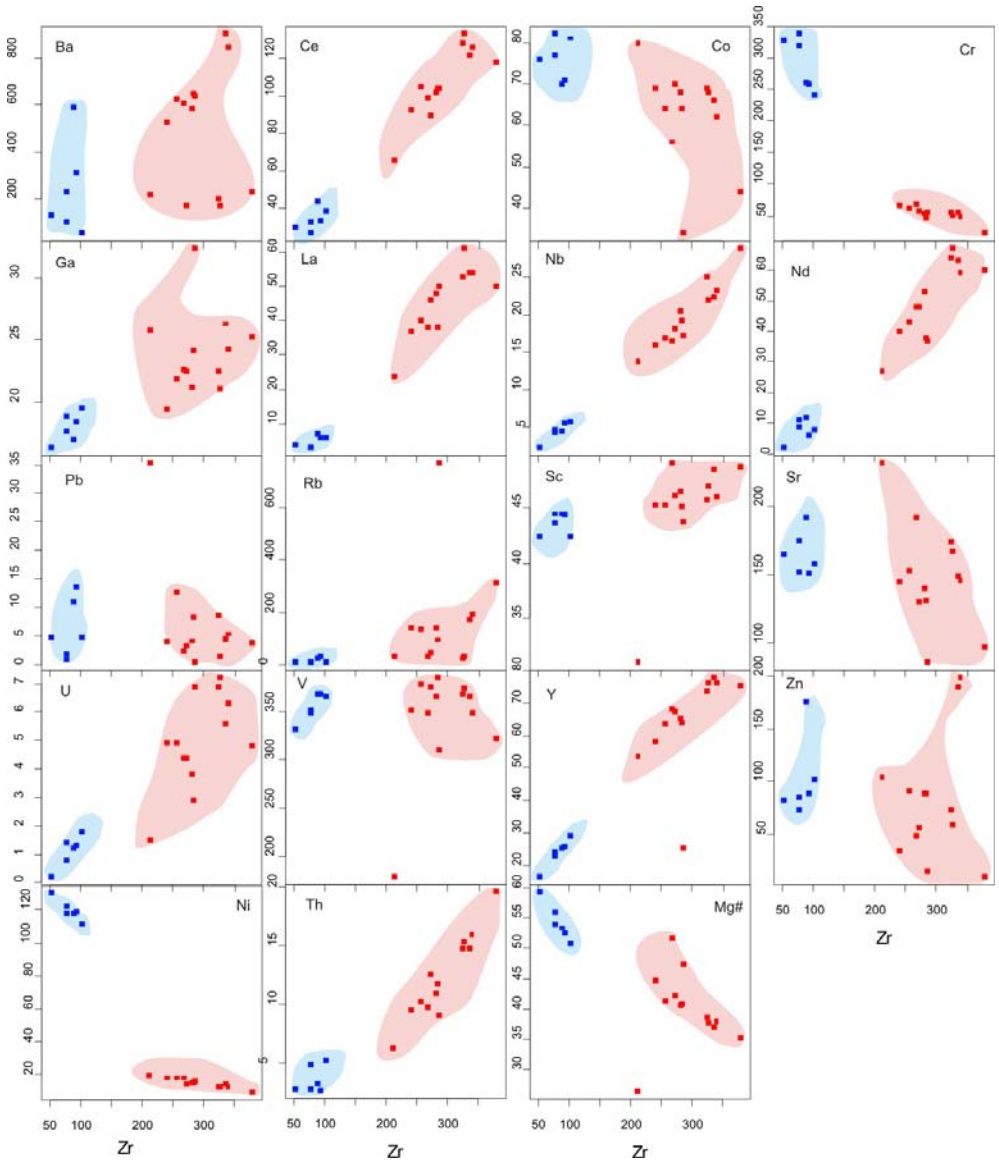

Figure 5.12 Binary plots of Zr versus selected trace elements for Group I and III mafic dykes (Symbol; blue: Group I and red: Group III).

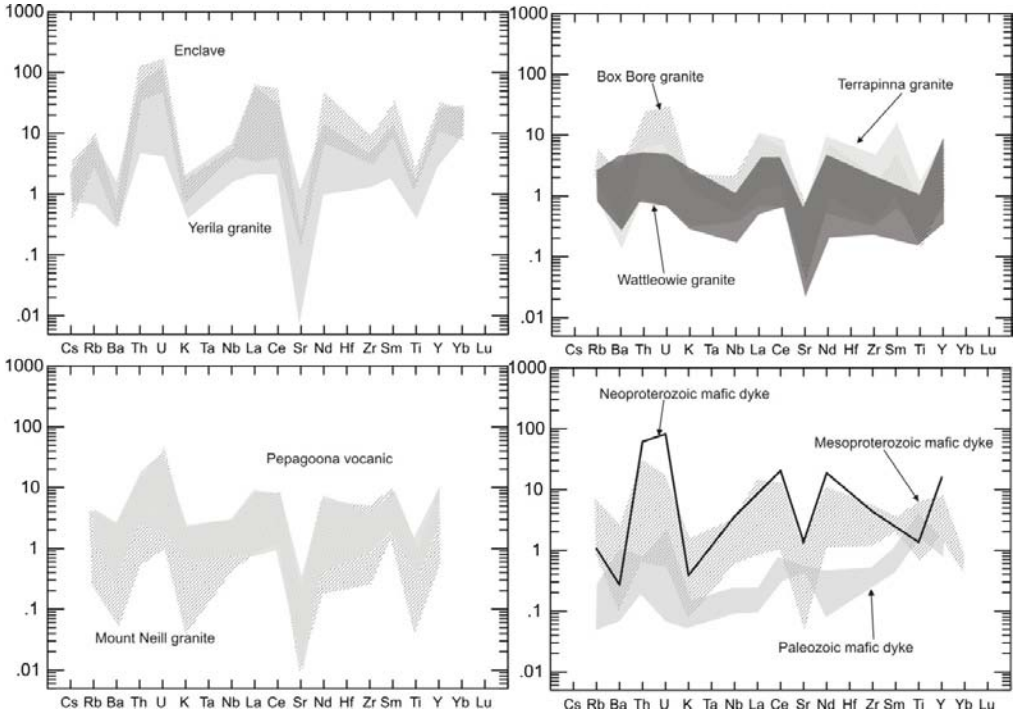

Figure 5.13 Incompatible element diagrams or spidergrams of the Mt Painter Province igneous rock that normalise to primordial mantle value of Wood et al. (1979).

5.1.3 Rare Earth Elements

The Mt Painter granitic and mafic rocks are normalised to values of Sun and McDonald (1989). The REE patterns of Mesoproterozoic mafic and felsic rocks have similar patterns (Figure 5.14) and show moderately fractionated light rare earth elements (LREEs) and relatively flat heavy rare earth elements (HREEs). The chondrite normalised La/Yb ratio representing the relative abundance of LREE to HREE can be used as an index of the degree of REE fractionation during magmatic evolution. Fractionation trends (La/Yb ratio) of felsic igneous samples range from 1.9 and 113.8 with an average of 17.1. Fractionation trends for LREE (La/Sm ratio) average 6.5 and fractionation trends for HREE (Sm/Yb ratio) average 2.0 for volcanic and granitic samples. Mafic samples have fractionation trends (La/Yb ratio) from 2.3 to 40; fractionation trends for LREE (La/Sm ratio) are from 1.5 to 15 and fractionation trends for HREE (Sm/Yb ratio) are from 1.5 to 2.7. Most samples have a prominent negative europium anomaly. The Yerila Granite and enclave samples that contain high REE concentrations display very strong negative Eu anomaly in particular enclave sample showing Eu/Eu* average of

0.14. In contrast, the REE pattern of a Wattleowie Granite shows a slightly positive europium anomaly.

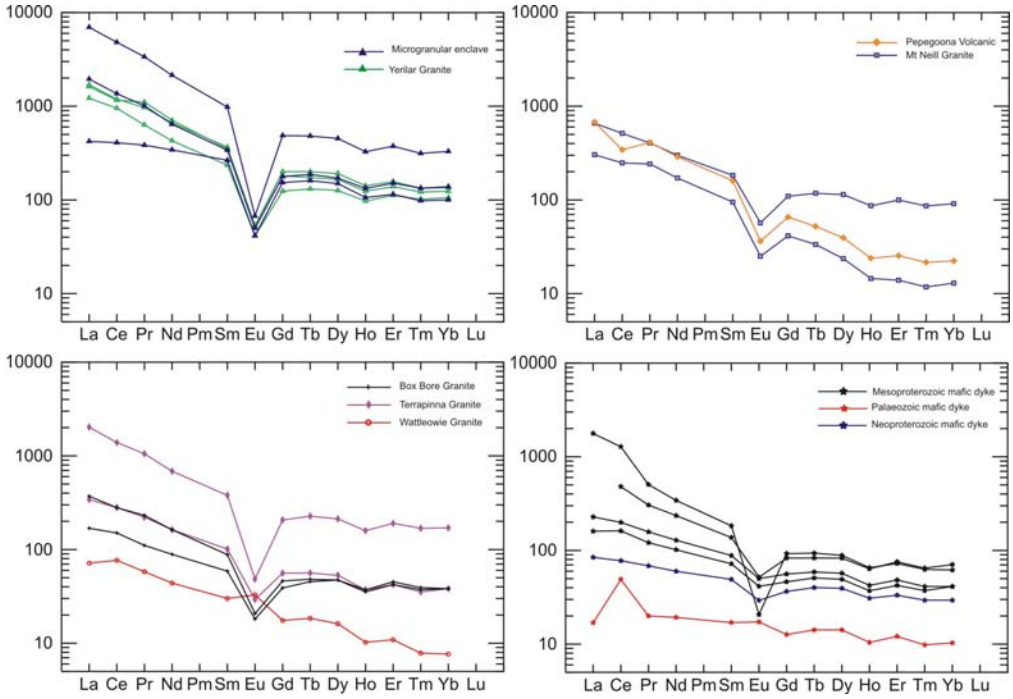

Figure 5.14 Rare earth elements patterns of the Mt Painter rocks normalised to values of Sun and McDonald (1989).

5.2 Discussion

5.2.1 Relationships between felsic suites

The oldest igneous suite comprises the co-magmatic Mt Neill Granite and Pepegoona Volcanics, which are commonly found together in outcrop and have an overlapping age range (see Chapter 4). The Mt Neill Granite and The Pepegoona Volcanic typically contain similar amounts of major and trace elements and similar REE and spidergram patterns (Figure 5.13 and 5.14). Moreover, they commonly show continuing trends in binary plots (Figure 5.15). The Terrapinna and Wattleowie granites that are grouped by Stewart and Foden (2002) have different major and trace concentrations. The Terrapinna Granite has a lower SiO_2 content but higher trace element concentrations than the Wattleowie Granite, in particular HFSE. Nevertheless, there is evidence suggesting that the two granites are co-magmatic including; field relationships, geochronology and isotope compositions and their

continuing trend in binary plots. The higher SiO_2 content of the Wattleowie Granite is possibly due to greater felsic magma fractionation.

In fact, the Pepegoona Volcanics and the Mt Neill, Terrapinna and Wattleowie granites could be derived from the same magma source but have different ratios of concentrations of the elements in their sources. This interpretation is suggested by incompatible binary plot of Ti versus Zr (Figure 5.16). The Pepegoona Volcanic, Mt Neill, Terrapinna and Watlleowie Granites have very similar bulk composition coefficients showing variations in the ratio that reflect differing propotions of accessory phases.

The Box Bore Granite, which was grouped in the Moolawatana Suite and separated from the Terrapinna and Wattleowie granites, contains high SiO_2 and REE elements such as La, Rb, Th, U and Ce. Geochemical characteristics of the granite are similar to other felsic igneous rocks (except the Yerila granite) regarding the REE and spider diagram patterns. Therefore, the Box Bore granite is probably derived from same source as the other felsic rocks (suggested by overlapping ages and isotopic compositions; detail in Chapter 4 and 6) but it involves more crustal input because of its enriched Th, U and Ce concentrations.

The Yerila Granite, which has the highest heat producing values, is relatively more mafic in composition having a lower SiO_2 content than other suites. This granite shows different trends within many binary diagrams compared to other units. This observation may indicate that the Yerila Granite was derived from different sources or involved in different processes from the other felsic rocks. Geochronology and isotope composition of the Yerila Granite and other units do not show obvious distinct values (see Chapter 4 and 6). Therefore, the Yerila Granite is possibly derived from the same sources as the other felsic rocks (see Chapter 6) but has higher degree of fractional crystallization.

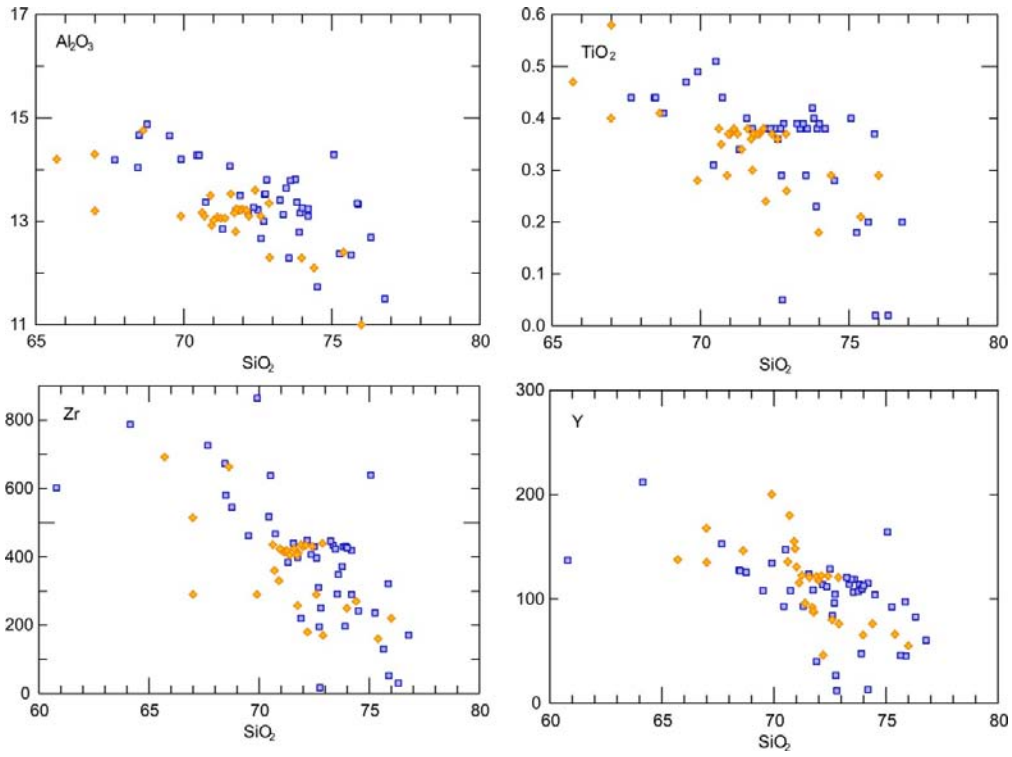

Figure 5.15 Harker diagrams of SiO_2 versus selected elements for Mount Neill Granite and Pepegoona Volcanic showing the continuing trends.

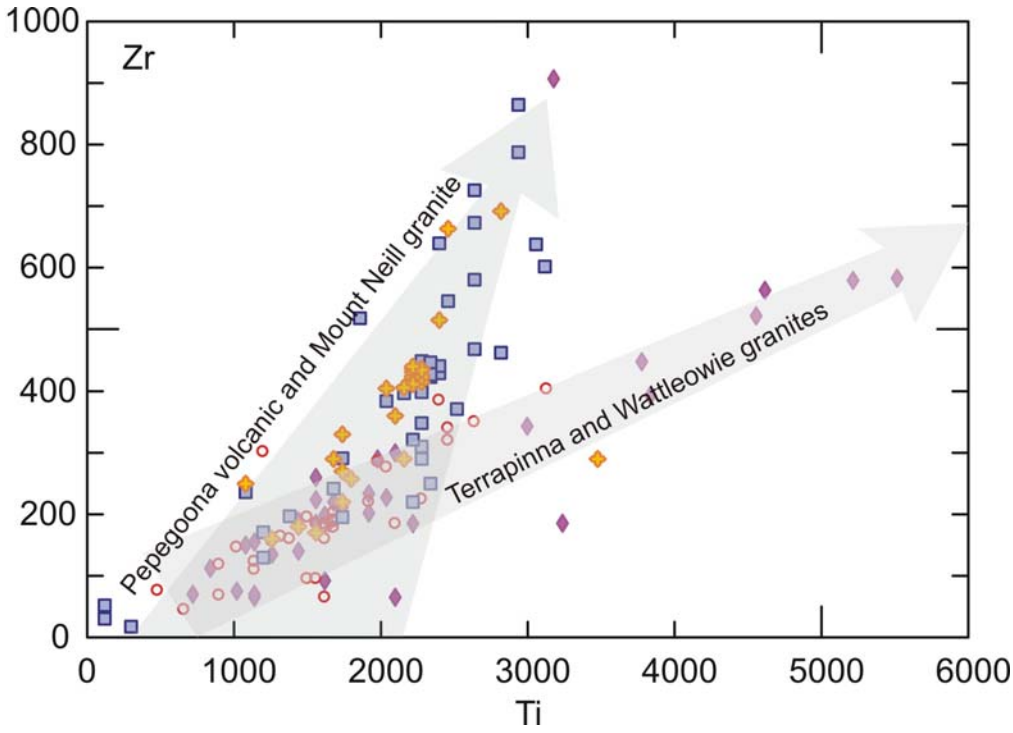

Figure 5.16 Binary plot of Ti and Zr showing continuing trends in the Terrapinna and Wattleowie granites and in the Pepegoona Volcanics and Mount Neill Granite.

5.2.2 Relationships between microgranular enclaves and the host Yerila granite

The microgranular enclaves vary in composition from mafic to felsic compositions with SiO_2 ranging from 56.5 to 70.0 wt%, which is more mafic than the host Yerila Granite. They commonly show continuing trends with the host Yerila Granite in various binary diagrams (Figure 5.17) suggesting that they are coeval. However, some element pairs shown in the scatter plots might be caused by an incomplete mixing and hybridization in intermediate compositions. Major and trace element concentrations of the microgranular enclaves are commonly in the same range as, but with slightly higher concentrations than the Yerila Granite. The REE patterns of the enclaves is similar to the Yerila Granite but with higher REE concentrations. More enriched HREE and strongly depleted Eu in the enclaves (Figure 5.14) suggest that they are more highly fractionated than the host granite.

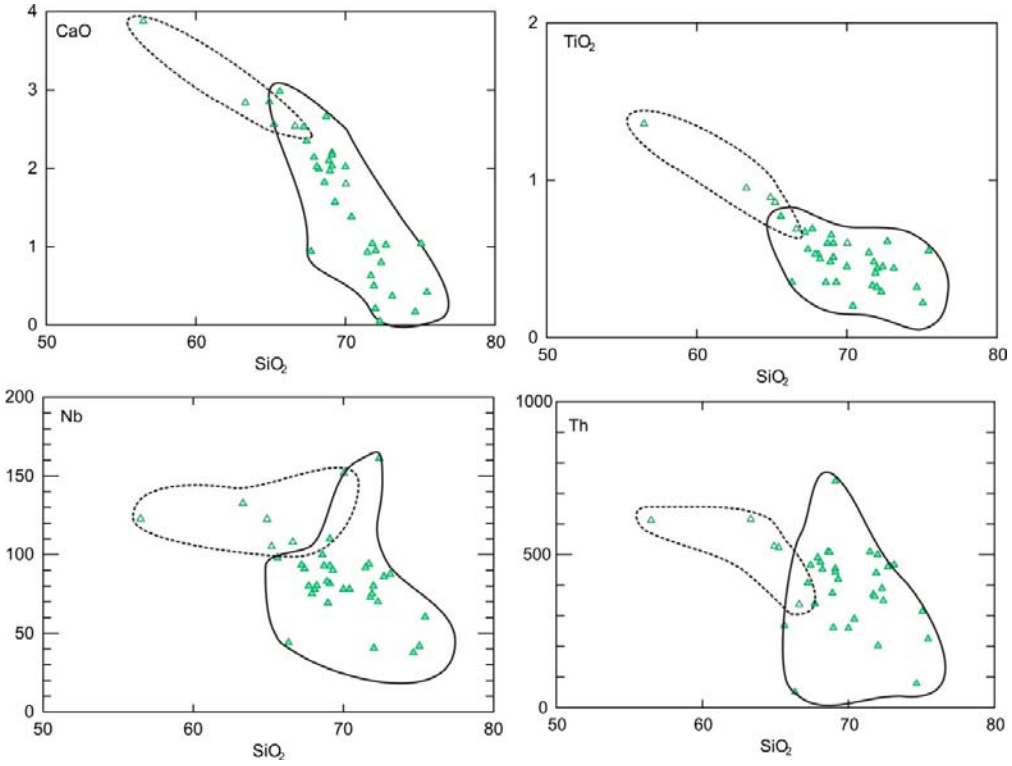

Figure 5.17 Binary plot of SiO_2 versus selected elements for microgranular enclave and host Yerila granite.

5.2.3 Relationships between felsic and mafic igneous rocks

Mafic dykes from this study are divided into three groups by using geochronology of U-Pb of single zircons (see Chapter 4), radiogenic isotope (see Chapter 6) and geochemistry. Group I and II mafic dykes are Neoproterozoic and Mesoproterozoic in age respectively. The unknown age mafic dykes, Group III, have different geochemical characteristics from groups I and II, having a depleted REE pattern and being enriched in Ni, Cr and Sc indicating mantle involvement. Only one sample of Neoproterozoic age was analysed in this study and will not be included in the discussion. The relationship between Mesoproterozoic mafic and felsic rocks will be focussed on here.

Correlations between the enriched U and Th mafic dykes and HHP felsic igneous rocks are shown in Figure 5.18. A diagram of SiO_2 versus TiO_2 shows a continuing trend from the mafic to felsic rocks, which suggests that the mafic dykes may be highly fractionated and felsic rock pattern results from magma mixing processes. The Zr versus SiO_2 diagram suggests zircon fractionated crystallization from mafic magma, which was undersaturated. Once Zr becomes saturated in magma, high Zr, which is found in the Mt Painter Province felsic rocks and some mafic rocks, cannot be reached via fractional crystallization only. The felsic suites are more likely to involve mixing between mafic and felsic magmas. The similarity of REE and spider diagrams for mafic and felsic rocks suggest that they are coeval.

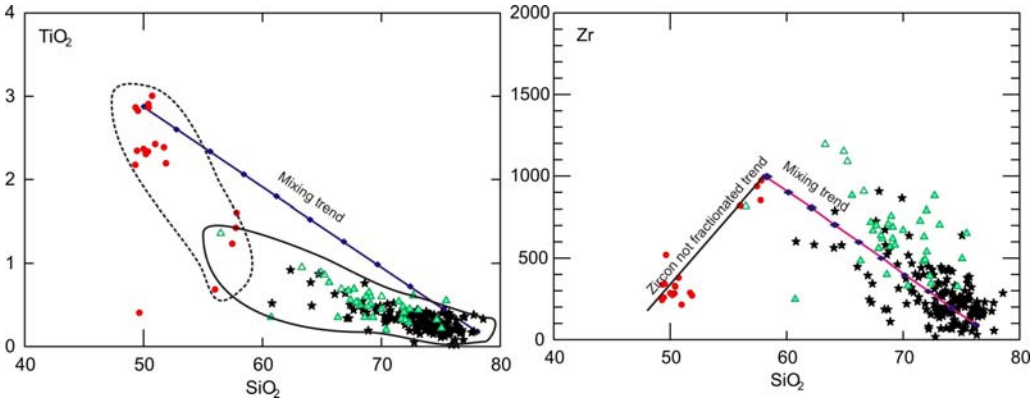

Figure 5.18 Binary plots of SiO2 versus TiO_2 and Zr for Mesoproteroic mafic and felsic rocks from Mount Painter province.

Chapter 6 Radiogenic isotopes

This chapter presents data on radiogenic isotopes from whole rocks (Nd-Sm, Rb-Sr and Pb-Pb), K-feldspars (Pb-U) and zircons (Hf) from the dominant magmatic suites of the Mt Painter Inlier. The results are used to constrain the petrogenesis of the Mt Painter igneous rocks. The interpretation and discussion of possible sources and petrogenetic processes combine data from this study and previous work that include whole rock Sm-Nd and Rb-Sr isotopes (Stewart and Foden, 2001; Neumann, 2001) and Pb isotope of whole rock and K-feldspar (Neumann, 2001). Whole-rock Nd-Sm, Rb-Sr and Pb-Pb and K-feldspar Pb-U analyses were made using TIMS at University of Adelaide and Hf isotope analyses of zircons were conducted using MC-ICPMS at GEMOC, Macquarie University. Detailed methodology is provided in Appendix 1.

6.1 Nd-Sm isotopes

Studying model ages and difference in isotopic ratio between the rocks and standard reservoirs will preset in this chapter. Moreover, the calculated difference at time of extraction of magma from the chondritic uniform reservoir (CHUR) using the $\varepsilon_{Nd}(T)$ as parameter which widely used model for the isotopic evolution of the mantle during Earth history also considerate here. Model ages are calculated using standard isotopic ratios (Table 6.1) including the chondritic uniform reservoir (CHUR) and depleted mantle (DM).

Table 6.1 Present day isotopic ratios for the model age calculation of CHUR and DM

	$^{143}Nd/^{144}Nd$	$^{147}Sm/^{144}Nd$	**Reference**
CHUR	0.512638	0.1967	Jacobsen and Wasserburg, 1984
DM	0.513114	0.222	Michard et al., 1985

6.1.1 Results

Twenty-five samples were analysed for whole rock Sm-Nd isotopic compositions including samples from the Pepegoona Volcanics (n=2), Mt Neill Granite (n=2), Box Bore Granite (n=2), Terrapinna Granite (n=2), Wattleowie Granite (n=2), Yerila granite (n=4), microgranular enclaves

(n=4), a tonalite (a felsic intrusion within the Wattleowie Granite; n=1), Paleozoic mafic dykes (n=3), a Neoproterozoic mafic dyke (n=1) and Mesoproterozoic mafic dykes (n=3). Measured $^{143}Nd/^{144}Nd$ ratios and εNd calculated for the sample crystallized ages is shown in Table 6.1 and Figure 6.1.

Two samples from the Pepegoona Volcanic (crystallization age of 1603±19 Ma) yielded εNd values of -2.7 and +0.6 with T_{CHUR} (Wassertburg et al., 1981) and T_{DM} (Michard et al., 1985) model ages of 1.86 and 2.10 Ga; 1.55 and 1.84 Ga (Sample MN010 and MN032, respectively).

Samples from the Mt Neill Granite that have a crystallization age of 1590±5 Ma include a fine-grained granite (MN026) and a coarse-grained granite (MN029). The εNd values yield -8.8 and -0.58; T_{CHUR} model ages of 3.91 and 1.64 Ga and T_{DM} model ages of 3.42 and 1.93 Ga for MN026 and MN029, respectively.

Sample SD011 and SD015 from the Box Bore Granite were selected for Nd-Sm isotope. The crystallization age of the Box Bore Granite is 1586±45 Ma. The samples have εNd values of -1.6 and -0.7 and yield T_{CHUR} and T_{DM} model ages of 1.72 and 1.98 Ga for sample SD011; 1.66 and 1.95 Ga from sample SD015.

Samples of the Terrapinna Granite including Sample MN047 and MN102 were selected for Nd-Sm isotope. The granite has crystallization age of 1569±22 Ma. The εNd values of MN047 and MN102 are +0.19 and -1.86 with T_{CHUR} and T_{DM} model ages of 1.55 and 1.86 Ga; and 1.76 and 2.02 Ga, respectively.

Two samples (BB02 and SD028) from the Wattleowie Granite, which has crystallization age of 1562±7 Ma yield εNd values of -1.3 and -0.8. T_{CHUR} and T_{DM} model ages of the samples are 1.71 and 2.03 Ga for sample BB02 and 1.63 and 1.88 Ga for sample SD028.

There are four samples from the Yerila Granite for Nd-Sm isotope analysis including sample MN092, SD025, SD42 and SD062. The granite yields crystallization age of 1556±20 Ma. Yerila Granite samples yield εNd values from -0.7 to -2.6 with T_{CHUR} and T_{DM} model ages average of 1.61 and 1.99 Ga, respectively.

Table 6.1 Nd-Sm, Rb-Sr and Pb-Pb isotopic data for mafic-felsic igneous rocks of Mt Painter Province.

Sample	Suite	Age(Ga)	$^{143}Nd/^{144}Nd$	2SE	$^{147}Sm/^{144}Nd$	εNdt	T_{DM}(Ga)	$^{87}Sr/^{86}Sr$	2SE	$^{87}Rb/^{86}Sr$	$^{206}Pb/^{204}Pb$	2SE	$^{207}Pb/^{204}Pb$	2SE	$^{208}Pb/^{204}Pb$	2SE
BB02	WG	1.56	0.511907	0.000015	0.1317	-1.3	2.03	0.849503	0.000077	6.911						
MN010	PV	1.6	0.511673	0.000032	0.1179	-2.6	2.1	1.327708	0.000050	33.524	32.008	0.002807	16.911	0.001627	48.124	0.005347
MN026	MN	1.59	0.511888	0.000080	0.1678	-8.8	3.42	0.903877	0.000036	17.263						
MN029	MN	1.59	0.511774	0.000008	0.1165	-0.5	1.93	1.066332	0.000092	20.697	29.416	0.002398	16.639	0.001548	47.058	0.005007
MN032	PV	1.6	0.511720	0.000008	0.1067	0.6	1.84				109.275	0.115223	22.238	0.023629	120.560	0.127159
MN047	TG	1.57	0.511802	0.000008	0.1147	0.2	1.86	0.856024	0.000037	7.264						
MN084	MF	1.57	0.511953	0.000009	0.1253	1.0	1.82	0.782820	0.000021	3.348	33.353	0.003317	16.898	0.001702	48.779	0.005058
MN090	MF	1.57	0.512005	0.000009	0.1407	-1.1	2.07	0.765561	0.000021	0.452						
MN092	YG	1.56	0.511507	0.000008	0.0990	-2.6	1.99	0.137564	0.000025	24.158	22.674	0.017761	27.161	0.004107	153.693	0.027751
MN099	MF	0.45	0.512536	0.000009	0.1672	-0.3	1.6	0.719607	0.000028	0.203	34.953	0.005447	17.398	0.002707	53.677	0.008376
MN102	TG	1.57	0.511736	0.000009	0.1184	-1.9	2.02				24.940	0.001691	16.184	0.001362	42.483	0.004405
SD004	MF	1.57	0.511859	0.000009	0.1343	-2.6	2.17	0.877924	0.000088	26.264						
SD011	BB	1.59	0.511637	0.000009	0.1085	-1.6	1.98	0.965879	0.000032	20.398	77.977	0.019482	20.225	0.005165	88.501	0.023703
SD015	BB	1.59	0.511771	0.000011	0.1171	-0.7	1.94	1.101916	0.000024	21.597						
SD025	YG	1.56	0.511561	0.000173	0.0991	-1.6	1.92	0.888218	0.000025	8.360	108.737	0.029851	22.870	0.006640	125.630	0.037791
SD028	WG	1.56	0.511603	0.000085	0.1001	-0.8	1.88									
SD029	MF	0.44	0.512679	0.000009	0.1669	2.5	1.2	0.757372	0.000021	0.379	20.017	0.001325	15.776	0.001070	40.064	0.002772
SD041	MF	0.44	0.512564	0.000012	0.1691	0.1	1.58	0.711811	0.000016	0.167	38.287	0.009074	17.774	0.004250	56.936	0.013592
SD042	YG	1.56	0.511529	0.000009	0.0915	-0.7	1.85	1.449129	0.000043	38.438						
SD043	ME	1.51	0.511541	0.000014	0.0991	-2.5	1.95	1.176919	0.000029	27.669	50.490	0.008493	18.094	0.004220	72.046	0.021929
SD046	ME	1.5	0.512239	0.000011	0.1709	-2.8	2.59	1.348676	0.000036	31.590	102.338	0.011904	22.442	0.003098	118.787	0.017906
SD050	ME	1.51	0.511427	0.000009	0.0855	-2.1	1.88	1.024049	0.000020	16.288						
SD051	MF	0.8	0.512507	0.000056	0.1645	0.7	1.61	0.746922	0.000042	20.376	39.727	0.006061	17.003	0.002493	41.498	0.006565
SD057	MF	1.52	0.511623	0.000013	0.1048	-2.0	1.93	0.773735	0.000036	17.008	133.026	0.026789	22.835	0.004578	159.026	0.032425
SD062	YG	1.56	0.511661	0.000009	0.1085	-1.5	1.94	1.160438	0.000021	22.643						
SD065	ME	1.51	0.511548	0.000009	0.0992	-2.4	1.94				152.864	0.081363	26.733	0.014118	176.989	0.094745
SD068	TN	0.11	0.512192	0.000066	0.1282	-4.9	1.50									

PV: Pepegoona Volcanic, MN: Mount Neill Granite , BB: Box Bore Granite, TP: Terrapinna Granite, WT: Wattleowie Granite , YG: Yerila Granite, ME: microgranular enclave, MF: Mafic dyke, TN: Tonalite

Sample SD043, SD045, SD050 and SD065 of microgranular enclave found in Yerila Granite yield εNd values between -2.1 and -2.8. Sample SD043, SD050 and SD065 are mafic microgranular enclaves which have T_{CHUR} model ages ranging from 1.66 to 1.71 Ga and T_{DM} model age ranging from 1.88 to 1.95 Ga. The felsic enclave, SD047, has older T_{CHUR} and T_{DM} model ages of 2.35 and 2.59 Ga than mafic enclaves.

Sample SD068 is a tonalite which intrudes the Wattleowie Granite yields εNd values (calculated for an age of 440 Ma) of -4.9 with T_{CHUR} and T_{DM} model ages of 1.00 and 1.50 Ga, respectively.

Mafic dyke samples selected for analysis can be divided into three groups including Mesoproterozoic (MN084, MN090, SD004 and SD057), Neoproterozoic (SD051) and Paleozoic (MN099, SD029 and SD041) mafic dykes. The Mesoproterzoic mafic dykes yield εNd values ranging between -1.1 and +1.0. These mafic dykes have T_{CHUR} model ages ranging between 1.46 and 1.90 Ga and T_{DM} model ages ranging between 1.82 to 2.17 Ga. The Neoproterozic mafic dyke yields εNd values of 0.7 with T_{CHUR} and T_{DM} model ages of 0.62 and 1.61 Ga. The youngest mafic dyke that has crystallization age around 440 Ma yields εNd values between -0.3 and +2.5 with T_{CHUR} model ages between 0.21 and 0.53 Ga and T_{DM} model ages between 1.25 and 1.60 Ga.

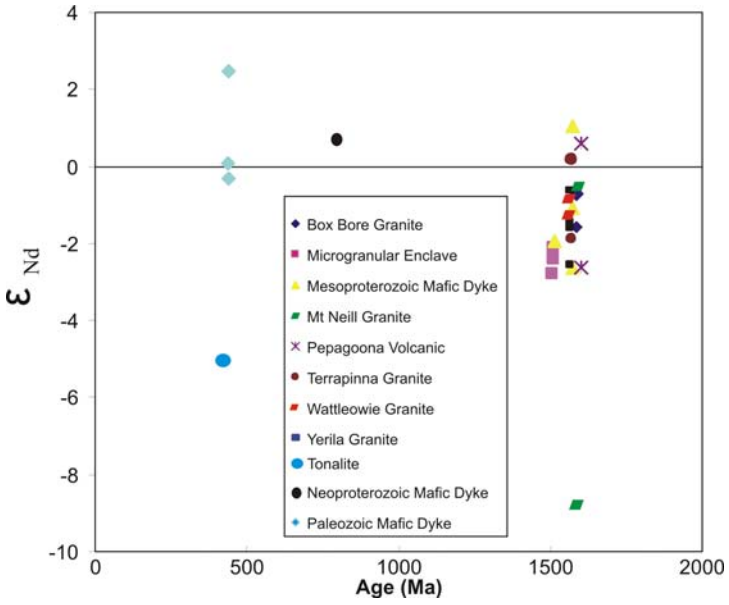

Figure 6.1 Initial εNd values versus crystallization ages of the mafic and felsic rocks from Mt Painter Province.

6.1.2 Discussion of Nd-Sm isotopes

Nd isotopic analyses of the Mesoproterozoic mafic and felsic samples from the Mt Painter Province mainly yielded negative initial εNd values, whereas the younger Palaeozoic mafic dykes yielded higher initial εNd values. The Mesoproterozoic felsic and mafic samples mainly have initial εNd values between -2.8 and +1.0 and overlapping in the coexisting mafic and felsic magmas. This evidence suggests these magmatic rocks contain a relatively homogeneous Nd isotopic signature source. The exception is one fine-grained sample from the Mount Neill Granite (sample MN026) containing very low εNd values of -8.7 and T_{DM} of 3.42 Ga together with an unusual low $^{143}Nd/^{144}Nd$ ratio and previous data of Scheaefer (1993) providing the Mt Neill Granite with T_{DM} of 3.4 and 3.7 Ga that may reflect unexposed older crusts underneath the Mt Painter Province.

The Mesoproterozoic samples from this study and previous studies (Neumann, 2001; Stewart and Foden, 2001) plot in the Sm-Nd isochron ($^{143}Nd/^{144}Nd$ versus $^{147}Sm/^{144}Nd$ suggesting an initial $^{143}Nd/^{144}Nd$ value of 0.510632±0.000082 and providing an isochron Nd-Sm age of 1403±110Ma (Figure 6.2). Although the Nd-Sm isochron age is considerably younger than the U-Pb zircon ages (see Chapter 4), both ages agree within analytical uncertainty, and the Nd-Sm whole rock isochron age may still be interpreted as a minimum estimate for the igneous age.

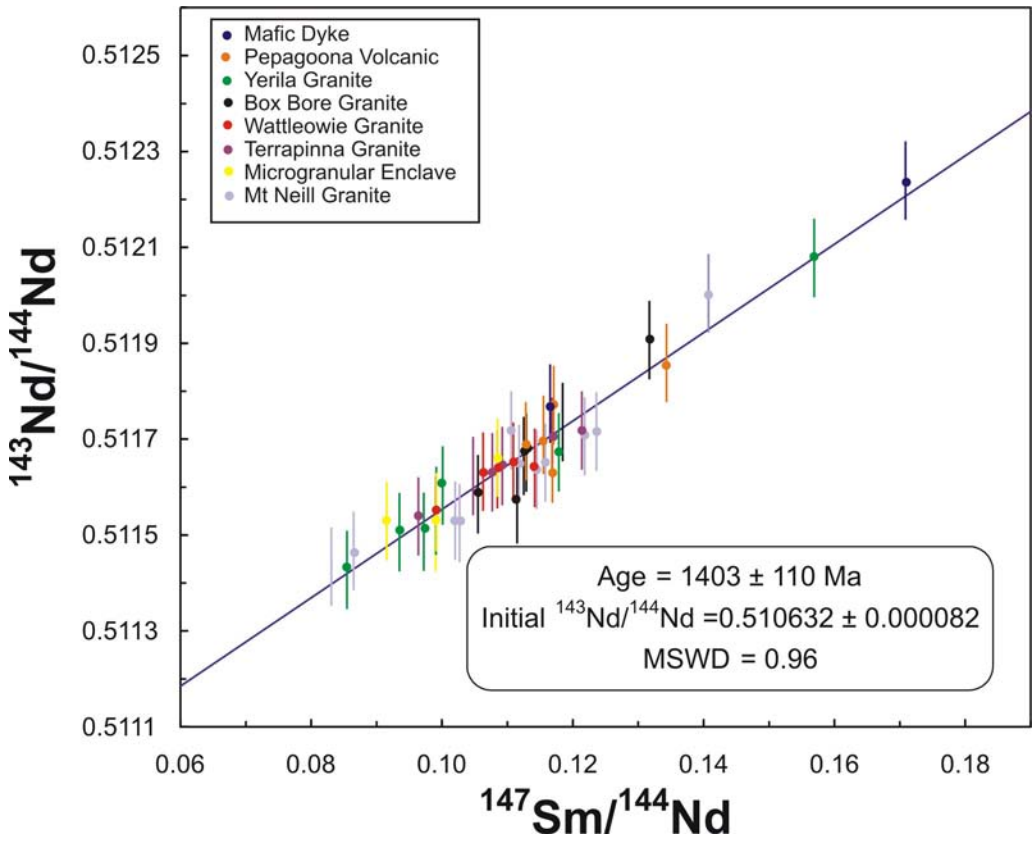

Figure 6.2 Sm-Nd isochron of mafic and felsic magmatic rocks from the Mt Painter Province (data from this study; Stewart and Foden, 2001; Neumann, 2001).

Initial εNd values for all Mesoproterozoic granitic and volcanic samples calculated at their crystallized ages are lower than depleted mantle at the time of intrusion (Figure 6.3) that indicate crustal components. Moreover, there are several evidences supporting old crust as an important source for generating the Mesoproterozoic magmatic rocks. These include;

- Higher $^{143}Nd/^{144}Nd$ isotopic composition than the chondritic uniform reservoir and low Sm/Nd ratios (ranging from 0.14 to 0.23) of the samples give evidence for the possible existence of underlying older crust.
- T_{CHUR} model ages, which provide estimates of the time that a sample (or its crustal precursor) separated from the mantle source region, for the Mt Painter rocks (except Sample MN026) are ranging between 2.35 and 1.46 Ga, with a cluster at 1.70 Ga that are older than the Mt Painter magmatic emplacement ages suggesting reworking of older crust.

- Depleted-mantle model ages (T_{DM}), which are the estimate time when sample separated from a mantle depleted reservoir, for the Mt Painter rocks (except Sample MN026) range between 1.82 and 2.59 Ga (Table 6.1) suggesting a long crustal history.

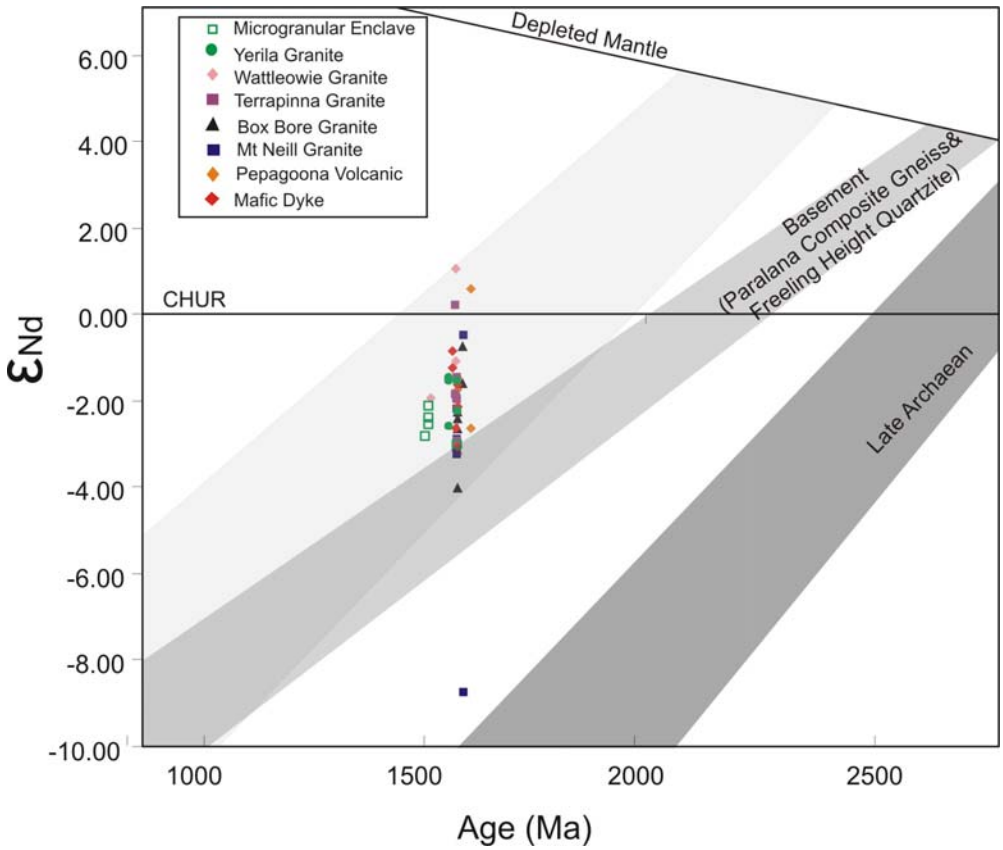

Figure 6.3 Initial εNd values versus ages of Mesoproterozoic mafic and felsic rocks from Mt Painter Province comparing to the Paralana Gneiss and Freeling Height Quartzite basements (data from Schaefer, 1993).

Based on the T_{DM}, the Mesoproterozoic igneous rocks appear controlled predominantly by widespread melting of heterogeneous 1.82 and 2.59 Ga lower crust. However, there is no report of any crustal growth or tectonic activity at this time on the Australian continent, so melting of a 1.82 and 2.59 Ga crustal source is unlikely to explain the observed Nd ratios. A more likely alternative is that the εNd values of the Mt Painter Mesoproterozoic magmatic rocks result from mixing of a juvenile source and pre-existing crust.

A mantle-derived source is suggested as one of the important sources as well as the older crustal source. This interpretation is based on the higher

initial εNd values of the Mesoproterozoic magmatic rocks than the Paralana Gneiss and Freeling Height Quartzite basements with some sample being positive initial εNd values (Figure 6.3). However, the positive εNd values from the Mt Painter rocks are less than other Mesoproterozoic magmatic rocks such as mafic rocks from the Broken Hill Domain, Curnamona Craton where initial εNd values are up to +3.5 (Raveggi et al., 2007); metabasites from the Olary Domian, Curnamona Craton have initial εNd values up to +2.7 (Rutherford et al., 2006); and ultramafic dykes from the Olympic Dam, Gawler Craton have initial εNd values up to +4 (Johnson and McCulloch, 1995). The less primitive isotopic magma in the Mesoproterozoic HHP rocks from Mt Painter Province suggests that these rocks are probably not derived directly from mantle. They were more likely derived from heat source related to an input material from depleted mantle as interpreted in A-type Olary Domain (Ashley et al., 1996).

The Sm-Nd isotopic data suggests that both mantle-derived magma and reworking of old crust are important sources. To generate a crustal-contaminated magma, partial melting of lower crust by magma underplating and mantle-derived mantle magma is suggested.

A Neoproterozoic mafic dyke comparable to the Wooltana Volcanics (see Chapter 4) yields initial εNd values within the range of εNd values observed for the Wooltana Volcanics themselves (Figure 6.4). Palaeozoic mafic dykes have high εNd values (calculated at 440 Ma) suggesting thay were possibly derived from a juvenile mantle source. One sample of the tonalite that is interpreted as a later felsic intrusion intruded the Wattleowie Granite and has an εNd value of -4.8, which overlaps the εNd values of the Mudnawatana tonalite from the Mt Painter Province ($\varepsilon Nd_{(T=500)}$ of -4.31; Neumann, 2001; Figure 6.4).

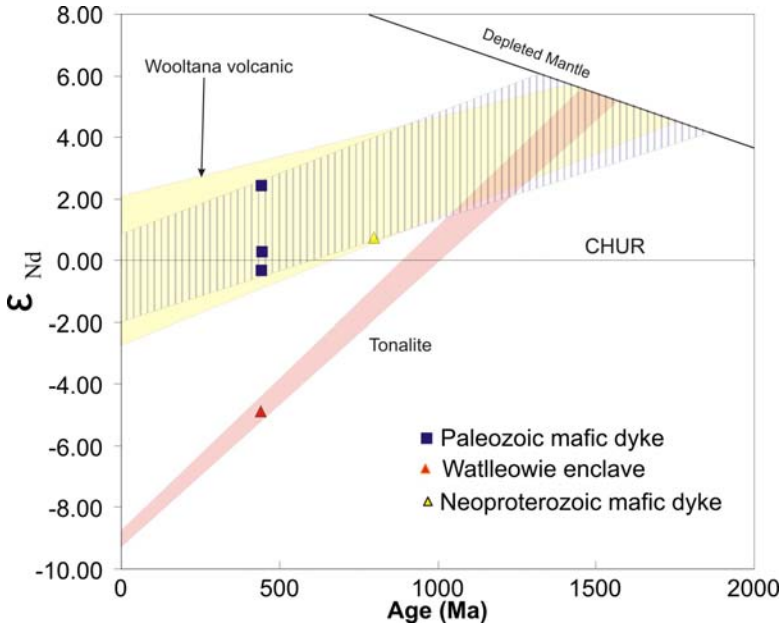

Figure 6.4 εNd values versus ages of Nesoproterozoic and Palaeozoic magmatic rocks from Mt Painter Province.

6.2 Rb-Sr isotopes

6.2.1 Result

Twenty-two samples were selected covering felsic (volcanic and granitic rocks) and mafic suites including Pepegoona Volcanic (n=1), Mount Neill Granite (n=2), Box Bore Granite (n=2), Terrapinna Granite (n=1), Wattleowie Granite (n=2), microgranular enclave within the Wattleowie granite (n=1), Yerilar Granite (n=3), microgranular enclaves of the Yerila Granite (n=3), Palaeozoic mafic dykes (n=3), Neoproterozoic mafic dyke (n=1) and Mesoproterozoic mafic dykes (n=3).

The measured $^{87}Sr/^{86}Sr$ ratios of mafic and felsic samples are very variable ranging between 0.137564 and 1.449129 (Table 6.1). Most of the results are extremely high $^{87}Sr/^{86}Sr$ ratios, which do not represent the primary ratios. These rocks were possibly affected by later fluid influx into cooling plutons. The scatter in the Rb/Sr versus SiO_2 (Figure 6.5) suggests variable post-magmatic disturbance. Samples that possibly contain primary $^{87}Sr/^{86}Sr$ ratios are mafic suites, especially Palaeozoic mafic dyke yielding $^{87}Sr/^{86}Sr$ ratios of 0.719607 to 0.757372.

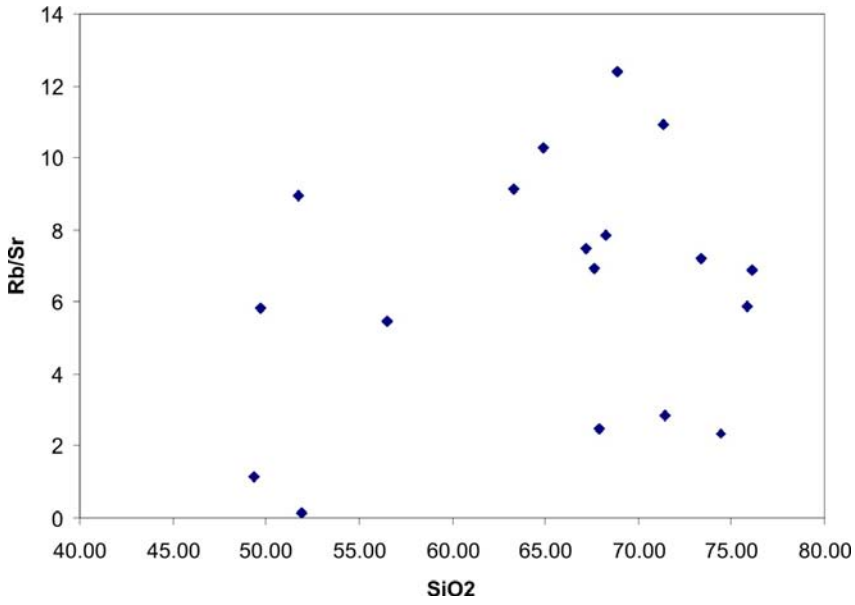

Figure 6.5 Rb/Sr versus SiO_2 of selected samples for Rb-Sr isotope

6.2.2 Discussion of Rb-Sr isotopes

At the magmatic stage, the Mt Painter rocks were likely disturbed by active interaction between coeval silicic and mafic magma. The $^{87}Sr/^{86}Sr$ ratio of silicic magmas is sensitive to input basaltic injection. Generally, Rb in mafic dykes is concentrated in subordinate K-feldspar while Sr is hosted in plagioclase that makes up ~60% of the rock volume (Katzir et al., 2007). Alteration of K-feldspar may result in resetting $^{87}Rb/^{86}Sr$ and $^{87}Sr/^{86}Sr$ ratios; however, if Sr dominates over Rb, the whole rock $^{87}Sr/^{86}Sr$ value would not be greatly impacted (Katzir et al., 2007). This could apply for some mafic samples that have higher Sr concentrations compared to Rb (e.g. MN084, MN090 and MN099; Table 6.1).

A Rb-Sr isochron for the Mesoproterozoic granitic and volcanic rocks indicates an apparent age of 1165±120 Ma (Figure 6.6), which is significantly younger than the U-Pb zircon ages. The Rb-Sr isochron age suggests that the Mt Painter magmatic rocks have been affected by fluid infiltration or thermal event. Although, there is no tectonic event recorded in South Australia Craton at the time. The 1.16 Ga thermal event of the Mt Painter Province based on the Rb-Sr isochron age could be related to the Musgrave Event in the Musgrave Block, which is characterized by medium-pressure granulite facies

and emplacement of syn-orogenic magmas and post-orogenic granite (e.g. White et al., 1999; Camacho et al., 1997).

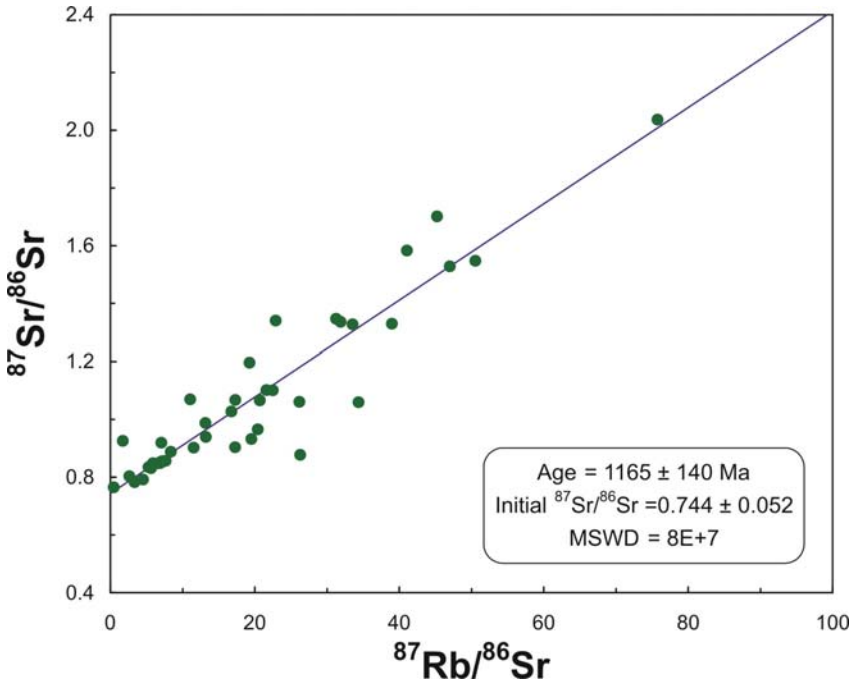

Figure 6.6 Rb-Sr whole-rock isochron for the Mesoproterozoic magmatic rocks of the Mt Painter Province.

6.3 Whole Rock Pb isotopes

Whole-rock Pb-Pb isotopic ratios can be used to understand rock petrogenesis. Different U/Pb and Th/Pb ratios for each environment affect the isotopic evolution of Pb; therefore Pb isotope compositions might record chemical environments in which Pb has resided. However, the U/Pb and Th/Pb ratios are affected by magma fractionation, hydrothermal, metamorphism and weathering which may modify the U and Th concentrations and and alter Pb isotope composition.

6.3.1 Result

Sixteen samples were selected for whole-rock Pb-Pb isotope analyses in this study including Pepegoona Volcanic (MN010 and MN032), Mount Neill Granite (MN029), Box Bore Granite (SD011), Terrapinna Granite (MN102), Wattleowie Granite (SD028), Yerila Granite (MN092, SD025 and SD042), microgranular enclaves of the Yerila Granite (SD045 and SD049) and mafic dykes (Mesoproterozoic mafic dykes- MN084 and SD057;

Neoproterozic mafic dyke-SD051; Paleozoic mafic dykes-sample MN099 and SD029).

The igneous rocks from the Mt Painter Province have a widely variable $^{206}Pb/^{204}Pb$, $^{207}Pb/^{204}Pb$ and $^{208}Pb/^{204}Pb$ ratios (Table 6.1), which calculated to crystallized ages with Some sample show extremely low values of $^{206}Pb/^{204}Pb$, $^{207}Pb/^{204}Pb$ and $^{208}Pb/^{204}$ Pb (e.g. MN032, MN092, SD011, and SD065). The low ratios are possibly caused by late thermal event; therefore, the whole rock Pb-Pb isotope from the Mt Painter rocks in this study is not a reliable petrogenetic indicator.

6.3.2 Discussion of Pb isotopes

The Pb-Pb whole rock isochron age ($^{207}Pb/^{204}/Pb$ versus $^{206}Pb/^{204}/Pb$ ratios; Figure 6.7) provides an age of 1246±80 Ma which is considerably younger than the U-Pb zircons ages. The Pb-Pb isochron age is consistent within analytical error with the Rb-Sr isochron age supporting that the Meosproterozoic magmatic rocks from the Mt Painter Province have been affected by later hot fluids during the Musgrave Event.

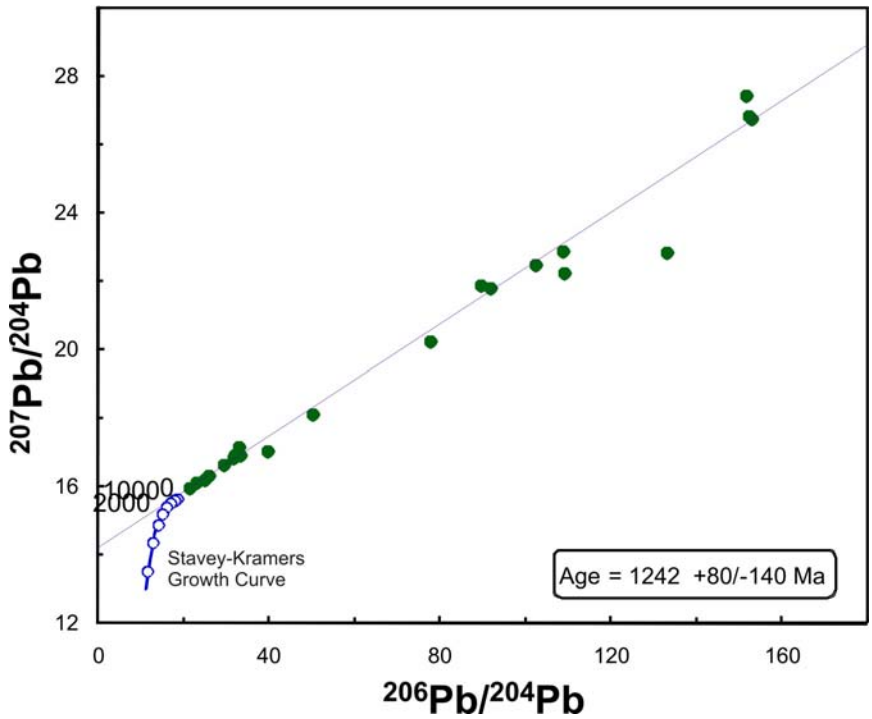

Figure 6.7 Pb-Pb whole-rock isochron for the Mesoproterozoic magmatic rocks of the Mt Painter Province. Stavey-Kramers model after Stavey and Kramers (1975).

6.4 Pb isotopes in K-feldspar

Using whole-rock Pb isotopes to study the magmatic origin of Mt Painter igneous rocks is difficult because U and Pb are relatively mobile during metamorphism and hydrothermal alteration that subsequently affected these rocks. A potential solution to this problem is to analyse minerals characterised by low U/Pb ratio such as alkali feldspar. K-feldspars containing low U and Th contents and high Pb contents should be insensitive to late U mobility and better preserve the initial lead ratios, and so can potentially be used to trace magmas and petrogenetic processes.

6.4.1 Result

Ten potassium feldspar samples from the Mesoproterozoic Mt Painter granitic and volcanic rocks were selected for the Pb isotope including Pepegoona Volcanic (MN004 and MN067), Mt Neill Granite (MN001 and MN039), Box Bore Granite (SD008 and SD010), Terrapinna Granite (MN100), Wattleowie Granite (BB02), Yerila Granite (SD022) and microgranular enclave of Yerila Granite (SD043). The K-feldspars from these rocks have variable concentrations of U and Pb. The U concentration ranges between 1 and 8 ppm and the Pb concentration ranges between 6 and 60 ppm with Pb/U ratios ranging from 2 to 99 (Table 6.2). The $^{206}Pb/^{204}Pb$, $^{207}Pb/^{204}Pb$ and $^{208}Pb/^{204}Pb$ ratios from these analyses are fairly consistent. The measured $^{206}Pb/^{204}Pb$ ratios mainly range from 19.970 to 39.388; the measured $^{207}Pb/^{204}Pb$ ratios largely range from 15.809-17.886; the $^{208}Pb/^{204}Pb$ ratios of most samples range from 39.439-62.493 with average of 49.197. Only two samples (MN100 and SD022) display extremely high values of $^{206}Pb/^{204}Pb$ (98.807 and 83.454), $^{207}Pb/^{204}Pb$ (24.021 and 22.670) and $^{208}Pb/^{204}Pb$ (100.913 and 97.766).

6.4.2 Discussion of Pb isotopes in K-feldspar

U and Pb concentrations and $^{206}Pb/^{204}Pb$, $^{207}Pb/^{204}Pb$ and $^{20}Pb/^{204}Pb$ ratios for the K-feldspars generally vary, the Pb isotopic ratios fall on the same line on the $^{207}Pb/^{204}Pb$ versus $^{206}Pb/^{204}Pb$ diagram (Figure 6.8) suggesting close systems. Therefore, the K-feldspar Pb isotopic compositions

can be used as an estimate of the initial lead isotope ratios in parent magma and in the source. The K-feldspars have same Pb-isotope compositions as the granite melts at the time they were crystallized and separated. Isochron ages between high $^{206}Pb/^{204}Pb$ and low $^{206}Pb/^{204}Pb$ are different. The low $^{206}Pb/^{204}Pb$ group ($^{206}Pb/^{204}Pb<41.689$) yields a Pb-Pb isochron age for the K-feldspars of 1660 (+120/-310) Ma, which overlap with the magmatic ages of the HHP granites and associated rocks. The high $^{206}Pb/^{204}Pb$ group ($^{206}Pb/^{204}Pb>82.833$) yields a Pb-Pb isochron age for the K-feldspars of 2234 (+360/-390) Ma, which may record a prehistory. The 2.22 Ga isochron age of the K-feldspar may suggest that pre existing continental crust source is one an important source generating the HHP granites. However, a Pb-Pb isochron age for both groups is 1761±41 Ma (Figure 6.8), which may suggests a reservoir-separation date for the K-feldspars. The 1.76 Ga isochron age may record the time when a pre-existing crustal source (2.22 Ga?) melted.

Table 6.2 Pb isotopic data for K-feldspar from felsic igneous rocks of Mount Painter Province

Sample	Suite	Pb ppm	U ppm	$^{206}Pb/^{204}Pb$	2SE	$^{207}Pb/^{204}Pb$	2SE	$^{208}Pb/^{204}Pb$	2SE
BB02	WG	10	1	26.322	0.003369	16.353	0.002303	47.4321	47.432
MN001	MN	20	3	35.988	0.007171	17.467	0.001937	51.8137	51.814
MN004	PV	7	4	29.920	0.009851	16.633	0.005358	44.9303	44.930
MN039	MN	60	1	19.970	0.008801	15.809	0.008195	39.4390	39.439
MN067	Vol	9	6	34.780	0.148055	17.063	0.073618	47.9915	47.992
MN100	TG	31	8	98.808	0.013961	24.021	0.003279	100.9136	100.914
SD008	BB	12	1	39.388	0.006488	17.886	0.003889	62.4938	62.494
SD010	BB	11	1	32.450	0.112267	17.173	0.00703	49.1914	49.191
SD022	YG	36	6	83.455	0.01113	22.670	0.002921	97.7658	97.766
SD043	ME	6	4	36.489	0.010538	17.401	0.005447	50.2822	50.282
SD046	ME	67	10	22.674	0.004861	15.921	0.001007	38.3312	38.331

PV: Pepegoona Volcanic, MN: Mt Neill Granite , BB: Box Bore Granite, TP: Terrapinna Granite, WT: Wattleowie Granite , YG: Yerila Granite, ME: microgranular enclave.
Pb isotope values for all samples corrected for mass fractionation of 0.0010 amu.

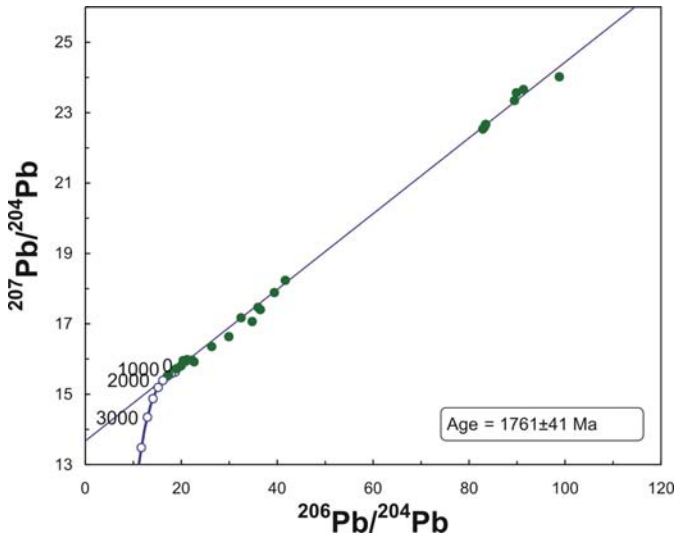

Figure 6.8 Pb-Pb K-feldspar isochron for the Mesoproterozoic magmatic rocks of the Mt Painter Province.

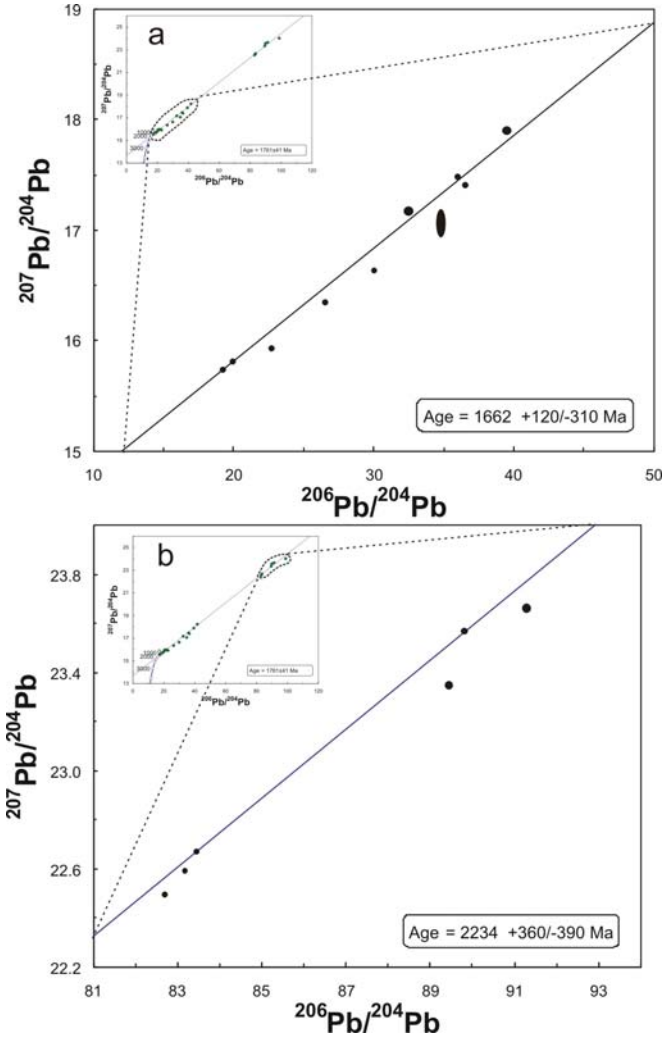

Figure 6.9 Pb-Pb K-feldspar isochron for the Mesoproterozoic magmatic rocks of the Mt Painter Province; a) low $^{206}Pb/^{204}Pb$ group and b) high $^{206}Pb/^{204}Pb$ group

Some K-feldspars have high U and Th contents, which are observed in the Yerila granite, Mount Neill granites and Pepegoona volcanic K-feldspars (data from this study and Neumann, 2001) reflecting U- and Th-enriched sources of the K-feldspars. There are two factors that may have caused the U- and Th-enriched K-feldspars.

- Firstly, a U-Th rich protolith could be generated during an extended time gap between crystallization and high-grade metamorphism (Halla, 2005).
- A second possibility is a time gap between U-enrichment and melt generating in the source (e.g. by subduction-related slab dehydration processes and melting; Halla, 2005).

The first factor could possible cause the U- and Th-enriched K-feldspars because the basement protolith of the Mt Painter Province are high-grade metamorphisms (sillimanite bearing metasediments).

For the second factor, the K-feldspar isochron age for all data of 1761±41 Ma is significantly older than the magmatic U-Pb ages which may indicate an extended time gap between formation of a U- and Th-enriched source and melting causing the U- and Th-enriched K-feldspar.

Crustal contamination through the remelting of pre-existing crust and/or assimilation of crust in mantle-derived magmas is an important process for producing the HHP granites and associated rocks. The K-feldspar isochron age of ~1.76 (±0.4) Ga, which could be ralated to a collision of the Archaean nuclei of the Gawler Craton with the southeastern margin of the central Australia along the Kimban Orogen (*ca* 1.74-1.69 Ga; Hand et al, 2007), may suggest the time of melt generating. The unusally long (~200 Ma) HHP melt residence time in the crust could possibly cause by the extension during Kimban Orogeny, which resuted in crustal melting.

6.5 Hf isotopes of zircon

Hf isotopes in zircons can use as a tracer for crustal evolution (e.g. Davis et al., 2005; Hawkesworth and Kemp, 2006) and magmatic processes (Kemp et al., 2005; Yang et al., 2007). Zircon naturally contains relative low Lu concentration but high Hf concentration with very low Lu/Hf ratios,

therefore they retain close to their initial Hf isotopic compositions. Combining Lu-Hf isotopes with U-Pb dating of single zircon is a useful tool for studying the evolution of crustal reservoirs and crustal growth over time (e.g. Nebel et al., 2007; Scherer et al., 2007). Hf isotope analysis in zircon was undertaken by MC-LA-ICPMS at GEMOC, Macquarie University. The calculation of ε_{Hf} for this study is adopted from Scherer et al. (2001) using a decay constant for ^{176}Lu of 1.865 x $10^{-11}y^{-1}$. Present-day chondritic values of $^{176}Hf/^{177}Hf$ = 0.033200 and $^{176}Lu/^{177}Hf$ = 0.282772 were used for this study (Blichert-Toft and Albarede, 1997). To calculate depleted mantle model ages (T_{DM}), a present day $^{176}Hf/^{177}Hf$ = 0.283250 (Nowell et al., 1998) and $^{176}Lu/^{177}Hf$ = 0.038400 (Griffin et al., 2000; see Appendix 6 for a full description of the methodology). Zircons were selected for Lu-Hf analyses that were <10% discordant when they were U-Pb dated using LA-ICPMS (see Chapter 4). Combination of the $^{207}Pb/^{206}Pb$ minimum formation ages and Hf isotope within same zircon grains yields important information about the petrogenesis of Mt Painter igneous rocks.

6.5.1 Result

Lu-Hf isotopes were measured in 172 zircons, extracted from twelve mafic and felsic samples.

Fourteen zircons from sample MN003 (Pepegoona Volcanic), with $^{207}Pb/^{206}Pb$ ages ranging from 1587 to 1622 Ma yielded variable εHf values ranging from -3.1 to +4.1 (Figure 6.10; Table 6.3) with average of +0.8; median of +1.0; standard derivation of +1.7, corresponding to initial $^{176}Hf/^{177}Hf$ ratios of 0.281666-0.2818786.

The Mt Neill Granite has a slightly younger Pb/Pb zircon crystallization age than the Pepegoona Volcanic. Fifteen Mt Neill zircons from sample MN029 selected for Hf isotope analyses yield U-Pb ages ranging from 1575 to 1625 Ma. The εHf from the Mt Neill Granites is ranging from -1.2 to +4.2 with average of +1.4; median of +1.6; standard derivation of +1.4, corresponding to initial $^{176}Hf/^{177}Hf$ ratios of 0.281777-0.281880.

The εHf analyses of seventeen zircons from the Box Bore Granite (sample SD015) have a wide range of εHf from -9.3 to +2.1 with average of -

1.7; median of -0.3; standard derivation of +3.9, corresponding to initial $^{176}Hf/^{177}Hf$ ratios of 0.281653-0.281901.

The measured Hf isotopes in zircons from the Terrapinna Granite (n=11) gives εHf values ranging from -0.3 to +3.7 with average of +1.6; median of +1.3; standard derivation of +1.3, corresponding to initial $^{176}Hf/^{177}Hf$ ratios of 0.281825 and 0.281810.

Eighteen zircons from the Wattleowie Granite yield a wide range of ε_{Hf} values from -4.1 to +4.2 with average of +0.3; median of +0.1; standard derivation of +2.4, corresponding to initial $^{176}Hf/^{177}Hf$ ratios of 0.281360 to 0.281910. Analyses of zircons from the Yerila Granite yield εHf values ranging from of -2.9 to +4.2 with average of +1.0; median of +1.5; standard derivation of +2.1, corresponding to initial $^{176}Hf/^{177}Hf$ ratios of 0.281833 and 0.282161.

Zircons from the microgranular enclaves of the Yerila Granite (n=39 from sample SD047 and 050) ages ranging from 1450-1693 Ma. Hf isotope compositions have wide ranges; εHf values vary from ε_{Hf} (1497 Ma) of -12.9 to +12.8 with average of +0.8; median of +0.6; standard derivation of +3.5, corresponding to initial $^{176}Hf/^{177}Hf$ ratios of 0.281729 to 0.282045.

Zircons from the Mesoproterozoic mafic dykes from sample MN084, SD031 and SD057 were analysed for Hf isotope compositions. Zircons from sample MN084 have U-Pb crystallization ages between 1565 and 1685 Ma and they yield εHf values ranging from -9.2 to +5.1 with average of +0.8; median of +0.8; standard derivation of +4.2, corresponding to initial $^{176}Hf/^{177}Hf$ ratios of 0.281620 and 0.281912. Hf isotope analysis from sample SD031 (n=16) were on zircons with U-Pb ages ranging from 1558 to 1638 Ma, εHf values between -1.6 and +6.4 with average of +1.3; median of +1.1; standard derivation of +1.9, correspond to initial $^{176}Hf/^{177}Hf$ ratios from 0.281844 to 0.282013. Fifteen zircons from a younger mafic dyke (sample SD057) have U-Pb ages from 1425 to 1625 Ma and ε_{Hf} from -3.4 to +3.0 with average of +1.2; median of +1.7; standard derivation of +1.1, corresponding to initial $^{176}Hf/^{177}Hf$ ratios of 0.281782 and 0.281840.

Table 6.3 Selected Lu-Hf isotopic data in zircons form the mafic-felsic igneous rocks of the Mt Painter Province.

Sample_spot	Unit	Hf^{176}/Hf^{177}	1 S.D.	Lu^{176}/Hf^{177}	Yb^{176}/Hf^{177}	U/Pb Age (Ma)	εHf	T(DM) (Ga)
MN003_01	PV	0.281840	0.000010	0.00080	0.04134	1621	+2.2	1.97
MN003_03	PV	0.281687	0.000011	0.00069	0.03447	1622	-3.1	2.18
MN003_55	PV	0.281763	0.000015	0.00062	0.03457	1601	-0.8	2.07
MN003_06	PV	0.281926	0.000043	0.00159	0.07557	1606	+4.1	1.89
MN003_14	PV	0.281826	0.000010	0.00120	0.06460	1587	+0.5	2.01
MN003_166	PV	0.281851	0.000014	0.00138	0.05107	1604	+1.6	1.99
MN029_03	MN	0.281833	0.000011	0.00133	0.07063	1585	+1.6	2.02
MN029_05	MN	0.281822	0.000011	0.00053	0.02839	1600	+2.4	1.92
MN029_06	MN	0.281845	0.000010	0.00070	0.03793	1585	+1.8	1.97
MN029_07	MN	0.281866	0.000013	0.00084	0.04488	1614	+4.2	1.87
MN029_08	MN	0.281835	0.000011	0.00087	0.04791	1585	+0.0	2.03
MN029_09	MN	0.281854	0.000010	0.00059	0.03098	1583	-1.2	2.06
SD015_05	BB	0.281845	0.000011	0.00116	0.06635	1578	+1.1	1.99
SD015_07	BB	0.281847	0.000009	0.00095	0.05576	1574	+1.3	1.97
SD015_88	BB	0.281831	0.000011	0.00219	0.11771	1590	-0.3	2.06
SD015_14	BB	0.281854	0.000078	0.01113	0.81232	1571	-9.3	2.68
SD015_16	BB	0.281865	0.000020	0.00218	0.11514	1577	+0.7	2.01
MN101_01	TP	0.281867	0.000010	0.00174	0.09372	1575	+0.6	1.96
MN101_02	TP	0.281469	0.000015	0.00188	0.09734	1587	+1.3	1.93
MN101_03	TP	0.281735	0.000059	0.00391	0.15569	1893	+0.9	1.93
MN101_04	TP	0.281898	0.000037	0.00294	0.16816	1576	+1.2	1.92
MN101_06	TP	0.281879	0.000006	0.00138	0.06971	1602	+2.9	1.87
SD047_01	ME	0.281872	0.000011	0.00140	0.07232	1526	+3.0	1.85
SD047_06	ME	0.281937	0.000011	0.00136	0.05907	1522	-1.6	2.05
SD047_07	ME	0.281936	0.000018	0.00129	0.06270	1538	+0.9	1.92
SD049_04	ME	0.281836	0.000018	0.00208	0.13670	1486	+2.2	2.00
SD049_08	ME	0.281874	0.000013	0.00068	0.03471	1514	-0.6	2.02
SD050_03	ME	0.281875	0.000009	0.00137	0.06566	1520	-1.1	2.08
SD050_04	ME	0.281887	0.000010	0.00117	0.05367	1512	+1.8	1.97
SD050_14	ME	0.281893	0.000009	0.00116	0.05547	1535	-0.1	2.04
SD050_15	ME	0.281890	0.000015	0.00131	0.06282	1534	+1.1	1.94
SD060_01	YG	0.281851	0.000010	0.00135	0.06516	1502	+2.2	1.96
SD060_02	YG	0.281910	0.000015	0.00223	0.11557	1518	-0.2	1.98
SD060_03	YG	0.281833	0.000016	0.00372	0.18564	1616	+3.7	1.96
SD060_04	YG	0.281897	0.000012	0.00137	0.06963	1664	+0.1	2.04
SD060_05	YG	0.281894	0.000011	0.00403	0.24105	1546	-1.8	2.11
SD022_01	WG	0.281875	0.000012	0.00288	0.15576	1569	+1.5	1.99
SD022_02	WG	0.281805	0.000013	0.00236	0.16208	1568	-2.1	2.13
SD022_05	WG	0.281860	0.000008	0.00107	0.05827	1551	-0.1	2.00
SD022_07	WG	0.281883	0.000008	0.00059	0.03139	1541	+1.9	1.92
SD022_08	WG	0.281875	0.000007	0.00107	0.06307	1559	+1.1	1.99
MN084_01	MF	0.281834	0.000022	0.00088	0.04738	1583	+1.4	1.98
MN084_04	MF	0.281760	0.000029	0.00208	0.12157	1585	-2.2	2.07
MN084_05	MF	0.281792	0.000014	0.00155	0.07241	1615	+0.3	1.96

Table 6.3 (continued) Selected Lu-Hf isotopic data in zircons form the mafic-felsic igneous rocks of the Mt Painter Province

Sample_spot	Unit	Hf^{176}/Hf^{177}	1 S.D.	Lu^{176}/Hf^{177}	Yb^{176}/Hf^{177}	U/Pb Age (Ma)	εHf	T(DM) (Ga)
MN084_06	MF	0.281858	0.000018	0.00066	0.03255	1573	+0.8	1.94
MN084_07	MF	0.281912	0.000014	0.00043	0.02142	1572	+5.1	1.76
SD057_01	MF	0.281861	0.000010	0.00103	0.04326	1510	+1.7	1.88
SD057_03	MF	0.281843	0.000011	0.00065	0.03085	1520	-0.7	2.00
SD057_04	MF	0.281859	0.000015	0.00062	0.02891	1519	-3.4	2.02
SD031_06	MF	0.281905	0.000009	0.00157	0.07959	1562	-1.6	1.94
SD031_07	MF	0.281861	0.000010	0.00126	0.06536	1590	-0.3	1.92
SD031_08	MF	0.281962	0.000011	0.00206	0.10348	1575	-0.6	1.99
SD031_09	MF	0.281843	0.000012	0.00197	0.09748	1572	+0.5	1.95

Hfi = 176Hf/177Hf ratio - (176Lu/177Hf ratio * (EXP(0.0193 * 207Pb/206Pb ratio / 1000)$^{-1}$))
^{176}Lu decay constant (1.865x10^{-11}); Scherer et al. (2001)
PV: Pepegoona Volcanic, MN: Mount Neill Granite , BB: Box Bore Granite, TP: Terrapinna Granite, WT: Wattleowie Granite , YG: Yerila Granite, ME: microgranular enclave, MF: Mafic dyke.

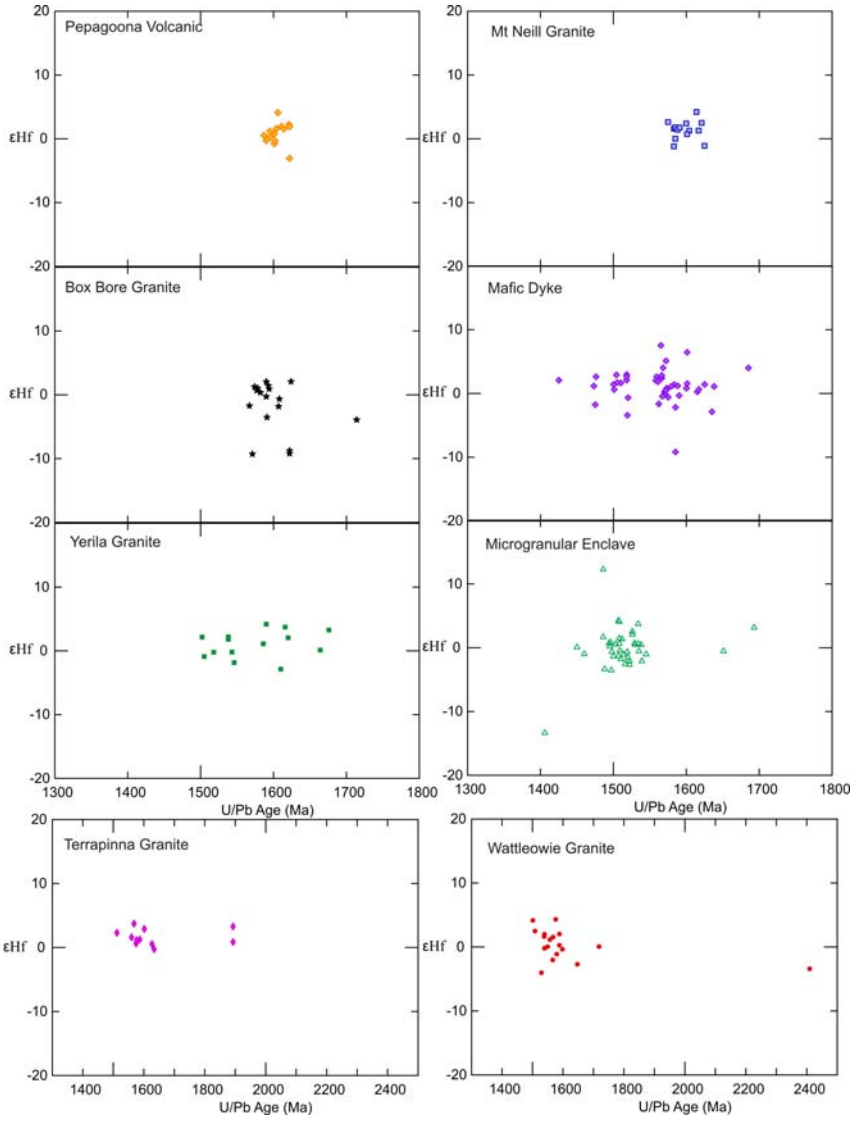

Figure 6.10 εHf values versus U-Pb zircon ages of the Mt Painter mafic and felsic igneous rocks.

6.5.2 Discussion of Hf isotopes

Hf isotope ratios were measured zircons from thirteen samples within different mafic and felsic suites of Mesoproterozoic igneous rocks from Mount Painter. Hf isotope compositions of selected zircons, which yield Pb/Pb crystallization ages from 1406 to 2411 Ma (majority from 1475 to 1650 Ma), have initial $^{176}Hf/^{177}Hf$ ratios over a narrow range from 0.28136 to 0.282161. The εHf values show large variation from -12.9 to 12.8, with a weighted mean of 0.73.

Sixty percent of the zircons have positive εHf values and plot close to the depleted mantle curve (Figure 6.11), suggesting that the primary sources of these zircon contained a significant amount of mantle-derived magma components. The zircons from microgranular enclaves and the mafic dykes have realtively high εHf values compared to the other felsic suites suggesting very juvenile crustal or mantle sources. However, most of results are lower than the DM line, only one zircon from microgranular enclave plots above the DM line. Therefore, the Mesoproterozoic granitic and associated rocks cannot represent products of juvenile mantle melts; if they had they would have εHf values close to the depleted-mantle evolution curve (e.g., values of about +10 to +11 at ~1.55 Ga). A mixing of material from the depleted mantle and older crust and/or lithosphere is necessary to account for the Hf isotopic data. The crustal sources may add into depleted-mantle magmatic sources through restite separation, wall-rock assimilation or magma mixing.

The microgranular enclaves have been interpreted that are not a restitic origin (see Chapter 2 and 3). Therefore, restite separation is unlikely to have produced the zircon Hf isotopic variations. Some granites and volcanic rocks have inherited zircons, potentially indicating wall-rock. Reaction between magma and its wall rocks could result in isotopic variations during crystallization of magmas. However, a small variation in εHf values and lack of inherited zircons from the basements in the HHP granities and associated rocks suggests that reaction between the magma and its wall-rock is not significant.

Zircon Hf model age on interpreted zircons could provide an age of source rocks because radiogenic Hf isotopes in the zircons can survive partial

melting (Kemp et al., 2006; Nebel et al., 2007). A model age (T_{DM}) of the zircons, which gives a minimum age for the source material of the magma from which the zircon crystallised, is ranging between 1.55 and 2.68 Ga with peak values around 1.85 to 2.10 Ga (Figure 6.12). This suggests that the parental magma was derived from reworking of the juvenile material added during Late Archaean to Palaeoproterozic Era.

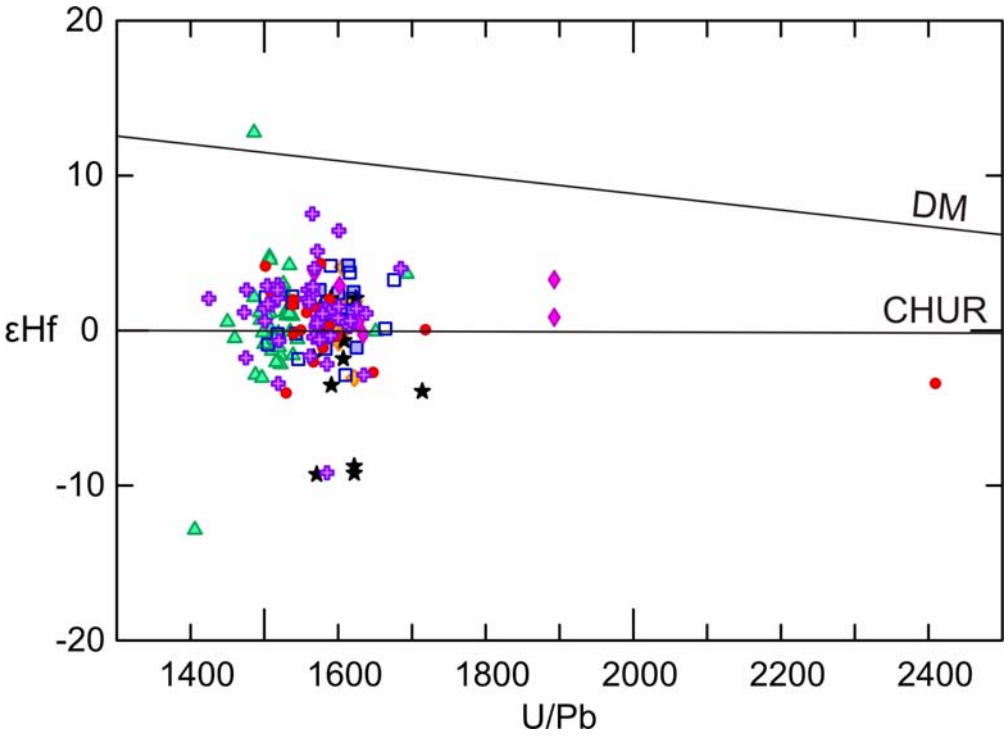

Figure 6.11 εHf versus crystallization ages of the Mt Painter mafic and felsic zircons.

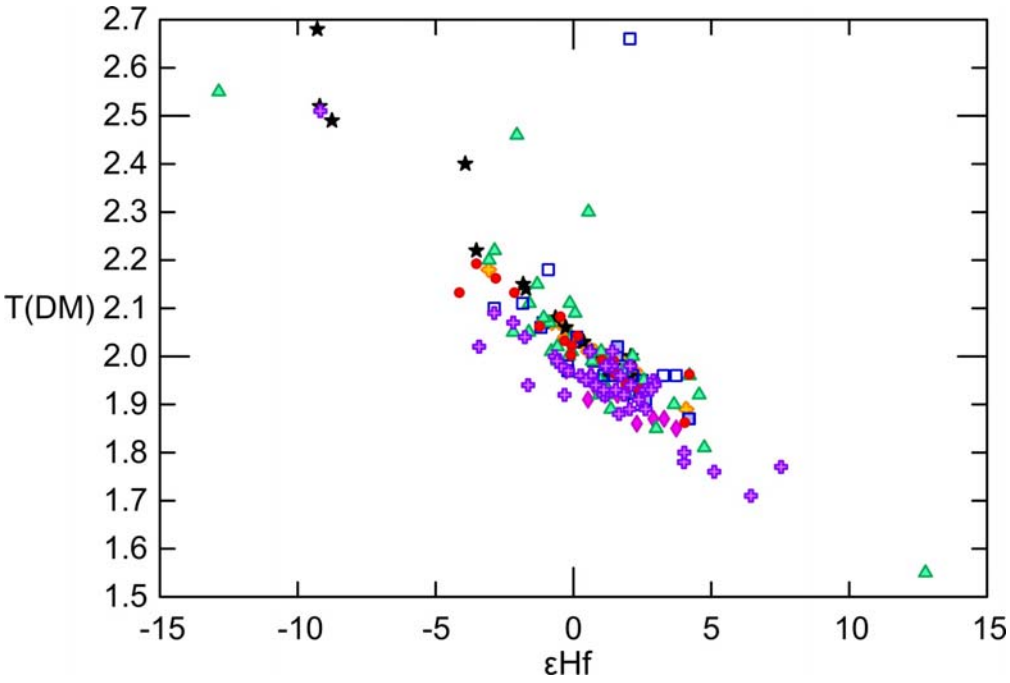

Figure 6.12 εHf values versus model ages (T_{DM}) of the zircons of the Mt Painter mafic and felsic zirconss.

6.6 Summary

The whole rock Nd-Sm, K-feldspar Pb-U and zircon Lu-Hf isotopic compositions of the granitic and associated rocks from the Mt Painter Province are consistent suggesting that these rocks were derived from homogeneous sources. Mixing between mantle-derived magmas and crustal sources together with extreme fractionation crystallization is required to produce the εNd and εHf values and large amount of trace elements in these rocks. Partail melting of the lower crust mixed with mantle-derived mafic magma at the deep hot zone is preferred to explain a relatively narrow range of isotopic signatures and enriched U and Th melts for the granitic and associated rocks. These rocks were affected by ~1.2 Ga thermal event (the Musgrave Event) as recorded in the Rb-Sr and Pb whole-rock isotopes.

Chapter 7 Petrogenesis of the HHP granites and associated rocks from Mt Painter Province

7.1 Typology

In this section, the HHP granites will be classified following a traditional alphabet granitic classification as I-, S-, and A-type granites (e.g. Chappell and White, 1974; Collins, 1982; Pitcher, 1983). P_2O_5 and Na_2O contents are used as criteria to identify S-type granites as they commonly contain much higher P_2O_5 and lower Na_2O than other granite types. Moreover, S-type granites show increasing P_2O_5 with fractionation, and are always peraluminous (Chappell and White, 1992). The Mesoproterozoic mafic and felsic rocks of the Mt Painter Province are characterised by low P_2O_5 and high Na_2O contents and do not contain garnet, cordierite, and sillimanite, therefore they are not S-type.

Discriminating between A-type and I-type granites is not simple. The Mt Painter granites which contain high Fe/Fe+Mg, Ga, Zn and HFSE (e.g. Zr, Nb and Y) could be grouped within A-type granites. The Ga/Al vs Zr and Ce discrimination diagrams after Whalen et al. (1987) classify most of the Mt Painter granitic and volcanic rocks as A-type granites (Figure 7.1a and b). A few samples, in particular from the Wattleowie Granite, plot outside the A-type box. These could be a result of crystal accumulation. The FeO/FeO+MgO versus SiO_2 diagram of Frost et al. (2001; Figure 7.2) suggests that the Mt Painter rocks mostly have a ferroan character and can be classified as A-type granite. A few samples that plot in magnesian field, in particular the co-magmatic Mt Neill Granite and Pepegoona Volcanics are affected by alteration.

Comparisons of rare earth patterns of the Mt Painter rocks with well-defined A-type granites from Padthaway and Lachlan Fold Belt (LFB); (Turner et al, 1992; Collins et al., 1982, respectively) show that their REE patterns are similar but the Mt Painter rocks have relatively higher REE concentrations (Figure 7.3). A spider diagram of the Mt Painter igneous rocks compared to LFB A-type granites (Turner et al., 1992; Collins et al., 1982;

Chappell and White 1992; Figure 7.4) show that both have negative anomalies in Ba, Nb, Sr and Ti but the Mt Painter rocks contain much higher element concentrations such as U, Th, Zr and REEs. These observations suggest that the Mt Painter rocks are A-type granites.

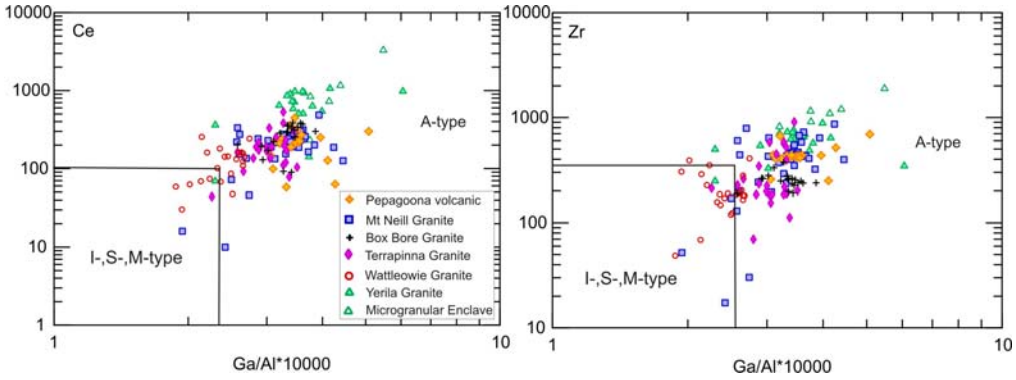

Figure 7.1 Discrimination diagram after Whalen et al., 1987 classifying the Mesoproterozoic granitic and volcanic rocks from Mount Painter Province as A-type granites.

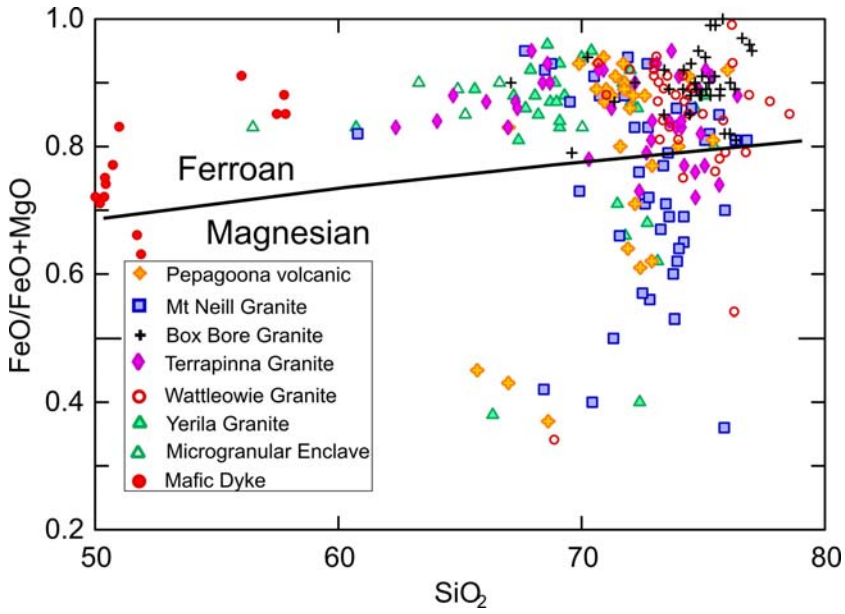

Figure 7.2 Diagram of SiO_2 versus FeO/FeO+MgO after Frost et al. (2001) suggesting the Mt Painter rocks having Ferroan characteristics.

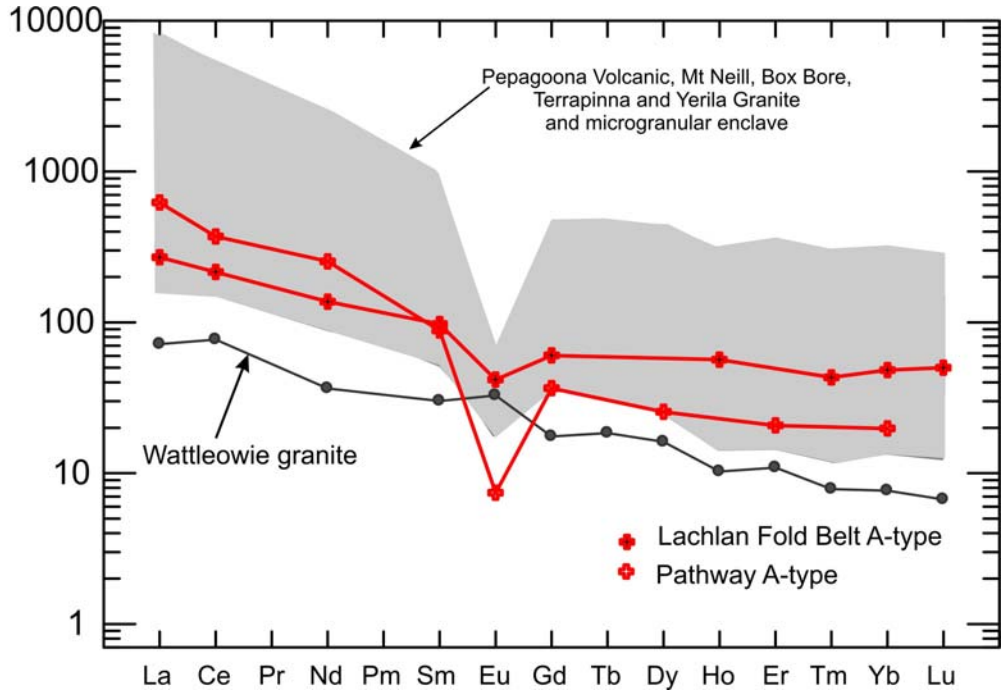

Figure 7.3 REE patterns of the MP rocks comparing to Lachlan Fold Belt A-type granite (data from Turner et al, 1992) and Pathway A-type granite (data from Collins et al., 1982) normalised to values of Sun and McDonald (1989).

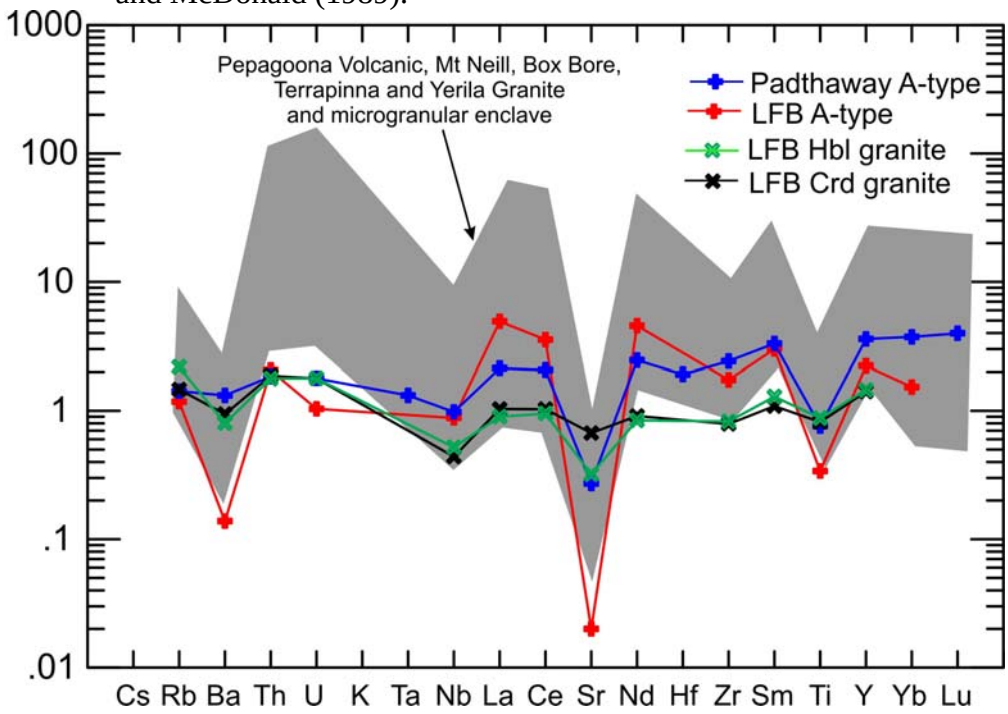

Figure7.4 Spidergram of the Mt Painter rocks comparing to Pathway A-type granite (data from Collins et al., 1982), Lachlan Fold Belt A-type granite (LFB A-type data from Turner et al, 1992), Lachlan Fold Belt hornblende granite (LFB Hbl granite; Chappell and White, 1992) and Lachlan Fold Belt cordierite granite (LFB Crd granite; Chappell and White, 1992) normalised to primordial mantle value of Wood et al. (1979).

Most mafic samples plot within the tholeiitic basalt field however a few Meosproterozoic mafic dykes are classified as alkali basalt due to their high Zr and P_2O_5 concentrations (Figure 7.5). The Mesoproterozoic mafic dykes and mafic microgranular enclaves can be further classified as continental tholeiitic basalt from the Y/Nb versus TiO_2 diagram (Figure 7.6) after Floyd and Winchester (1975).

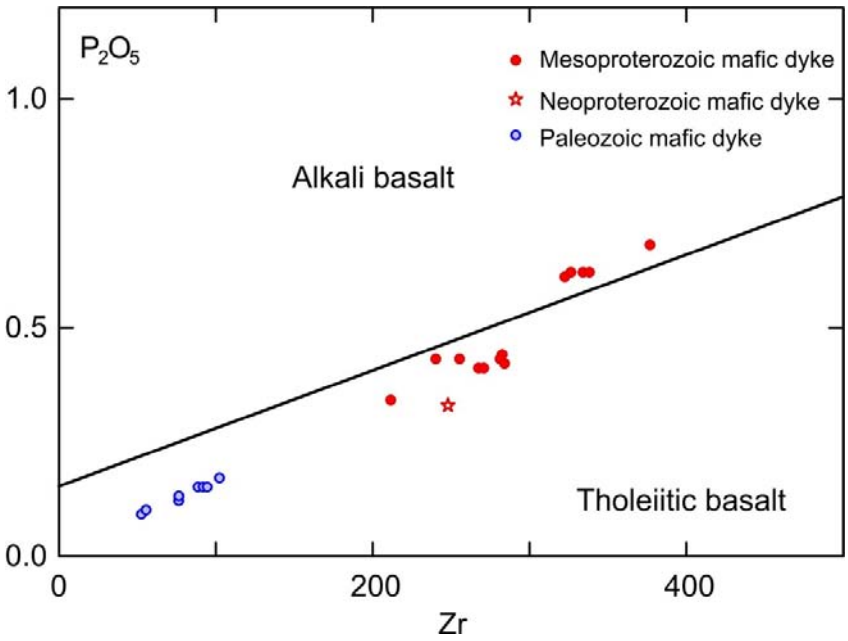

Figure 7.5 Binary plot of Zr versus P_2O_5 for mafic dykes.

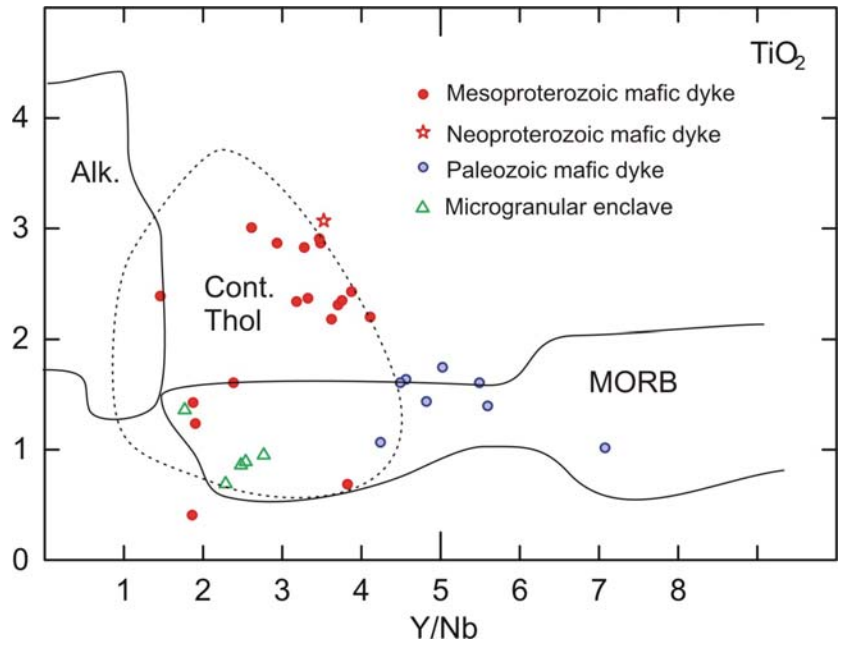

Figure 7.6 The Y/Nb versus TiO_2 discrimination diagram after Floyd and Winchester (1975) for mafic dykes and microgranular enclaves of the Mount Painter Province.

7.2 Tectonic environments

Geochemistry of the Mt Painter granites could be used to identify the tectonic setting of their formation. Discrimination diagrams of Rb, Y and Nb after Pearce et al., (1984) suggest that most granitic and volcanic suites from the Mt Painter province are within-plate granites (Figure 7.7a and b). Using diagrams of Rb, Y and Nb after Pearce et al., (1984) to classify sodic granites such as the Mt Neill and Box Bore Granites could be difficult because of a mobility of Rb. Therefore, scatter plots of geochemical data from some samples from the Mount Neill and Box Bore Granites are the result of Rb mobility. The Wattleowie Granites that are classified as volcanic-arc granites or volcanic arc could be a result of the limitation of Pearce Diagram (Pearce et al., 1984) or affected by crystal accumulation of plagioclase in granites. The plagioclase accumulation in Wattleowie Granite is also found within the REE pattern showing positive Eu anomalies (Figure 5.14).

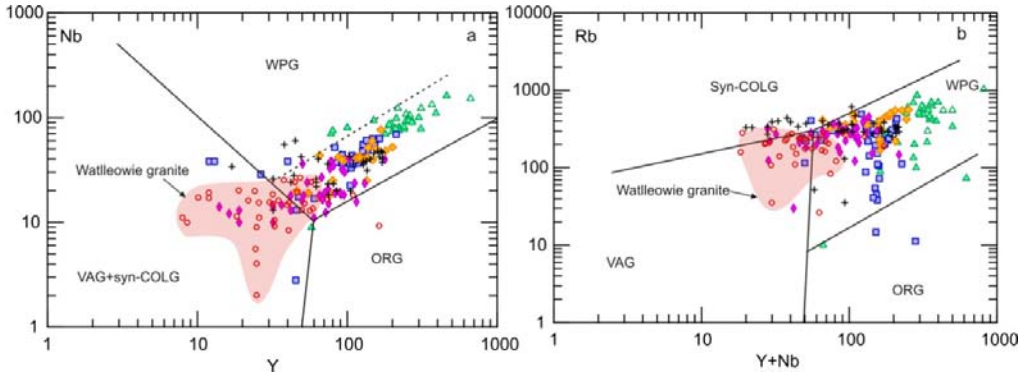

Figure 7.7 Discrimination diagrams for tectonic setting suggesting most MP rocks are within plate granites; a) Y versus Nb and b) Y+Nb versus Rb.

The HHP granites from Mt Painter are classified as A-type and within plate granites, thus implied to be formed in either post-orogenic or anorogenic settings. For further classification, the Rb/Nb versus Y/Nb and Y-Nb-Ce triangular discrimination diagrams of Eby (1992) can be used. These diagrams subdivide A-type granites into 2 classes; A_1, mantle-derived granites emplaced in an anorogenic setting and; A_2 granites, derived from the melting of continental or underplated mafic crust and emplaced in various tectonic environments. The Mt Painter granitic and associated rocks mainly plot within subtype A_2 granite (Figure 7.8). In the tectonic setting R1-R2 discrimination diagram after Batchelor and Bowden (1985; Figure 7.9), the

HHP granites overlap around the syncollision-anatectic field. The Freeling Height Quartzite having maximum depositional age of 1590 Ma is deformed and metamorphosed before the intrusions of the HHP granites, which could be realted to the Kararan Orogeny (*ca.* 1570 to 1540 Ma) in the Northern Gawler Craon. This evidence could indicate that the generation of the Mt Painter HHP granites is possibly in a syncollision-anatectic setting. However, there is no evidence indicating an orogenic event affecting the Mt Painter Province during the Meosproterozoic. Geochemical data of the Mt Painter HHP granites that suggests syncollision-anatectic setting could reflect the magma source characteristics rather than an environmental setting. If this observation is true, the granites could be generated from crust which had been through a cycle of subduction-zone or continental-continent collisional magmatism.

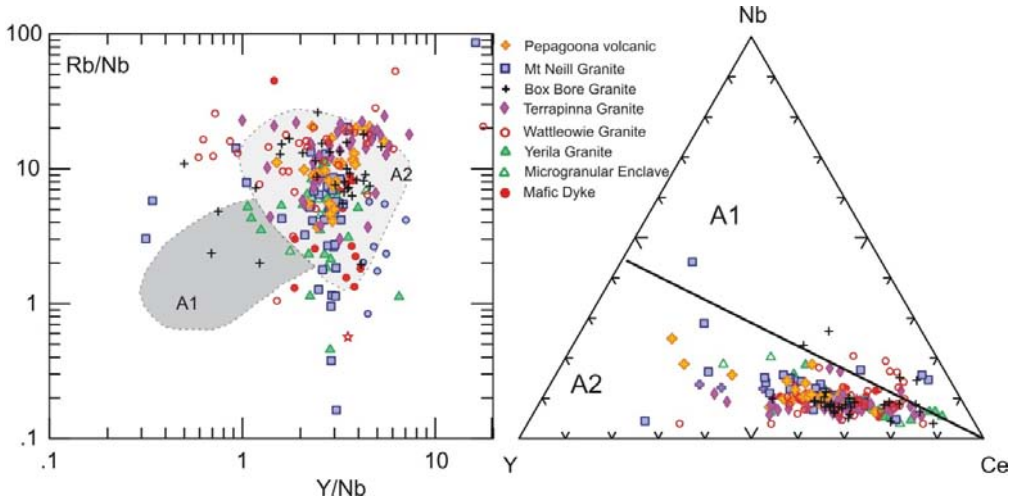

Figure 7.8 Discrimination diagrams for Mesoproterozoic mafic and felsic rocks from the Mount Painter Province suggesting an A2-type tectonic setting a) after Wu et al, 2002 and b) after Eby (1990). Y/Nb versus Rb/Nb and Y-Ce-Nb.

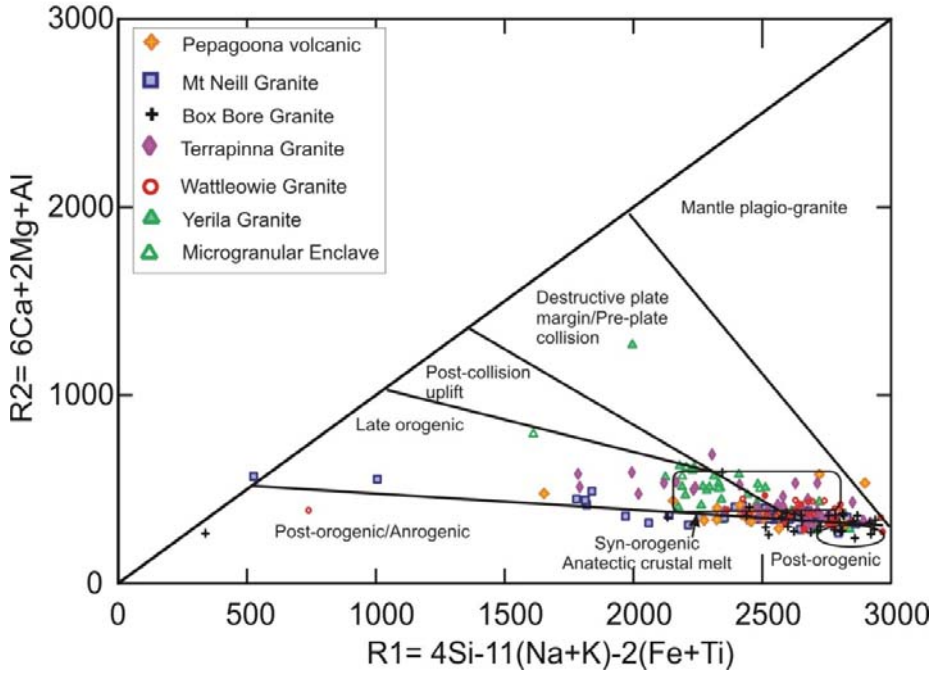

Figure 7.9 R1-R2 tectonic setting discrimination diagram for the HHP granite and associated rocks after Batchelor and Bowden (1985).

On the Zr-Y-Nb basalt discrimination diagram after Meschede (1986 Figure 7.10a), which is designed to differentiate between mid-ocean ridge basalts (MORB) and continental tholeiite, the Mesoproterozoic mafic rocks primarily plot in the volcanic arc basalt and within plate tholeiite fields. On the Pearce and Cann (1973) basalt discrimination diagram, the mafic dykes from Mt Painter mainly plot within the calc-alkaline basalt field (Figure 7.10b). Therefore, geochemical data of the Mt Painter mafic rocks is not suitable for identifying their tectonic settings.

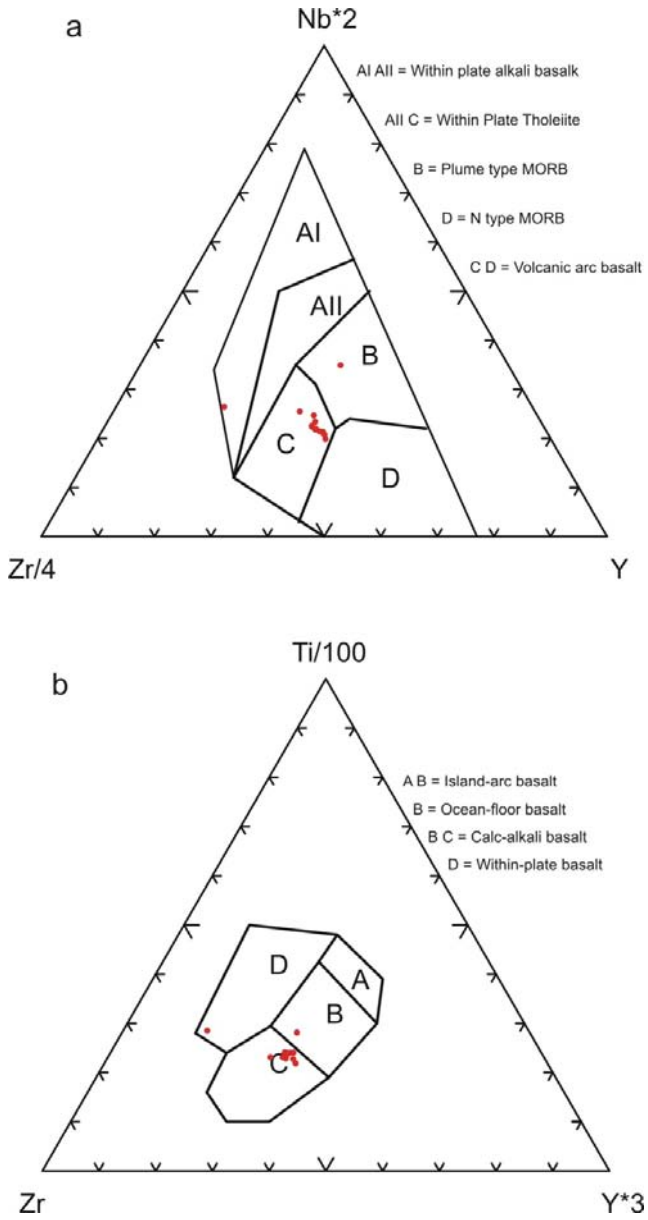

Figure 7.10 Tectonic setting discrimination diagram for the Mesoproterozoic mafic dykes from The Mt Painter Province; a) Zr-Y-Nb diagram after Meschede (1986); b) Zr-Y-Ti after Pearce and Cann (1973).

7.3 Emplacement conditions

The level of emplacement for the microgranular enclaves can be derived in a more quantitative way by using the composition of hornblende, which is temperature and pressure dependent and several calibrations (Hammarstrom and Zen, 1986; Hollister et al., 1987; Johnston and Rutherford, 1989; Blundy and Holland, 1990; Schmidt, 1992; Anderson and Smith, 1995). In hornblende, the total Al content (atoms per 23 oxygens)

increases with pressure and temperature. Application of this thermobarometer requires the mineral assemblage quartz+plagioclase+K-feldspar+hornblende+ biotite+titanite+Fe–Ti oxide phase (Vyhnal et al., 1991), which the mafic rocks and microgranular enclaves from the Mt Painter Province have. The total Al content of hornblende in the microgranular enclaves is consistent. Therefore the hornblende thermobarometer is appropriate to apply to the microgranular enclaves.

The amphibole-plagioclase equilibration thermobarometer (Blundy and Holland, 1990; Vyhnal et al., 1991) for the hornblende of microgranular enclaves estimates corresponding temperatures ranging from 794 to 944 ºC with an average of 843 ºC (Table 7.1) and pressures ranging from 3.6 to 5.9 kbar with an average of 4.7 kbar, equivalent to depths of 11-18 km.

Hornblendes are found in the mafic rocks, which also have the mineral assemblage quartz+plagioclase+K-feldspar+hornblende+biotite+titanite+Fe–Ti oxide phase, however total Al contents of mafic rock hornblende vary widely. The corresponding pressure estimates for the Mesoproterozoic mafic dykes show extremely variations from 0.7 to 10.5 kbar with an average of 6.3 kbar and at temperatures ranging from 355 to 607 ºC. The widely different pressures calculated from the Mesoproterozoic mafic dyke possibly suggest the amphiboles are affected by late hot fluids.

Biotite compositions are used as a geothermometer following the equation of Luhr et al. (1984). The biotite geothermometer provides consistent high temperatures (>870 °C) in each of the rock units (Table 7.2).

Feldspar geothermometers based on synthetic ternary feldspar composition after Deer et al. (1992; detail in Chapter 3) mainly give temperatures of approximately 700 °C, however feldspars from the Yerila Granite and its felsic microgranular enclaves may have crystallized at higher temperatures (800-900 °C).

Table 7.1 Pressure and temperature estimates from amphiboles-plagioclase equilibration thermobarometer of microgranular enclaves and mafic dykes after Anderson and Smith (1995); Holland and Blundy, 1994.

Sample	Spot	Unit	T (C)	P(Kb)
MN096	Mn96_02	Enclave	944	
MN096	Mn96_03	Enclave	822	4.8
MN096	Mn96_04	Enclave	862	3.6
MN096	Mn96_05	Enclave	795	5.9
MN096	Mn96_06	Enclave	808	5.2
MN096	Mn96_07	Enclave	824	5.1
MN096	Mn96_08	Enclave	860	3.6
MN096	Mn96_09	Enclave	829	4.8
average			843	4.7
Standard division			44	0.8
Median			827	4.8
MN090	Mn91_01	Mafic Dyke	589	8.2
MN091	Mn91_02	Mafic Dyke	509	6.9
MN092	Mn91_06	Mafic Dyke	436	2.7
MN093	Mn91_08	Mafic Dyke	515	7.1
MN094	Mn91_10	Mafic Dyke	493	6.8
MN095	Mn91_11	Mafic Dyke	421	1.2
MN096	Mn91_12	Mafic Dyke	548	8.4
MN097	Mn91_13	Mafic Dyke	607	10.5
MN098	Mn91_14	Mafic Dyke	562	9.0
MN099	Mn91_15	Mafic Dyke	405	0.7
MN100	Mn91_20	Mafic Dyke	355	
MN101	Mn91_21	Mafic Dyke	560	7.7
MN102	Mn91_23	Mafic Dyke	392	1.3
MN103	Mn91_26	Mafic Dyke	530	6.9
MN104	Mn91_27	Mafic Dyke	544	9.1
MN105	Mn91_28	Mafic Dyke	536	8.2
average			500	6.3
Standard division			76	3.2
Median			523	7.1

Zircon saturation thermometry, which is calculated from the Zr concentration in a bulk rock analysis (Watson and Harrison, 1983), provides an estimate of melt temperatures. Saturation temperatures for zircons from the Mesoproterozoic mafic and felsic igneous rocks of the Mt Painter Province fall within the range of 703 to 1059 °C (Appendix 5). The Yerila Granite and its enclaves display the highest zircon saturation temperatures among the mafic and felsic rocks. Most Mesoproterzoic samples are ‘hot granite’ with respect to their high temperatures (>800 °C), which is typically found in inheritance-poor granitoid (Miller et al., 2003). These zircon saturation temperatures from the Mesoproterozoic samples are consistent with felsic

magma generation models including; dehydration melting in crust; fractionation of mantle melt with or without crustal contamination, and with the transport of magma in crystal-poor states. The calculated maximum zircon saturation temperatures are possibly greater than the real values because the Mesoproterozoic mafic and felsic rock contain some inherited zircons (see Miller et al., 2003). A binary diagram of Zr versus SiO_2 (Figure 7.11) shows a positive correlation at SiO_2 contents less than ~65 wt% suggesting Zr undersaturation; but a negative correlation at SiO_2 contents of more than 65 wt% suggesting zircon fractionation crystallization. The microgranular enclave (SD050), which plots at the zircon saturated point (Figure 7.11), can be used to calculate zircon saturation temperature, giving a zircon saturation temperature for the HHP Mt Painter melts of 986 ºC. However, this temperature may be unrealistic if zircons are accumulated. The spidergram for the Yerila Granite and its enclave exhibits negative Zr anomalies suggesting no zircon accumulation (Figure 7.12). Exceptionally, one sample of the microgranular enclave (SD049) shows a positive Zr anomaly indicating zircon accumulation, which has extremely high Zr concentration (1886 ppm). The Zr cumulating sample is not included in the calculated zircon saturation temperature.

Table 7.2 Representative or average of hornblende-plagioclase and biotite geothermometers and zircon saturation temperatures.

Unit	Temperature (°C)			
	Hornblende-plagioclase (average)	Biotite	Zircon (average)	Pressure (kbar) Hornblende-plagioclase (average)
Pepegoona Volcanic	-	885	886	
Mt Neill Granite	-	877	871	
Box Bore Granite	-	888	820	
Terrapinna Granite	-	-	819	
Wattleowie Granite	-	-	796	
Yerila Granite	-	895	913	
Microgranular enclave	843	870	975	4.7
Mesoproterozoic mafic dyke	615	928	765	6.3

Hornblende-plagioclase geothermometer using calculation of Blundy and Holland (1990), biotite geothermometer using calculation of Luhr et al. (1984); and average zircon saturation temperature using calculation of Watson and Harrison (1983).

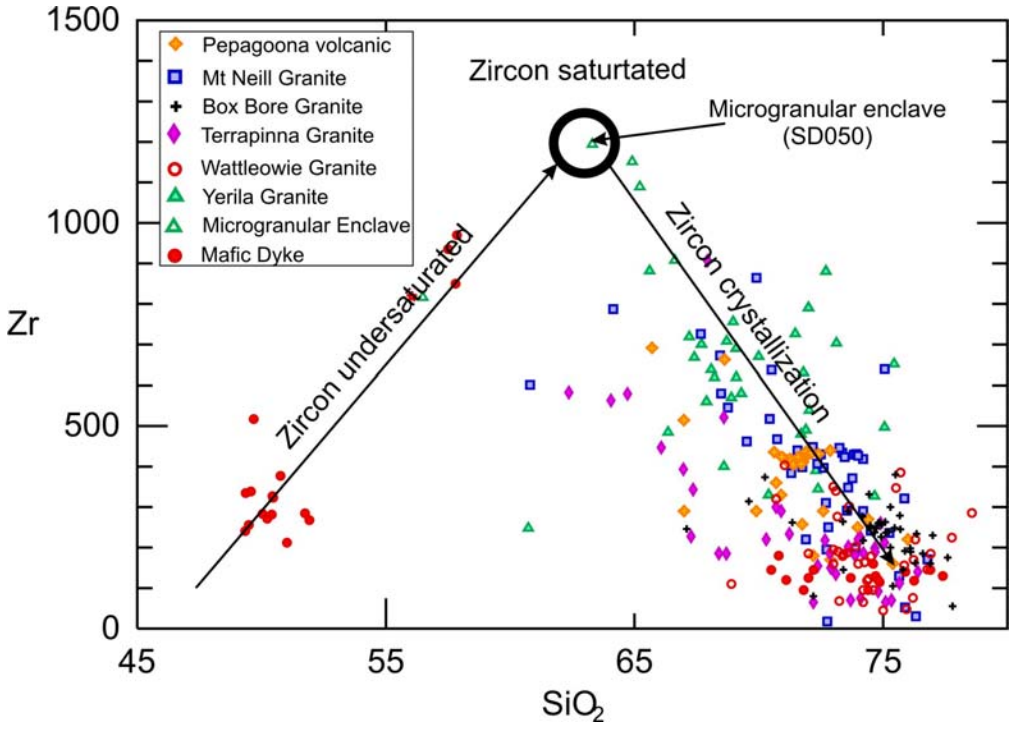

Figure 7.11 Binary plot of Zr versus SiO2 showing zircon saturation point.

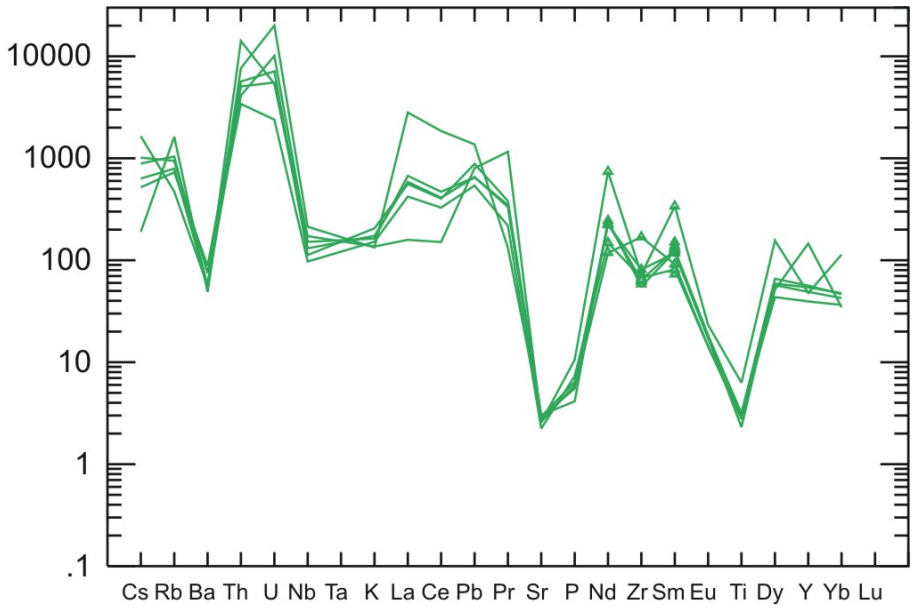

Figure 7.12 Spider diagrams for the Yerila Granite and microgranular enclave normalized to Sun and McDonald, 1989.

An accurate value of water activity cannot be calculated here; however there is evidence that suggests water-poor melt conditions applied for the HHP Mt Painter rocks. It includes; positive Eu anomalies in the REE pattern in K-feldspars (see Chapter 3), the appearance of magnesiumhastingite, and paragenesis of hornblende and biotite within the microgranular enclave

(Chapter 5), and abundant magmatic fluorine in most mafic and felsic rocks. Low oxygen fugacity is suggested for the HHP emplacement conditions based on the Fe/(Fe+Mg) of biotite, negative Eu and positive Ce anomalies in the REE pattern of zircons and enriched LREE of the REE pattern of apatites (e.g. Koreshkova et al., 2009; Broska et al., 2004; Bea, 1996).

7.4 Source regions

Considering field observations (Chapter 2), lithologies (Chapter 2), geochronology (Chapter 4), geochemistry (Chapter 5) and isotopes (Chapter 6), the Mesoproterozoic HHP mafic and felsic magmatic rocks of the Mt Painter Province having A-type characteristics are interpreted to be coeval and derived from similar source regions.

There is evidence that suggests mantle-derived magmas play an important role in generating the HHP granites including; the initial εNd values of theses rocks are higher than the Paralana Gneiss and Freeling Height Quartzite country rocks and; most zircons from the HHP rocks exhibit positive εHf values and plot close to the depleted mantle curve.

The lithospheric mantle and mixed lithospheric-asthenospheric mantle are suggested as main source regions for the HHP mafic dyke; this interpretation is based on a diagram of La/Yb versus Nb/La after Abdel-Rahman (2002; Figure 7.13).

However, mantle-derived magmas cannot be the only component generating the HHP granites and coeval mafic dykes. If these rocks were derived from mantle-derived magmas without crustal contaminations, extensive fractionation crystallization and large volumes of mafic rocks were required. Mafic rocks make up a very small proportion of igneous rocks found in the Mt Painter Province. Besides, the region sources for generating the HHP mafic dyke including lithospheric mantle and mixed lithospheric-asthenospheric mantle seem unlikely to explain the geochemical enrichment in the HHP rocks. Therefore other components are needed rather than only mantle-derived magmas.

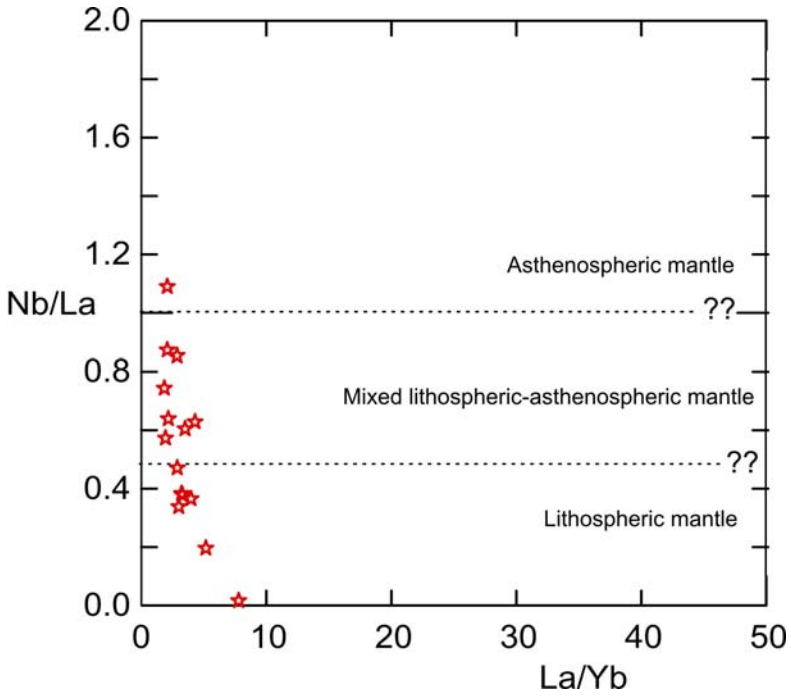

Figure 7.13 La/Yb versus Nb/La diagram for the Mesoproterozoic mafic rocks from the Mt Painter Province; modified after Abdel-Rahman (2002).

Crustal contamination (through the re-melting of pre-existing crust and/or assimilation of crust in mantle-derived magmas through restite separation, wall-rock assimilation or magma mixing) is possibly another component in the production of the HHP granites. There are several observations to support this interpretation. Firstly, inherited zircons are found in the HHP granites and associated rocks suggesting contamination by pre-existing crust. Geochemically, positive Th, Pb and Nd anomalies in the spider diagrams can also be interpreted to indicate a significant crustal component in the source of these rocks. Moreover, radiogenic isotopic compositions including Nd isotope from whole rocks, Hf isotopes in zircons and Pb in K-feldspars confirm the significance of crustal components in the melts required to produce the HHP granites. The lower εNd values from the Mt Painter mafic rocks, compared to other mafic Mesoproterozoic magmatic rocks in the Curnamona Craton (Broken Hill and Olary Domains; Raveggi et al., 2007; Rutherford et al., 2006), suggests a less primitive isotopic magma in the Mt Painter HHP rocks and that they are probably not derived directly from mantle. The εHf values of zircons from the Mt Painter granites are mostly less than εHf values of depleted mantle at ~1.55 Ga indicating crustal

composnents added into mantle magmatic melts. The HHP granites have typically high silica, alkali and incompatible element (e.g. Rb, Th, U and REE except Eu) contents but low alkaline-earth (Ca, Ba and Sr) and Al contents, whereas some rocks contain zircons with older cores of metamorphic origin. These features are consistent with melting of old sialic continental crust (Brueckner, 2009).

In summary, the HHP granites and associated rocks were derived from hybrid magma or crustal-contaminated magma with both mantle and crustal components.

7. 5 Processes

7.5.1 Fractional crystallization

Geochemical compositional variations of the Mt Painter Province granites suggest varying degrees of fractional crystallization. Negative Eu anomalies in the REE patterns indicate extensive fractionation of feldspar. Moreover, a plot of Ba versus Sr suggests that fractionation of K-feldspar and plagioclase played an important role in the differentiation of most felsic rocks, whereas plagioclase fractionation is more dominant in mafic rocks (Figure 7.14). Enrichment in REEs (in particular HREEs) can be explained by either concentrations of hornblende and possibly apatite or by preferential partitioning of REE between mafic and felsic liquids (Watson, 1976; Ryerson and Hess, 1978). The behaviour of elements in the spider diagram is controlled by individual minerals. Negative anomalies of Ba and Sr in the spider diagram for the Mt Painter magmatic rocks can be ascribed to the substantial fractionation of plagioclase from the melt through fractional crystallization. The spider diagrams also shows anomalies of Zr, Ti and Nb for both mafic and felsic rocks; the Zr concentration might be controlled by zircon, while Ti and Nb concentrations are controlled by Ti-bearing minerals such as ilmenite and sphene. Fractionation of Ti-bearing minerals is also confirmed by the decrease of TiO_2 with increasing SiO_2 (see Chapter 5). A decrease in Fe_2O_3 with increasing silica content of the mafic and felsic rocks (see Chapter 5) suggests that fractionation of primary ferromagnesian silicate

minerals. P and Ce anomalies in the spider diagrams are probably controlled by apatite and allanite fractional crystallization, respectively.

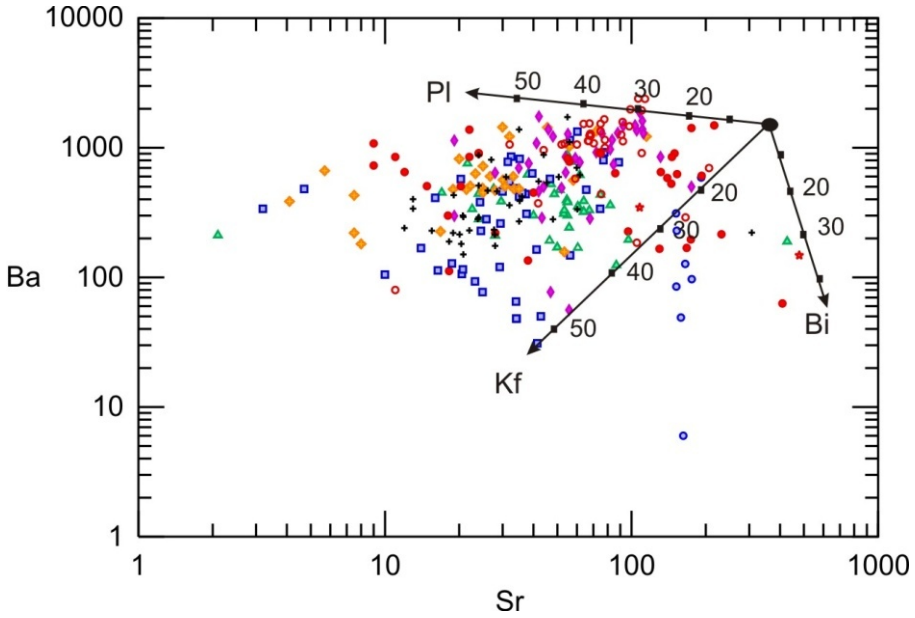

Figure 7.14 Binary plot of Ba versus Sr showing fractionation crystalisation of K-feldspar played an important role in the differentiation of the Mt Painter mafic and felsic rocks Partition coefficients of Sr and Ba from Arth (1976).

Generally, trends in bivariant element plots of the Yerila Granite and microgranular enclaves are distinct from other Mt Painter granites. Strongly fractional crystallization in the Yerila Granite and microgranular enclaves is suggested here by their steeper trends in binary diagrams (see Chapter 5). High fractionation crystallization for the Yerila granite and its enclave is also confirmed by the REE patterns (see Chapter 5). LREEs, which are compatible with fractionation of LREE-enriched phases such as sphene and allanite (Miller and Mittlefehlt, 1982), are more abundant in the Yerila Granite and its enclaves. The Mesoproterozoic mafic dykes have Mg# ranging from 22 to 54, suggesting that fractional crystallization is an important factor in the evolution of the mafic magma.

To investigate the fractionation of the granites from the contaminated mafic melt, fractional crystallization modelling was done using the Pele program (developed by Boudreau, 1999, Figure 7.15). Models were run to investigate the effects of temperature, pressure, crystallisation mode, oxygen fugacity and water content on fractional crystallization in an attempt to match

the calculated fractionated melts with the observed HHP granites. This model assumes that sample MN084, Mesoproterozoic mafic rock from the Mt Painter Province, is representative of contaminated primary mafic magmas. The estimated pressures and temperatures of 4.7 kbar and 986 ºC for contaminated mafic melts, which are based on the hornblende thermobarometer and zircon saturation temperatures (see section 7.3), are applied in this model. The temperatures for the model are incrementally decreased by 15 ºC from 1200 to 700 ºC and pressures are incrementally decreased by 0.1 kbar from 4.7 to 0.7 kbar.

The model suggests that the Mesoproterozoic mafic magma could fractionate to generate some of the HHP granites (e.g. the Pepegoona Volcanic, Mt Neill and Box Bore Granites). However, some granitic rocks (most of the Yerila, Terrapinna and Wattleowie Granites) require other processes such as mixing and mineral accumulations. Fractional crystallization from an incompatible-enriched source like the Mesoproterozoic mafic magma alone could not produce the extremely-enriched U and Th Yerila granite. Abundance of U and Th host minerals, such as allanite, zircon and sphene in the Yerila Granite, which they possibly concentrated in the Yerila Granite from crystal accumulations, is a key of U and Th enrichments. These accessory minerals were separated out from magma and concentrated in melts; then they were picked up the Yerila Granite and its enclaves. The youngest Yerila Granite and its enclaves contain the excess allanite, zircon and sphene.

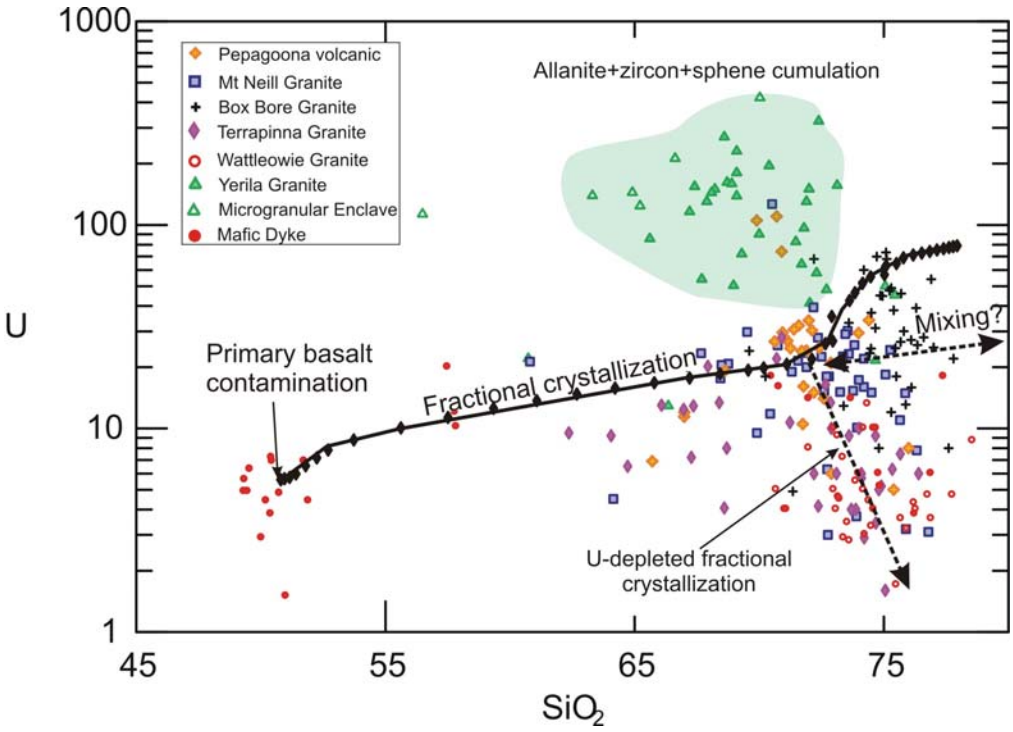

Figure 7.15 Fractional crystallization modelling from the Pele program for the HHP granites; assuming the Mesoproterozoic mafic dyke from the Mt Painter province is the primary magma.

7.5.2 Mixing

Based on geochemical, Sm-Nd and Lu-Hf isotopic data, both mantle-derived magma and reworking of old crust are important sources for the HHP granites. Therefore, fractionation crystallization is not the only process generating the granites. Mixing of two end members including mantle-derived magmas and crustal contamination (through assimilation and/or remelting of pre-existing crust or melting of a subduction-related slab) and mixing of mafic and felsic magmas are also suggested as other important processes to generate the Mesoproterozoic granitic and volcanic rocks.

Geochemical data of the granitic and associated rocks from Mt Painter display strong correlations in the Harker diagrams (detail in Chapter 5). Typically, strong linear geochemical trends on bivariant element plots suggest mixing between different magmas (Rollinson, 1993). These strongly suggest the importance of mixing in the genesis of the Mt Painter felsic rocks. However, some correlations are not perfect and may result from inhomogeneity in the mixing of end members, loss or gain of components,

element mobility, or fractionation during mixing (Rollinson, 1993). Intermediate compositions of microgranular enclaves are likely the result of mixing between mafic and felsic magmas.

A simple mixing model using a relationship of εNd values and Nd concentrations of average country rocks (Paralana Gneiss and Freeling Height Quartzites; data from Schaefer, 1993) and the high-Fe tholeiitic basalt from the Olary Domain (data from Rutherford et al., 2006) is shown in Figure 7.16. The selected high-Fe basaltic sample (M24) from the Olary Domain for this model has initial εNd values of 2.4 and Nd concentration of 3 ppm (Rutherford et al., 2006). The narrow range of initial εNd values and various Nd concentrations suggests that mixing of mantle-derived magma with assimilation of the basement is not the only process required to produce the HHP granitic and associated rocks. The juvenile magmas mix with various amounts of crustal materials (10-25% of crustal materials) and undergo fractional crystallization. Extreme fractional crystallization is required to produce the high Nd concentrations in the HHP granitic and associated rocks from the Mt Painter Province, in particular the Yerila Granite. Moreover, the Mt Painter mafic and felsic rocks have slightly negative to slightly positive εNd values; hence mixing between larger amounts of the mantle-derived magmas over the assimilated old crust is preferred. A plot of T_{DM} and $^{147}Sm/^{144}Nd$ (Figure 7.17) shows that the Mesoproterozoic rock data is clustered together supporting the conclusion that assimilation of the old crust was not important (Lui et al 2005). On the Zr/Y versus Nb/Y binary plot (after Fitton et al., 1997), most mafic dykes from the Mt Painter Province are similar to average lower crust (Figure 7.18) suggesting partial melting of the lower crust could be a source of these rocks.

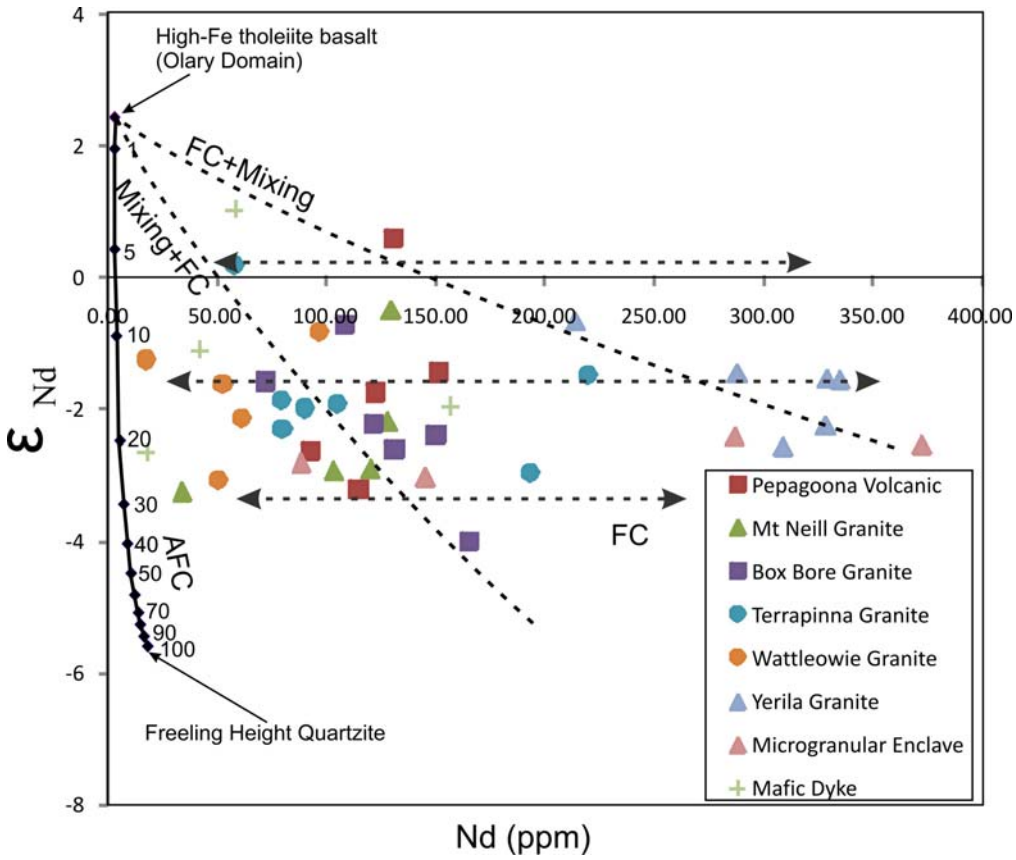

Figure7.16 Mixing modelling of Nd versus εNd(t) diagram for the Mesoproterozoic mafic and felsic rocks from the Mt Painter Province; assuming high-Fe tholeiite basalt as a mantle source assimilate various degree with the Freeling Height Quartzite bastment.

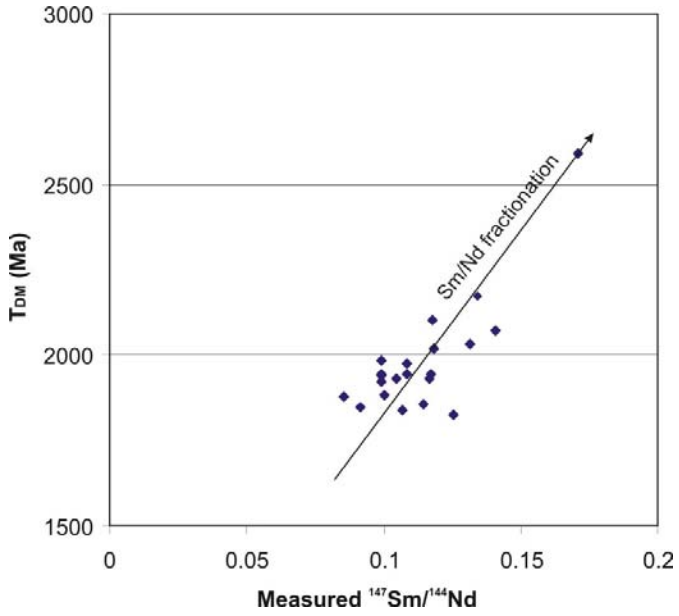

Figure 7.17 $^{147}Sm/^{144}Nd$ versus T_{DM} plot for the Mesoproterozoic mafic and felsic rocks showing the overall positive correlation.

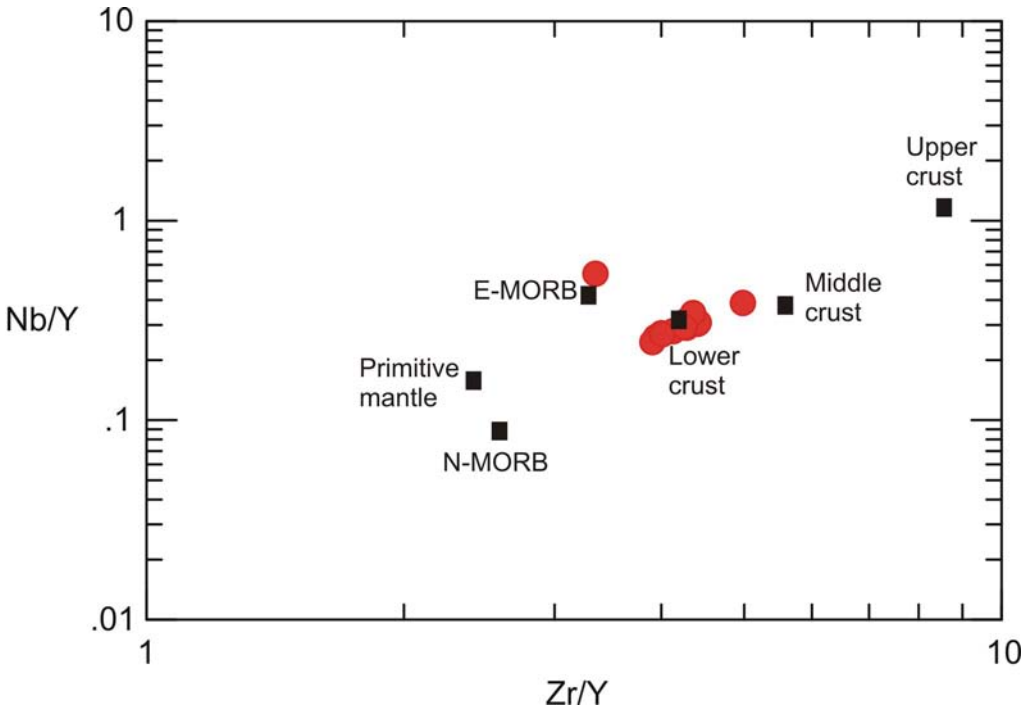

Figure 7.18 Source region discrimination diagram of Zr-Y versus Nb/Y for the Mesoproterozoic mafic dyke from Mt painter Province after Fitton et al. (1997).

7.5.3 Crustal melting

Partial melting of crustal materials is another possible process to generate the HHP granites. The HHP granites from the Mt Painter Province are grouped as A2-type granites (see Section 7.2), which derived from melting of continental crust or underplated mafic crust that has been through a cycle of continent–continent collision or island-arc magmatism (Eby, 1992). Following this generalisation, the Mt Painter A2-type granites were likely generated by crustal partial melting. Moreover, radiogenic isotopic compositions and geochemistry of these rocks suggest that crustal component is an important source to form crustal-contaminated magmas (see section 7.4). Data of εNd and εHf in the HHP granites and associated rocks suggests that the crustal-contaminated magmatic source is uniform and homogeneous. To generate the homogeneous source, mixing between mantle-derived magmas and crustal components were possibly occurred at the 'Hot Deep Zone'. At the lower crust and mantle interface, mafic sill could be repeatedly injected in the lower crust developing the 'Hot Deep Zone' (Annen et al., 2008). The mafic magmas, which could be brought up by mantle upwelling or extension

tectonism, transfered heat to the crust, which progressively rised in temperature (Annen et al., 2006). After the incubation period, the temperature at the injection depth reached that of mafic magma solidus and partial melting of the crust could start when the fluid-absent solidus is reached (Annen et al., 2006). To generate larger amount of mafic magma proportion compared to crustal proportion in the melt, partial melting of the granulitic crust is suggested as a crustal source (Annen et al., 2008). The crustal contaminated soure for generating the HHP granites have small amount of crustal melt compared to mafic melt the partial melting. Thus, partial melting of granulite protolith is suggested as a regional source to form the HHP granites.

7.6 Formation of the HHP granites

In this study, a model for the formation of the HHP mafic and felsic rocks adopts crustal-contaminated mantle-derived mafic magmas as a primary and main source of the melt involving fractional crystallization, mixing, partial melting and minor wall rock assimilation.

The primary contaminated mantle-derived magmas sourced from mantle-derived magma and partial melting of the lower crust from mantle upwelling. During ascent of the mantle-derived mafic magma, it was trapped at the lower crust and possibly acted as mafic underplating of the lower crust, allowing thermal exchange. At the deep crust, silicic melt could be generated because temperatures increase with depth. When temperature reached conditions of partial melting, partial melting and assimilation of the surrounding rocks in the lower crust were occurred. Mixing of partial melting of the lower crust and mantle-derive mafic magma at the mantle and lower crust interface produced a isotopically homogeneous contaminated melt. These partial melting and mixing process could occur at ~1.75 Ga then they possibly were sunsequently remelted at ~1.60 Ga. This melt being high K, Fe, F, HFSE contents in a reduced environment, with low fO_2 and H_2O was brought up that could be a result of crutal extension or rifting (1; Figure 7.19). This extension event could occur between ca. 1680 and 1640 Ma coincident with the Ooldean event in the western Gawler Craton which occurred follow the Kimban orogeny (Hand et al., 2007). Subsequent to the Kimban orogeny

and extension possibly results in emplacements of widespread magmatic rock suites (Hand et al., 2007) such as A-type affinities of the Olary Domain (Ashley et al., 1997), Gawler Range Volcanic and Hiltaba Suite of the Gawler Craton (Hand et al., 2007). Assimilation of solid wall rocks could happen during the contaminated magma ascent (2; Figure 7.19), but had limited affect on the magma. The felsic A-type magmas were generated from fractional crystallization of the contaminated mantle-derived magmas (3; Figure 7.19), then mixed with the following up mafic contaminated mantle-derived magmas resulting in the generation of the first felsic magmatic event including the Pepegoona Volcanics, and Mt Neill and Box Bore granites. This mixing of felsic and mafic contaminated mantle-derived magmas occurred by convection before the felsic suites ascended to the near surface (3; Figure 7.19). After generating the Pepegoona Volcanics, and the Mt Neill and Box Bore Granites, the ascending mafic magma mixed with the felsic rocks, forming the Terrapinna Granite, which has a mafic component due to its emplacement at a deeper level. While the Terrapinna Granite was generated, the accumulated Wattleowie Granite was produced.

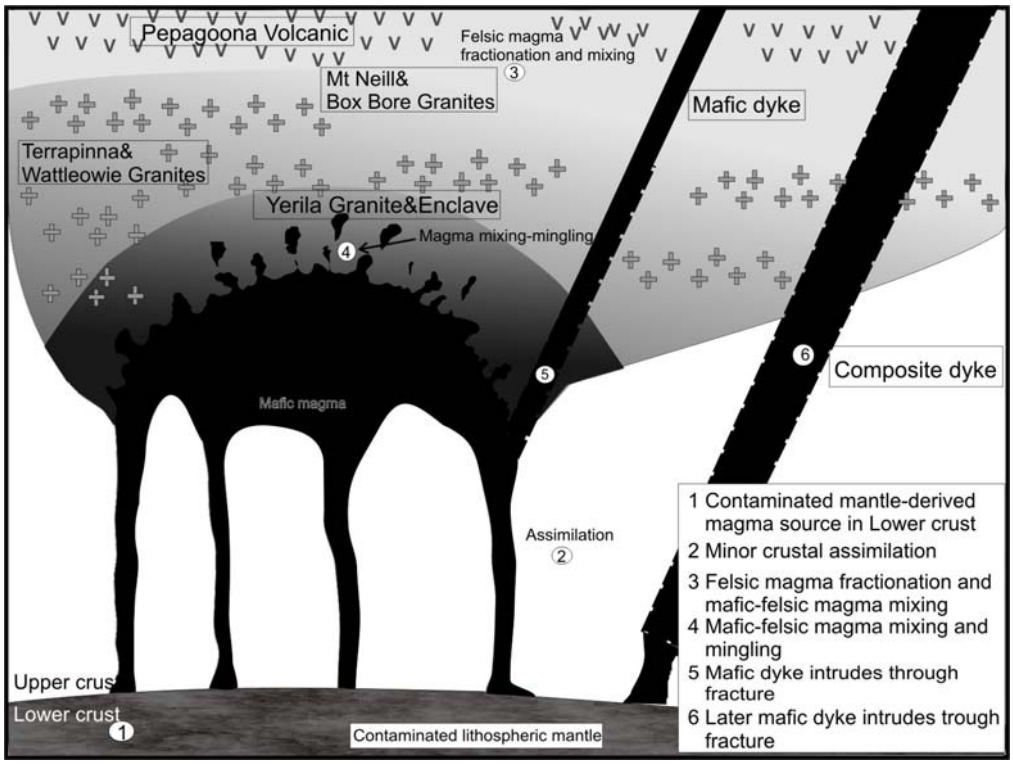

Figure 7.19 Illustration of formation and evolution of the HHP granites and associated rocks (see text for description).

The Yerila Granite, which is the most mafic of the felsic rocks, formed by a large (relative to the older granites) volume of mafic contaminated mantle-derived magmas being injected into the previous felsic magma and were generated by highly fractionated crystallization. At a later stage, the mafic contaminated mantle-derived magmas were rapidly injected in an open system when the felsic magmas were already moving upward, thereby having sufficient time to mix with the felsic magma. Small scattered blobs of disrupted mafic magma were carried within the moving granitic magmas. Different viscosities between the two magmas resulted in mingling, which continued during magma ascent and emplacement. The emplacement of the Yerila Granite and its enclaves took place very close to the surface. At the emplacement level, incompletely crystallized granitic magmas were affected by early fractures, which channelled the residual liquid and fluids (Hibbard and Watters, 1985; Barbarin et al., 2005). A later mafic contaminated mantle-derived magma injected into fractures in an essentially solid felsic rocks formed the composite dykes (4 and 5; Figure 7.19). Various amounts of upper continental crustal mixed or were assimilated into the contaminated mantle-derived magma during melting or magma ascendance.

Accessory minerals such as allanite, sphene and zircon, which are main hosts for U, Th and REE, were crystallized from melts and were partly captured by the early granitic and volcanic rocks. The larger proportion of these accessory minerals were not taken up and were stored in the melts. The later highly-fractionated Yerila Granite and its enclaves, which formed at high temperature, incorporated the excess allanite, sphene and zircon in the melts. It is this abundance of allanite, sphene and zircon in the Yerila Granite that results in the high heat production values in the granite.

7.7 Implication for tectonic evolutions

It is proposed that a crustal-contaminated mantle is a major source of the HHP granites and associated rocks from the Mt Painter Province. Partial melting of the lower crust played a major role to generate the HHP granites. Partial melting of the lower crust occurred, due to heating the crust that

possibly was caused by mantle underplating, which may be a result of post-orogenic extension and/or mantle plume activity occurred following collision.

This interpretation is supported by tectonic reconstruction models during the Proterozoic Era. Subduction-dominated accretionary growth of a new crust is proposed in many Proterozoic terranes such as the 1.8–1.7 Ga Yavapai province, 1.7–1.6 Ga Mazatzal province and Labradorian Orogen of the Laurentian margin (e.g. Karlstrom and Bowring, 1993; Gower, 1996), the Transcandinavian Igneous Belt and Gothian terrances of Baltica (e.g. Ahall and Gower, 1997; Ahall and Larson; 2000), the Arunta Region and Capricorn Orogen of Australia (e.g. Foden et al., 1988; Zhao, 1994; Zhao and McCulloch, 1995), *ca.* 1590-1555 Ma arc-related magmatism in the Musgrave Province (Wade et al., 2006) and the 1620-1608 Ma St Peter Suites (Swain et al., 2008).

The following evolution of southern margin of the Australian plate during the Proterozoic has been proposed by Betts et al. (2008). Between 1.8 and 1.5 Ga, the North Australia Craton and the South Australia Craton had a shared tectonic evolution with the South Australia Craton, reconstructed in a *ca.* 50º counterclockwise orientation (Betts and Giles, 2006). The model from Betts and Giles (2006) suggests the Australian continent grew laterally southward as crustal fragments were accreted to the margin at *ca.* 1.8-1.6 Ga. During this period, the convergent plate margin migrated southward (Betts et al., 2008). Accretion of the West Australian Craton with the North Australia Craton occured during the Yapungku Orogeny (*ca.* 1790-1765 Ma; Bagas, 2004; Figure 7.20), then accretion of the Mawson Continent, which comprises Gawler, East Antarctica, and Mojave Province onto the southern margin of Australia–Laurentia continent occurred at *ca.* 1750 Ma (Betts et al., 2008; Figure 7.20).

A Potential heat source for partial melting the lower crust as a crust source component was an increasing mantle heat flux. Main mechanisms causing heat fluxes in the intracontinent have been proposed by Neves and Mariano (2004) including thickening of previously thinned lithosphere (based on Thompson et al., 2001), mantle convection beneath the overriding plate in

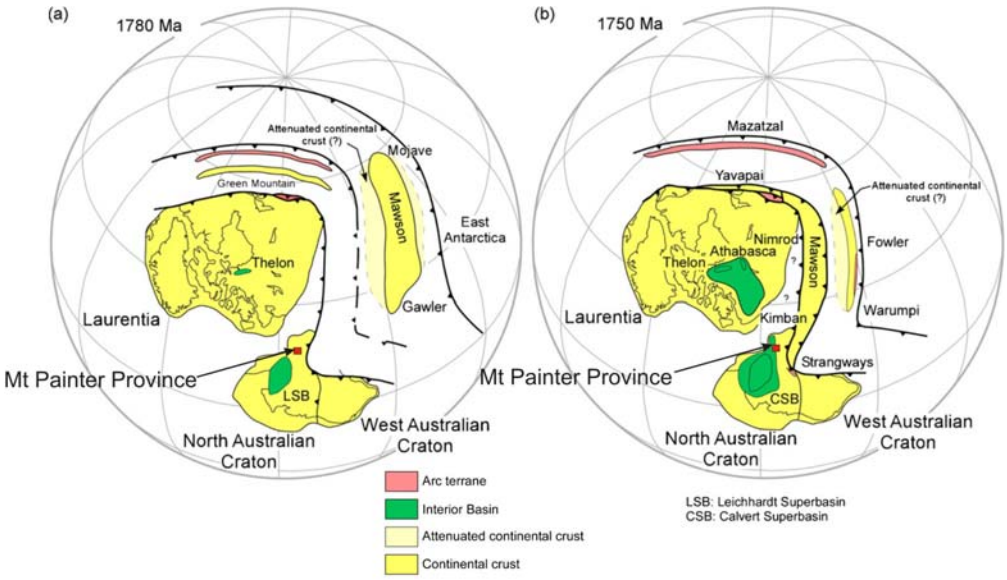

Figure 7.20 Evolutionary reconstructions of the Australia–East Antarctica–Laurentia between ca. 1780 and 1650 Ma. (a) Accretion of the West Australian Craton with the North Australia Craton during the Yapungku Orogeny (Bagas, 2004); (b) Accretion of the "Mawson Continent", which comprises Gawler, East Antarctica, and Mojave Province, onto the southern margin of Australia–Laurentia continent (modified after Betts et al., 2008).

a subduction setting (Giles et al., 2002) and heat delivered to the base of the lithosphere by a plume of deep mantle origin. The three modes of intracontinental contractional deformational is shown in Figure 7.20. The mantle plume model for generating the HHP granitic and mafic rock maybe ruled out because the Mt Painter Province loosely fits the definition of Large Igneous Province (LIP); which defined as follows: are a extents >1 Mkm^2; igneous volumes > 0.1 Mkm^3 with igneous pulse(s) of short duration (~1 to 5 Ma) during which > 75% of the total igneous volume has been emplaced; a maximum lifespan of ~50 Ma; intraplate tectonic settings (Bryan and Ernst, 2008). However, LIP that is found in surrounding areas (Gawler Range Volcanic and Hiltaba Suite of the Gawler Craton) fit well with the LIP definition. This evidence may suggest that mantle plume can possible be a cause of heat flux generating the HHP granites of the Mt Painter province. The Pb K-feldspar isochron age of 1761±41 Ma for the HHP granitic and volcanic rocks from the Mt Painter Province, which could suggest a possible time generating the melts, is coincided with significant tectonic events e.g. the Yapungku Orogeny (Bagas, 2004), accretion of the Mawson Continent onto

the southern margin of Australia–Laurentia continent (Betts et al., 2008), the 1740 Ma Kimban Orogeny and the 1.78 and 1.73 Ga north-dipping Arunta subduction (Zhao, 1994; Zhao and McCulloch, 1995). Therefore, crustal thickening and extensional collapse and/or extension preceding thickening in a continental back-arc setting could cause heat fluxes that generated a crustal contaminated magma.

Moreover, crustal thickening could lead to an increasing of the total heat production of the crust (Kukkonen and Lauri, 2009). The thermal and geochemical modelling of Paleoproterozoic southtern Finland that has been proposed by Kukkonen and Lauri (2009) suggests that high heat production migmatitic granites in southern Finland was a result of a rapid crustal thickening in a plate collision at *ca.* 1870-1860 Ma followed by conductive heating of the crust, simultaneous exhumation and partial melting of middle crust and emplacement of the melts in the upper crust. This similar process could apply for a formation of the HHP granites of the Mt Painter Province. If the lower crust experienced high-temperature–low pressure metamorphism forming the magmatic lower crust, which is enriched in heat production elements, partial melting of this crust could provide large amount of U and Th concentrations entering the melt phase.

The crustal contaminated magma ascended to a shallow level in intraplate or back arc settings by rifting or crustal extension at *ca.* 1600 Ma. The evidence of crustal extension in the Mt Painter Area is suggested by the deposition of the Freeling Height Quartzite. Moreover, ensialic rifting has been proposed as the depositional environment for Willyama Supergroup rocks in the Southern Curnamona Craton (e.g. Willis et al., 1983; Stevens et al., 1990; Cook and Ashley, 1992; Slack and Stevens, 1994; Gibson and Nutman, 2004; Gibson et al., 2004; Betts and Giles, 2006) which is analogous to the Mt Isa Rift system in northern Australia (Betts and Lister, 2001) generated the A-type felsic rocks from the Olary Domain (Ashley et al., 1996).

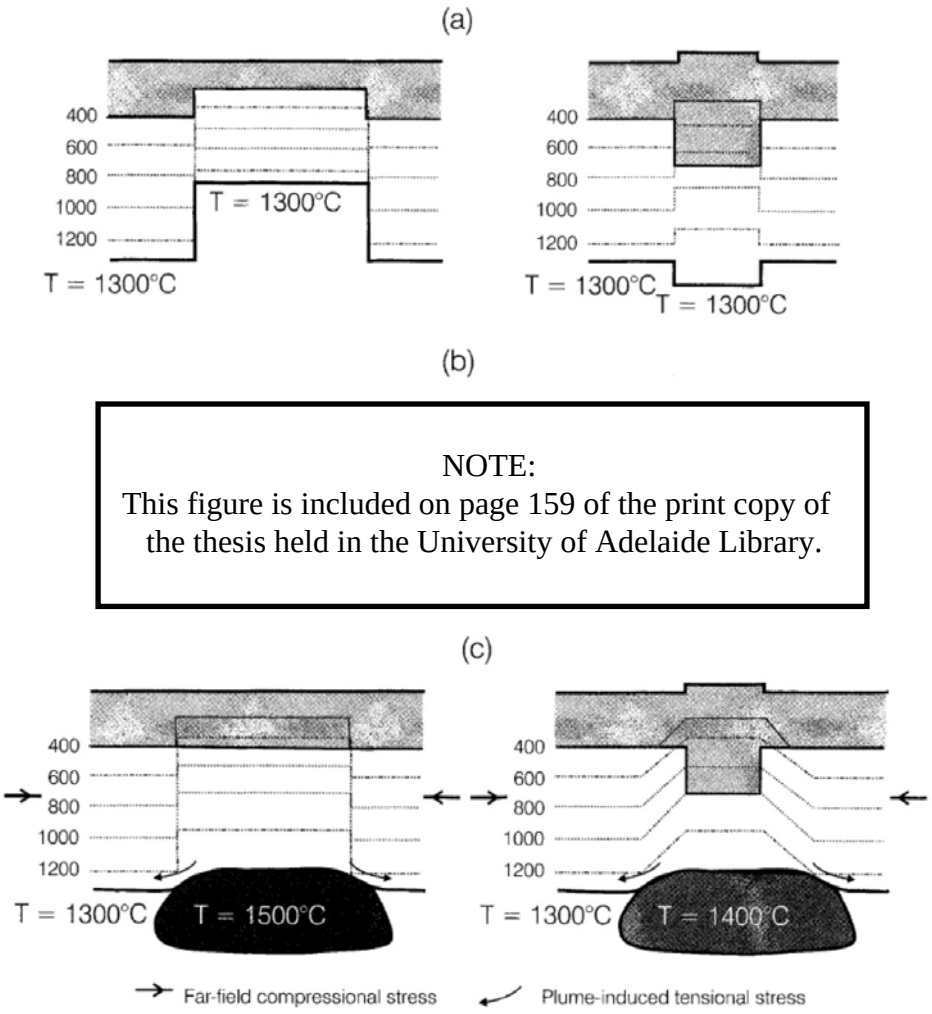

Figure 9.20 Three possible modes of intracontinental contractional deformational (Neve and Mariano, 2004): (a) extension preceding thickening in an intraplate setting (based on Thompson et al., 2001); (b) extension preceding thickening in a continental back-arc setting (Giles et al., 2002); (c) plume-lithosphere interaction in a mildly compressive continental setting.